UCRL-18476

cy. 2

RECEIVED
DEC 19 1968
LIBRARY AND
DOCUMENTS SECTION

AN ABSOLUTE TEMPERATURE SCALE FOR CERIUM MAGNESIUM NITRATE BELOW 0.002°K

James John Huntzicker
(Ph.D. Thesis)

September 1968

TWO-WEEK LOAN COPY

This is a Library Circulating Copy which may be borrowed for two weeks. For a personal retention copy, call Tech. Info. Division, Ext. 5545

UCRL-18476 cy. 2

LAWRENCE RADIATION LABORATORY
UNIVERSITY of CALIFORNIA BERKELEY

DISCLAIMER

This document was prepared as an account of work sponsored by the United States Government. While this document is believed to contain correct information, neither the United States Government nor any agency thereof, nor the Regents of the University of California, nor any of their employees, makes any warranty, express or implied, or assumes any legal responsibility for the accuracy, completeness, or usefulness of any information, apparatus, product, or process disclosed, or represents that its use would not infringe privately owned rights. Reference herein to any specific commercial product, process, or service by its trade name, trademark, manufacturer, or otherwise, does not necessarily constitute or imply its endorsement, recommendation, or favoring by the United States Government or any agency thereof, or the Regents of the University of California. The views and opinions of authors expressed herein do not necessarily state or reflect those of the United States Government or any agency thereof or the Regents of the University of California.

UCRL-18476

UNIVERSITY OF CALIFORNIA

Lawrence Radiation Laboratory
Berkeley, California 94720

AEC Contract No. W-7405-eng-48

AN ABSOLUTE TEMPERATURE SCALE FOR CERIUM MAGNESIUM NITRATE BELOW 0.002°K

James John Huntzicker

(Ph.D. Thesis)

September 1968

AN ABSOLUTE TEMPERATURE SCALE FOR CERIUM MAGNESIUM NITRATE BELOW 0.002°K

Contents

Abstract v

I. Introduction and Historical Review 1

II. Theoretical Background 4

A. Adiabatic Demagnetization 4

B. The Measurement of Absolute Temperature Below 1°K . 8

C. Thermal Equilibrium Nuclear Orientation 14

III. Experimental 25

A. ^{3}He Refrigerator 25

B. Vapor Pressure Measurements 30

C. The Experimental Chamber and its Contents 34

D. Magnetic Field 39

E. Counting System 43

F. Summary 46

IV. The Cerium Magnesium Nitrate Temperature Scale 48

A. Physical Properties of CMN and ^{137m}Ce 48

B. Sample Preparation 59

C. Data Reduction 67

D. Results 86

E. Discussion 112

V. The Nuclear Orientation of ^{137m}Ce in Cerium Zinc Nitrate: Preliminary Results 130

A. Theoretical 130

AN ABSOLUTE TEMPERATURE SCALE FOR CERIUM MAGNESIUM NITRATE BELOW 0.002°K

James John Huntzicker

Department of Chemistry and Lawrence Radiation Laboratory
University of California
Berkeley, California 94720

September 1968

ABSTRACT

The absolute temperature scale for single crystal cerium magnesium nitrate (CMN) has been extended to S/R = 0.002 by adiabatic demagnetization from values of H/T up to 68 kOe/°K. The temperature dependence of the highly anisotropic angular distribution of the 255 keV γ-ray from oriented ^{137m}Ce in the CMN provided the thermometric parameter. The nuclear orientation results were interpreted with the spin Hamiltonian $\mathcal{H} = g_{\perp}\beta H_x S_x + B(S_x I_x + S_y I_y)$ where H_x (a calculated dipolar field) = 60.67 Oe and B/k = 0.00820 ± 0.00042°K. The hyperfine structure constant B was determined by normalizing the nuclear orientation results to the calorimetric results of Hudson and Kaeser in the entropy range $0.063 \leq (\ln 2 - S/R) \leq 0.164$. Analytic relations between temperature and entropy are presented for the entropy range $0.002 \leq S/R \leq 0.640$. The lowest temperature measured was 0.00135 ± 0.00008°K. The present results are in reasonable agreement with both the earlier nuclear orientation results of Frankel, Shirley, and Stone and with the calorimetric results of Hudson and Kaeser. These results and the results of Hudson and Kaeser are compared in detail. The effect of recent high-field magnetization measurements on the CMN temperature scale are discussed.

The ^{137m}Ce γ-ray thermometer was also used to investigate the thermal behaviour of cerium zinc nitrate (CZN). The preliminary nuclear orientation results indicate a high degree of similarity between CZN and CMN.

I. INTRODUCTION AND HISTORICAL REVIEW

Until recently temperatures below 0.1°K were obtained primarily by adiabatic demagnetization of a paramagnetic crystal. With the advent of ^3He - ^4He dilution cooling it now seems possible to maintain temperatures of about 0.01°K for long periods of time and temperatures of 0.004°K for much shorter periods. At this writing the most common way of reaching temperatures below 0.004°K is by adiabatic demagnetization of the paramagnetic salt, cerium magnesium nitrate. This thesis will be concerned with the establishment of an entropy-temperature relation for single crystals of this salt and will present results over practically the whole entropy range.

Cerium magnesium nitrate, $Ce_2Mg_3(NO_3)_{12}\cdot 24H_2O$, hereafter designated as CMN, has long been recognized as a substance capable of being cooled by adiabatic demagnetization to extremely low temperatures. The studies of the temperature scale to date can be grouped into three categories: calorimetric investigation of single crystal CMN, nuclear orientation studies of single crystal CMN, and calorimetric studies of powdered CMN.

The pioneer investigation of the temperature scale was a calorimetric study by Daniels and Robinson[1] on a sample which they described as a single crystal fashioned into an approximate prolate spheroid. They found that Curie's law was obeyed to 0.006°K and that $\ln 2 - S/R = 3.2 \times 10^{-6} T^{-2}$ in this region. Below 0.006°K there were significant departures from Curie's law, and for $S/R < 0.45$ the temperature was constant and equal to 0.00308°K. In a subsequent re-analysis of the

Daniels and Robinson data, de Klerk[2] asserted that the temperature did not become constant at $S/R = 0.45$ but continued to decrease until at $S/R = 0.150$, $T = 2.25$m°K (millidegree K).

In 1965 Frankel, Shirley, and Stone[3] demonstrated that nuclear orientation could be used to determine the temperature of a paramagnetic crystal. They found that the Daniels and Robinson T-S scale was unable to explain the nuclear orientation results for ^{137m}Ce in CMN below 3.0°K. Using their results and the Daniels and Robinson scale above 6m°K, Frankel et al. derived a new T-S relation. They found that T did not become constant at any value of entropy in the range available to them and at $S/R = 0.303$ (the lowest entropy which they measured), $T = 1.94$m°K.

In the most recently reported investigation of single crystal CMN, Hudson and Kaeser[4] studied several single crystal samples – both spherical and ellipsoidal. They found no shape dependence in the correlation between absolute temperature and entropy and confirmed that Curie's law was obeyed down to 6m°K. However, they found that for this temperature region $\ln 2 - S/R = 2.88 \times 10^{-6} T^{-2}$ in significant disagreement with the earlier work. At the low temperature end of the scale their work was in disagreement with the results of Frankel et al. Below $S/R = 0.296$ they found the temperature to be essentially constant and equal to 1.53m°K. In addition a small anomaly in the heat capacity with a maximum at 0.025°K was discovered and was shown to be of non-magnetic origin.

As an outgrowth of their studies of liquid ^{3}He, Wheatley and collaborators[5,6,7] have established a $T - T^*$ relation for powdered CMN in the shape of a right circular cylinder with diameter equal to height. They have determined the thermodynamic temperature by considering the properties of liquid ^{3}He and ^{3}He in liquid ^{4}He as a function of magnetic temperature. Measurements of the self-diffusion constant of ^{3}He in both the pure liquid and in liquid ^{4}He and of the attenuation of zero sound in pure ^{3}He indicated that $T \approx T^*$ down to almost 2m°K. They have assumed, however, that the demagnetizing or shape correction to T^* is zero – an assumption which has recently been challenged by Abraham and Eckstein.[8] Black[9] and Anderson[10] have presented results contrary to Abraham and Eckstein, and this controversy has not yet been resolved.

The measurements reported in this thesis are concerned only with single crystal CMN, and so the subject of powdered CMN will not be discussed further. The remainder of this thesis is divided into five parts: theoretical background, experimental technique, the CMN temperature scale, preliminary results on the cerium zinc nitrate temperature scale, and appendices. The primary goals in this research have been to check the earlier nuclear orientation work and to extend the temperature scale to lower entropies and temperatures.

II. THEORETICAL BACKGROUND

In this section the theoretical background relevant to the experiments described in this thesis will be presented. The first topic to be discussed will be adiabatic demagnetization followed by the measurement of temperature below 1°K, and nuclear orientation.

A. Adiabatic Demagnetization

In 1926 Giauque[11] and Debye[12] independently proposed that the adiabatic demagnetization of a paramagnetic salt initially at 1°K would yield temperatures well below 1°K. In 1933 when liquid He first became available to Giauque, he and MacDougall[13] demagnetized $Gd_2(SO_4)_3 \cdot 8H_2O$ to 0.2°K. With the availability of appropriate magnets and liquid helium other investigators at Oxford and Leiden began research at temperatures below 1°K. The subject of magnetic cooling has been reviewed by Ambler and Hudson,[14] De Klerk,[2,15] and Kurti.[16]

The technique of magnetic cooling consists of two main steps: isothermal magnetization of the paramagnetic salt at a temperature near 1°K and adiabatic demagnetization to the lower final temperatures. In the first step the salt is thermally linked to a liquid helium bath either mechanically or by helium exchange gas. A direct current field of several thousand Oersteds partially aligns the electron spins of the paramagnetic ions along the field direction giving a state of lower entropy. The paramagnetic salt is then isolated from the liquid helium bath by breaking the mechanical link or by evacuating the experimental chamber to a low pressure. When the isolation is complete, the magnetic field is slowly reduced. If the crystal is demagnetized adiabatically

and reversibly to zero magnetic field, then a net entropy reduction in the electronic spin system (and in the crystal) at zero magnetic field will be achieved. Consequently the final temperature of the crystal will be lower than the initial temperature.

Thermodynamically, magnetic cooling is directly analogous to the cooling of a gas by isothermal compression and subsequent adiabatic decompression. Table II.1 presents the relevant formulae for an ideal gas and an ideal paramagnet. The latter is defined as a paramagnet whose magnetization M is a function only of external field H and temperature T. For simplicity we let the salt obey the Curie law:

$$\chi = M/H = C'_M/T \qquad \text{(II.A.1)}$$

where χ is the magnetic susceptibility and C'_M is the Curie constant. In Table II.1 h is enthalpy, C_H is the heat capacity at constant magnetic field, and C_p is the heat capacity at constant pressure. The familiar PV work for a gas is replaced by HM work for a magnetic system. For the isothermal steps there is a decrease in entropy for an increase in pressure or field. In the adiabatic step both $(\partial T/\partial P)_S$ and $(\partial T/\partial H)_S$ are greater than zero, and thus a decrease in pressure or field yields a lower temperature.

In the temperature region between 0.3°K and 4°K the magnetic properties of the salt are due primarily to the electronic ground state of the paramagnetic ion. This condition exists when the higher states are sufficiently removed in energy and only the lowest state is appreciably populated. If, in addition, the collective interactions

Table II.1. Comparison of an ideal gas and an ideal paramagnet.

$dE = \delta q + \delta W$	$\delta q = TdS$
Ideal Gas	Ideal Paramagnet
$\delta W = -PdV$	$\delta W = HdM$
$dE = TdS - PdV$	$dE = TdS + HdM$
$dh = TdS + VdP$	$dh = TdS - MdH$
$dA = -SdT - PdV$	$dA = -SdT + HdM$
$dF = -SdT + VdP$	$dF = -SdT - MdH$
$PV = nRT$	$\chi = M/H = C'_M/T$
Isothermal Compression	Isothermal Magnetization
$(\partial S/\partial P)_T = -(\partial V/\partial T)_P = -nR/P$	$(\partial S/\partial H)_T = (\partial M/\partial T)_H = -C_M H/T^2$
$\Delta S = -nR\,\ell n P_1/P_o < 0$ for $(P_1 > P_o)$	$\Delta S = -C'_M/T^2\,(H_1 - H_o) < 0$ for $(H_1 > H_o)$
Adiabatic Decompression	Adiabatic Demagnetization
$(\partial T/\partial P)_S = -(\partial S/\partial P)_T/(\partial S/\partial T)_P = T/C_P(\partial V/\partial T)_P = (T/C_P)(nR/P) > 0$	$(\partial T/\partial H)_S = -(\partial S/\partial H)_T/(\partial S/\partial T)_H = T/C_H(\partial S/\partial H)_T = C'_M H/TC_H > 0$
$\therefore$ An adiabatic decrease in P results in a lower T.	$\therefore$ An adiabatic decrease in H results in a lower T.

between the paramagnetic ions are small, the salt obeys a Curie law or a modified Curie law:

$$\chi = \frac{M}{H} = C'_M/T + \alpha \qquad \text{(II.A.2)}$$

where α is a temperature-independent term arising primarily from the second order Zeeman effect.[17] From Eqs. (II.A.1) and (II.A.2) we expect M to be directly proportional to H, but this is only true in the low-field limit. At high magnetic fields the magnetization saturates, and the expression for ΔS in Table II.1 is no longer valid. Thus in order to calculate the thermodynamic properties of the salt during the isothermal magnetization, it is necessary to recast the problem in terms of statistical thermodynamics.

If we let the ground state of the paramagnetic ion be characterized by angular momentum J, then in an external field H the $(2J+1)$ degeneracy is completely lifted and the energy levels are characterized by $E_m = -mg\beta H$. Here m takes on the values $J, J-1, J-2, \ldots. -J$, and β is the Bohr magneton and g the spectroscopic splitting factor. The last quantity depends in detail on the various interactions in the crystal and on the direction of the applied field. Theoretically it corresponds to the expectation value of the operator $\underline{L} + 2\underline{S}$ where $\underline{L}$ and $\underline{S}$ are the orbital and spin angular momentum operators. The partition function Q for N independent ions is then defined as

$$Q = \left[\sum_{m=-J}^{J} \exp\left(-E_m/kT\right) \right]^N \qquad \text{(II.A.3)}$$

and the thermodynamic functions may in turn be defined in terms of Q

$$F = -kT\ell nQ \text{ (Gibbs Free Energy)}^{*} \tag{II.A.4}$$

$$M = -\left(\frac{\partial F}{\partial H}\right)_T = kT\left(\frac{\partial \ell nQ}{\partial H}\right)_T \tag{II.A.5}$$

$$S = -(\partial F/\partial T)_H = k\ell nQ + kT(\partial \ell nQ/\partial T)_H \tag{II.A.6}$$

where R is the gas constant. The entropy removed during an isothermal magnetization is just a function of H/T, and a measurement of this quantity will uniquely define the entropy. This presupposes that the lattice entropy is negligible — an assumption which is usually well justified at magnetizing temperatures of 1°K or less. In zero external field the levels E_m are degenerate and $S/R = \ell n(2J+1)$. This value of S/R corresponds to the maximum amount of entropy which may be removed in the magnetic cooling process.

B. The Measurement of Absolute Temperature Below 1°K

In the nineteenth century Lord Kelvin[18] defined thermodynamic or absolute temperature with respect to a Carnot cycle. "The absolute values of two temperatures are to one another in the proportion of the heat taken in to the heat rejected in a perfect thermodynamic engine

---

*For a magnetic system with the independent variables T, V, and H, the Gibbs function (F) is more appropriate than the Helmholtz function (A). It can be shown for such a system that $Q = \exp(-F/kT)$ or $F = -kT\ell nQ$. An excellent discussion of this point is given by P. M. Morse in Thermal Physics (W. A. Benjamin, Inc., New York, 1964) pp. 292-3.

working with a source and a refrigerator at the higher and the lower of the temperatures respectively." This statement is equivalent to the second law of thermodynamics — the mathematical formulation of which may also be regarded as defining the thermodynamic temperature:

$$dS = (\delta q/T)_{reversible} \quad . \tag{II.B.1}$$

Using the methods of statistical thermodynamics (e.g. see Ref. 19) and the second law of thermodynamics it can be shown that entropy is related to the probability that an energy state is occupied by

$$S = -k \sum_j P_j \ln P_j \tag{II.B.2}$$

where j refers to the available energy states and P_j is the probability of occupation. It can also be shown that P_j is the familiar Boltzmann probability

$$P_j = e^{-E_j/kT} \Big/ \sum_{j'} e^{-E_{j'}/kT} \tag{II.B.3}$$

for a closed isothermal system. Here E_j refers to the energy of the state j and k is the Boltzmann constant. For our discussion then, we will regard (II.B.1) and (II.B.3) as equivalent definitions of the thermodynamic temperature.

The next subsection deals with the calorimetric measurement of temperature. Although this method was not used in this work, an understanding of the method is necessary for the discussion in Section IV.

1. Calorimetric Measurement of T

In a calorimetric determination of T Lord Kelvin's definition and Eq. (II.B.1) are used. Two temperature regions are of interest in such an investigation. The first is the Curie law region where Eq. (II.A.1) or (II.A.2) is valid while the second is the lowest temperature region, where the susceptibility is often no longer a useful thermometric parameter. In the discussion of the calorimetric method primary attention will be placed on the method used by Daniels and Robinson[1] and by Hudson and Kaeser[4] in their studies of CMN.

It is convenient to define a parameter T^* known as the magnetic temperature which is defined by Eq. (II.B.4),

$$\chi = C'_M/T^* = M/H \quad . \qquad \text{(II.B.4)}$$

In general T^* is dependent on the shape of the sample because of the demagnetizing factor. Kurti and Simon[20] have suggested that T^*'s be referred to $T^{\circledast}$, the magnetic temperature for a sphere. They have shown that the local field actually acting upon the ions rather than the external field is the fundamental quantity for determining susceptibilities and temperature. This field includes the interaction of other dipoles and also the demagnetizing effects. In the Lorentz approximation for the dipole field which is valid at high temperatures

$$H_{local} = H_{ext} - dM + H_{Lor} = H_{ext} - dM + (4\pi/3)M \qquad \text{(II.B.5)}$$

where d is the demagnetizing factor, M is the magnetization per unit volume, H_{ext} is the external field and H_{Lor} is the Lorentz field.

Equation (II.B.5) is valid only for ellipsoidal samples since only in these samples will the magnetization be uniform. For a sphere $d = 4\pi/3$ and $H_{local} = H_{ext}$. This implies that for a spherical sample, bulk susceptibility measurements in the high-temperature region will give $T^{\circledast}$'s which, to a high precision, are equal to T, the thermodynamic temperature. Thus in the following discussion we will concern ourselves only with $T^{\circledast}$; T^{*}'s for other sample shapes can be converted to $T^{\circledast}$ by the appropriate demagnetization correction.

In the Curie law region the S-T relation can be determined as follows. An $S/R - \chi - T^{\circledast}$ correlation can be established by demagnetizing from a known H/T and measuring the susceptibility just after demagnetization. This presupposes that the $\chi - T^{\circledast} - T$ correlation has been already established in the liquid He region (i.e. C'_M has been determined). The theoretical relation between S/R and T in the Curie law region, has been considered by Van Vleck,[21] Hebb and Purcell,[22] and Daniels.[23] If the only important interactions are dipole-dipole and isotropic exchange, they find

$$\ln (2J + 1) - S/R = bT^{-2} = bT^{\circledast\,-2} \quad . \qquad \text{(II.B.6)}$$

By fitting the S/R, $T^{\circledast}$ data to (II.B.6) the value of b can be obtained.

It is important, however, to choose the appropriate temperature region in which to apply Eq. (II.B.6) to the $T^{\circledast}$ data. As long as both the magnetic specific heat $C^{\circledast} = dQ/dT^{\circledast}$ and S/R are proportional

to $T^{\circledast -2}$, T is equal to $T^{\circledast}$.* To determine whether $C^{\circledast}$ is proportional to $T^{\circledast -2}$, it is necessary to introduce heat into the sample after the demagnetization. A convenient way of doing this is by exposing the salt to a large dosage of γ-radiation; this method has the advantage that the heating is quite uniform throughout the sample in the high temperature region and that the rate of heat influx is constant. It can then be shown that for a constant rate of heating the susceptibility decreases linearly with time of heating if $C^{\circledast}$ is indeed proportional to $T^{\circledast -2}$.†

---

*This can be shown by a simple thermodynamic argument.

$$\text{Let } C^{\circledast}/R = (1/R)\, dQ/d\,T^{\circledast} = (T/R)\, dS/d\,T^{\circledast} .$$

If it is found that $S/R = \ln (2J+1) - bT^{\circledast -2}$, then $(1/R)\, dS/dT^{\circledast} = 2bT^{\circledast -3}$ and $C^{\circledast} = 2bTT^{\circledast -3}$. Therefore $C^{\circledast} = 2bT^{\circledast -2}$ only when $T = T^{\circledast}$.

---

† $\chi = C'_M/T^{\circledast} + d$

$$d\chi/dt = (d\chi/dT^{\circledast})dT^{\circledast}/dt = -(C'_M/T^{\circledast 2})dT^{\circledast}/dt \quad \text{where } t = \text{time}$$

now $C^{\circledast} = dQ/dT^{\circledast} = 2bT^{\circledast -2}$

then $d\chi/dt = -(C'_M C^{\circledast}/2b)dT^{\circledast}/dt = (-C'_M/2b)dQ/dt = \text{constant}$

Q.E.D.

The temperature region where $\chi(t)$ is linear [here t denotes time] can be established by demagnetizing from various values of H/T and measuring the initial susceptibility just after demagnetization and the amount of time required to warm the sample to some reference susceptibility at a high temperature. In this way a χ - Q curve, can be constructed. By selecting the region in $T^{\circledast}$ where $\chi(t)$ is linear and S/R is proportional to $T^{\circledast\,-2}$, one can easily determine the constant b in Eq. (II.B.6). Thus the thermodynamic temperature is known for all values of S/R in the Curie law region. From footnote (†) we also see that $dQ/dt = -(d\chi/dt)(2b/C'_M)$ where dQ/dt is the heat absorbed by the crystal per unit time, $d\chi/dt$ the slope in the linear region, and b and C'_M known constants. Thus dQ/dt is determined in the absolute sense by a measurement of $d\chi/dt$.

For the lowest temperatures the thermodynamic temperature is obtained by constructing a Q-S curve. The sample is demagnetized from various H/T values, which determine the entropy, and measuring the time of γ-ray exposure necessary to warm the crystal to some reference temperature. As was shown above, time is directly convertible to heat input. Corrections for normal heat leak and for the fact that the sample cannot be instantaneously exposed to the γ-ray source must be made. The absolute temperature for any value of S is then determined by the slope of the Q-S curve: $T = dQ/dS$. Generally an analytic function is fitted through the data points and the differentiation performed on the chosen function. It is obvious that the slope depends critically on the chosen function and that great care must be taken in curve fitting. This comprises the greatest single difficulty in this type of determination.

2. Statistical Measurement of T

The second method of determining absolute temperatures is the statistical method, which was used in this research. The thermodynamic foundation for this method was given in Eqs. (II.B.2) and (II.B.3) which define the Boltzmann probability, P_j. For P_j to be a useful thermometric parameter, the separation of the energy levels must be of the order of kT; i.e. $E_j - E_{j'} \approx kT$. Because we are interested in measuring temperatures below 0.01°K, the only suitable energy levels are the hyperfine levels of an ionic-nuclear system in the paramagnetic salt. The method which we selected was to study the nuclear orientation of radioactive nuclei grown substitutionally into the paramagnetic crystal. The theory of nuclear orientation and its use in temperature measurement will be discussed in the next section.

C. Thermal Equilibrium Nuclear Orientation

An ensemble of nuclei is said to be oriented if the various nuclear magnetic substates are not equally populated. The nuclei will populate the available levels according to a Boltzmann distribution as described in Eq. (II.B.3). If the nuclei are radioactive and have spin greater than 1/2, then the spatial distribution of emitted radiation will be anisotropic and the degree of anisotropy dependent on the absolute temperature and the magnitude of the electron-nuclear interaction. The subject of nuclear orientation has been thoroughly reviewed,[24-31] and so only a summary of the pertinent results will be presented.

If we confine ourselves to γ-radiation and consider only the case where there is cylindrical symmetry about a quantization axis, then the angular distribution of radiation from oriented nuclei can be written as

$$W(\theta,T) = 1 + \sum B_k(T)\, U_k\, F_k\, g_k\, P_k\,(\cos\theta)\ . \qquad \text{(II.C.1)}$$

The summation runs from 2 to 2L or 2I whichever is lesser where L is the multipolarity of the transition of interest and I is the spin of the level which is oriented. In (II.C.1) θ is the angle (in the plane defined by the detector and the axis of quantization) between the axis of quantization and the direction of emission of the photon. $P_k(\cos\theta)$ is a Legendre polynomial of degree k, and g_k is a factor correcting for the finite solid angle subtended by the detector. U_k and F_k are angular momentum factors, and $B_k(T)$ contains all the temperature information in the problem. These factors will be discussed in more detail below.

1. $\underline{U_k}$

In a series of nuclear transitions

$$I_o \xrightarrow{L_1} I_1 \rightarrow \ \cdots\ I_{n-1} \xrightarrow{L_n} I_n \rightarrow I_{n+1}$$

let us designate the observed transition as $I_{n-1} \xrightarrow{L_n} I_n$ and the state which is originally oriented I_o. If the lifetimes of the intermediate states are short, ($\lesssim 10^{-10}$ sec), and all the intermediate spins are greater than 1/2 then the orientation will be preserved through

the cascade. Because of conservation of angular momentum the magnitude of the angular anisotropy (although not the angular dependence itself) will be modified. If we consider a particular unobserved transition $I_{m-1} \xrightarrow{L_m} I_m$, then the modification factor is $U_k^{(m)}$ and is given by

$$U_k^{(m)} = [(2I_{m-1}+1)(2I_m+1)]^{1/2}(-1)^{I_{m-1}+I_m-L_m} \times W(I_{m-1},I_{m-1},I_m,I_m;kL_m) \tag{II.C.2}$$

where $W(I_{m-1},I_{m-1},I_m,I_m;k,L_m)$ is a Racah coefficient. If the transition is of mixed multipolarity and the mixing ratio is $\delta = \frac{\langle\| L+1 \|\rangle}{\langle\| L \|\rangle}$, then

$$U_k^{(m)} = \frac{U_k^{(m)}(L) + \delta^2 U_k^{(m)}(L+1)}{1+\delta^2} \tag{II.C.3}$$

For a series of preceding transitions,

$$U_k = U_k^{(1)} U_k^{(2)} U_k^{(3)} \text{------} U_k^{(n-1)} .$$

These transitions may be either β-decay or γ-emission and if the angular momentum properties of the transition are known, the U_k may be calculated exactly.

2. $\underline{F_k}$

This factor is an angular momentum coefficient concerned with the observed transition. The generalized F coefficient involves four angular momenta and may be written as:

$$F_k(LL'j_1j) = (-1)^{j_1-j-1}[(2L+1)(2L'+1)(2j+1)]^{1/2}$$

$$\times C_{1-1}^{LL'k} \; W(jjLL';kj_1) \tag{II.C.4}$$

where C is a Clebsch-Gordan coefficient and W is a Racah coefficient. In the notation of the previous paragraph the transition of interest is $I_{n-1} \xrightarrow{L_n} I_n$ where I_{n-1} corresponds to j, I_n to j_1, and L_n to $L = L'$ in Eq. (II.C.4). If the transition is not pure but contains an admixture δ^2 of $L+1$ multipolarity then F_k is written as

$$F_k = \frac{[F_k(L_n,I_n,I_{n-1}) + \delta^2 F_k(L_n+1,I_n,I_{n-1}) + 2\delta F_k(L_n,L_n+1,I_n,I_{n-1})]}{1+\delta^2} \tag{II.C.5}$$

The $F_k(LL'j_1j)$ have been tabulated by Ferentz and Rosenzweig.[32]

3. $\underline{B_k}$

The B_k are the orientation parameters and contain all the temperature and solid state physics information. The most general expression for the B_k may be written as:

$$B_k = (2I+1)^{1/2} \sum_{j=1}^{R} P(E_j) \left[\sum_{i=1}^{R} (A_i^j)^2 (-1)^{I-m_i} C^{IIk}_{m_i -m_i} \right] \tag{II.C.6}$$

$$P(E_j) = \frac{\exp(-E_j/kT)}{\sum_n \exp(-E_n/kT)} \quad . \tag{II.C.7}$$

In these formulae the following definitions apply:

I : nuclear spin of the oriented nucleus

E_j : the j-th eigenvalue of the electron-nuclear interaction Hamiltonian

A_i^j : the i-th element of the j-th eigenvector of the interaction Hamiltonian

R : $R = (2I+1)(2S+1)$ where S is the electron spin

C : a Clebsch-Gordan coefficient

$P(E_j)$: the population of the level E_j

m_i : eigenvalue of I_z

If the eigenvectors and eigenvalues of the electron-nuclear Hamiltonian can be determined, then the temperature dependence of B_k and therefore of $W(\theta,T)$ can be calculated. For an axially symmetric system (where z represents the quantization axis) Abragam and Pryce[33] have shown that the electron-nuclear interaction can be treated in terms of the phenomenological spin-Hamiltonian:

$$\mathcal{H} = g_{\parallel}\,\beta\,H_z\,S_z + g_{\perp}\,\beta(H_x\,S_x + H_y\,S_y) + A\,S_z\,I_z + B(S_x\,I_x + S_y\,I_y)$$

$$+ D[S_z^{\,2} - \tfrac{1}{3}\,S(S+1)] + P[I_z^{\,2} - \tfrac{1}{3}\,I(I+1)] - \vec{\mu}_I \cdot \vec{H} \quad . \qquad \text{(II.C.8)}$$

For a paramagnetic crystal, S in Eq. (II.C.8) is an effective spin and will – in general – not be equal to the actual electronic spin of the paramagnetic ion. S is defined by setting $2S+1$ equal to the number of states in the lowest lying group of levels. These states are usually complicated mixtures of spin and orbital states resulting from the interaction between the crystalline electric field and the paramagnetic ion. Generally these states are well separated in energy from the next group of states. The first two terms in Eq. (II.C.8) describe the interaction of the effective spin with an external magnetic field. The terms in A and B represent the hyperfine interaction between the paramagnetic ion and its nucleus while the term in D describes the splitting of the

levels of the effective spin S by the crystalline field. The final two terms represent the nuclear quadrupole and nuclear Zeeman interactions respectively.

At this point it is necessary to distinguish between two different types of orientation: polarization and alignment. The former occurs when there is a non-zero first moment of nuclear magnetization and requires a magnetic field (either external or internal) of well-defined direction. In the latter the first moment of nuclear magnetization is zero and the second moment is non-zero. One may think of polarization as when a majority of the nuclear spins are pointing in one direction and alignment as when the nuclear spins are oriented both parallel and anti-parallel (in equal proportions) with respect to a direction of quantization. In the next few paragraphs the three most important types of orientation will be discussed with reference to Eq. (II.C.8). An excellent discussion of these methods is given by Daniels in Chapter II of Reference 26.

4. <u>The "Universal" Method</u>

$$\mathcal{H} = -\vec{\mu}_I \cdot \vec{H} \quad . \qquad \text{(II.C.9)}$$

This may be subdivided into two separate topics: brute force polarization and polarization in ferromagnets. The first is simply the direct interaction of an external magnetic field with the nuclear moment μ_I and requires fields of 10^5 - 10^6 Oe and temperatures of about 0.01°K. Because of the difficulty of producing such large fields in the laboratory this technique has only been used for several particularly

favorable cases. Orientation in the ferromagnets Fe, Co, and Ni is a much more general case and has been used extensively since the discovery by Samoilov et al.[34] that large magnetic fields are present at impurity nuclei in ferromagnetic metals. Fields larger than 10^6 Oe have been measured, and with temperatures of 0.01°K obtainable by adiabatic demagnetization and contact cooling, many nuclei have been oriented. With the recent development[35,36] of the combined nuclear magnetic resonance-nuclear orientation technique, the universal method has yielded accurate information about nuclear magnetic moments, hyperfine magnetic fields, and nuclear spin-lattice relaxation times at very low temperatures.

5. Electric Quadrupole Alignment

$$\mathcal{H} = P[I_z^2 - \frac{1}{3} I(I+1)] = e\,Q\,q \left[\frac{3I_z^2 - I(I+1)}{4I(2I-1)} \right]. \qquad \text{(II.C.10)}$$

If a nucleus with an electric quadrupole moment Q experiences an electric field gradient q, then the nucleus will align parallel to the direction of the field gradient as first suggested by Pound.[37] It has been shown by Sternheimer[38] that closed electronic shells will be deformed by an electric field gradient, which may be produced either by the valence electrons of the atom itself or by the crystalline field of the lattice. This deformation can amplify the field gradient at the nucleus by as much as a factor of 100 in the case where the lattice is the source of the field gradient. Using the nuclear alignment technique, Blok and Shirley[39,40] have systematically studied Sternheimer anti-shielding effects for several rare earth ions in the cerium magnesium

nitrate and neodymium ethyl sulfate lattices. Field gradients capable of orienting nuclei can also be produced by chemical bonding, but the "Sternheimer" technique appears to be the most general and practical method for quadrupole alignment.

6. Magnetic Hyperfine Alignment or Polarization

$$\mathcal{H} = g_{\parallel}\, \beta\, H_z\, S_z + g_{\perp}\, \beta(H_x\, S_x + H_y\, S_y) + A\, S_z\, I_z + B(S_x\, I_x + S_y\, I_y)\ . \tag{II.C.11}$$

In this method we are specifically concerned with paramagnetic ions. Let us first consider the zero external field case – the so-called Bleaney[41] method. Large magnetic fields ($\sim 10^5$ Oe) are produced at the nuclei of paramagnetic ions by the d or f electrons responsible for the paramagnetism. The crystalline electric fields, which we assume to be axially symmetric, interact directly with the orbital angular momenta of the electrons and indirectly with the spin angular momenta through the spin-orbit interaction. Thus the symmetry of the magnetic field which the nucleus sees is dictated by the crystal field symmetry, and the nuclei will align with respect to the symmetry axis of the crystal field. The field at the nucleus results from the orbital motion of the electrons and from an electronic spin dipolar interaction. If we consider only systems with Kramers' degeneracy, A and B in Eq. (II.C.11) are the matrix elements: $4\beta\, \beta_N\, g_I\, \overline{(1/r^3)}\langle +|N_z|+\rangle$ and $4\beta\, \beta_N\, g_I\, \overline{(1/r^3)}\langle +|N_x|-\rangle$ respectively. Here β_N is the nuclear magneton, g_I the nuclear g-factor and $\underline{N}$ is the operator

$$\sum_i \left\{ \underline{\ell}_i - \underline{s}_i + \frac{3(\underline{r}_i \cdot \underline{s}_i)r_i}{r_i^2} \right\}$$ where $\underline{\ell}_i$ and $\underline{s}_i$ are electronic orbital and spin angular momentum operators. The $|+\rangle$ and $|-\rangle$ refer to the two members of the Kramers' doublet. If $A > 0$ and $B = 0$, the hyperfine energy level scheme consists of $2I+1$ equally spaced levels characterized by $|M_S, m_I\rangle$. For $S = 1/2$ the lowest level is doubly degenerate and corresponds to $|M_S = \pm 1/2, m_I = \pm I\rangle$. At low temperatures the nuclei will preferentially populate this level, and consequently the direction of orientation will be parallel to the quantization axis. For $A = B$ there are only two levels, and no nuclear orientation is produced at low temperatures. If $B \neq 0$ and $A = 0$, the hyperfine level scheme consists of $2I+2$ unequally spaced levels characterized by linear combinations of $|\pm M_S, \pm m_I\rangle$. For $S = 1/2$ and half integral I the lowest level corresponds to

$1/\sqrt{2}\ [|M_S = 1/2, m_I = -1/2\rangle - |-1/2, 1/2\rangle]$. At low temperatures the nuclei will align by populating this level preferentially. Phenomenologically, one may think of the nuclei as orienting in a plane perpendicular to the quantization axis, and consequently this is known as planar alignment.

When a small magnetic field (< 1000 Oe) is applied to the crystal, the electron spins will polarize and will in turn polarize the nuclei. This is known as Gorter[42]-Rose[43] polarization. The Kramers' degeneracy of the hyperfine levels is completely removed, but the wave functions are complicated linear combinations of the basis states. The primary disadvantage of this method is that the application of the magnetic field will — in general — warm the crystal.

7. Measurement of Absolute Temperature by Nuclear Orientation

Shirley and co-workers[3,44] have shown that thermodynamic temperature scales can be established for paramagnetic crystals by nuclear orientation. They determined T-S relations for cerium magnesium nitrate[3] above 0.002°K and for neodymium ethyl sulfate[44] between 1°K and 0.01°K using the techniques to be described in the following paragraphs.

In a nuclear orientation measurement of temperature the radioisotope is the thermometer, and as with any thermometer certain conditions must be satisfied. In general the thermometer must be in good thermal contact with the system to be measured; it must be sensitive to thermal changes in the system; and the relation between its thermometric parameter and temperature must be known. The first condition requires that the nuclear spin-electron spin relaxation time be short. An obvious first choice for a salt like CMN would be a Ce isotope. The second condition requires a temperature-sensitive angular distribution of radiation which does not saturate at even the lowest temperatures. The final condition demands that all the relevant U_k, F_k, and $B_k(T)$ are known.

Knowledge of $B_k(T)$ implies a knowledge of the spin Hamiltonian parameters. In general, however, only the form of the Hamiltonian is known by resonance work on stable isotopes of the atom in question, and the parameters must be determined separately. If an S-T or a $T^{\circledast}$ - T relation is known for the paramagnetic salt over part of the temperature range, then the parameters of the spin Hamiltonian can be determined as

follows. The sample is demagnetized to various known temperatures, and $W(\theta = 0)$ is measured at each temperature. The angle $\theta = 0$ is chosen because $W(\theta)$ assumes its maximum values for this angle. The W, T data are then fitted to Eq. (II.C.1), and the values of the spin Hamiltonian parameters in $B_k(T)$ are varied until the best fit is obtained. When the values of the parameters are known, $W(\theta, T)$ can be calculated for any value of T and θ.

The crystal is then demagnetized from known values of H/T (or entropy) to the low temperature, and $W(\theta = 0)$ is measured. When the $W(\theta)$'s are converted into temperature, an entropy-temperature relation is established. Unfortunately for each (S, T) point a separate demagnetization is required since the entropy is known only just after demagnetization. Irreversible heating effects due to natural heat leak and radioactive heating will change the entropy from the measured value over a period of time. It usually turns out however, that the sample remains isothermal sufficiently long to acquire resonable counting statistics in $W(\theta)$. If this is not the case, then warm-up corrections must be applied.

The major difficulties in this type of experiment arise from uncertainties in calculating $W(\theta)$ (e.g. background corrections). The details of the experimental technique and the data analysis will be discussed in the next two sections, and these difficulties will be dealt with then.

III. EXPERIMENTAL

In this section the important details of the experimental technique and apparatus will be discussed. Such topics as the ^{3}He refrigeration system, the production and measurement of the magnetic fields, and the gamma ray detection system will be emphasized. The section will be concluded by a chronology of an actual experimental situation.

A. ^{3}He Refrigerator

All the nuclear orientation experiments were performed in a ^{3}He refrigerator manufactored by Cryonetics Corporation[45] (Model 302) and substantially modified in this laboratory. The apparatus is a continuously operating refrigerator of the type described by Ambler and Dove[46] and will be discussed briefly. A diagram of the apparatus is shown in Fig. III.1, and a block diagram of the circulation system is depicted in Fig. III.2.

The warm incoming ^{3}He gas is partially condensed in the input capillary, which is soldered to the 1°K ^{4}He bath. The liquid-gas mixture flows downward to a porous plug of sintered stainless steel (the frit)[47] which acts as a flow impedance for the ^{3}He. The frit is at a temperature close to that of the ^{3}He bath, and consequently additional condensation of the ^{3}He gas is achieved at this point. The ^{3}He flows from the frit into the ^{3}He bath where refrigeration is obtained by pumping off the vapor above the ^{3}He liquid. The bath container is high-purity copper and is hard soldered to a stainless steel tube which is connected to the pumping system. Several vertical copper rods are imbedded in the

Figure III.1. ^{3}He Refrigerator.

The liquid N_2 dewar is not shown.

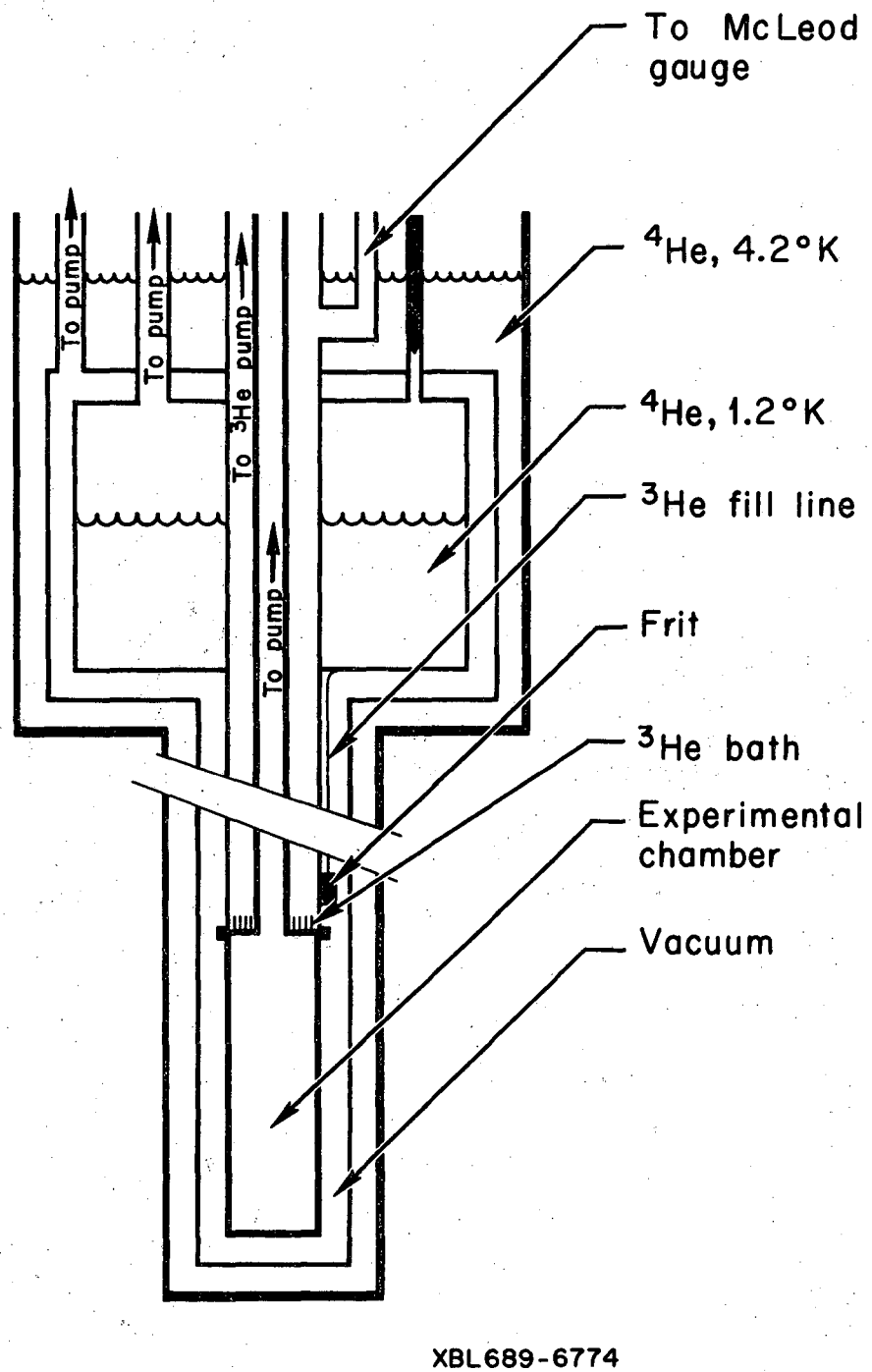

XBL689-6774

Fig. III.1.

Figure III.2. ^{3}He Circulation System.

The arrows indicate the direction of flow of the ^{3}He. The symbols in the drawing refer to the following: F (frit); DP (diffusion pump); MP (mechanical pump); EC (to experimental chamber); S (^{3}He storage tank); PG (Phillips gauge); HG (Hastings-Raydist thermocouple gauge); MG (McLeod gauge); $\boxed{X}$ (valves). The valve numbers refer to the following: 1. (fine circulation); 2. (coarse circulation); 3. (flow throttle); 4,5,6. (isolation valves); 7. (cryostat bypass); 8. (exchange gas admit).

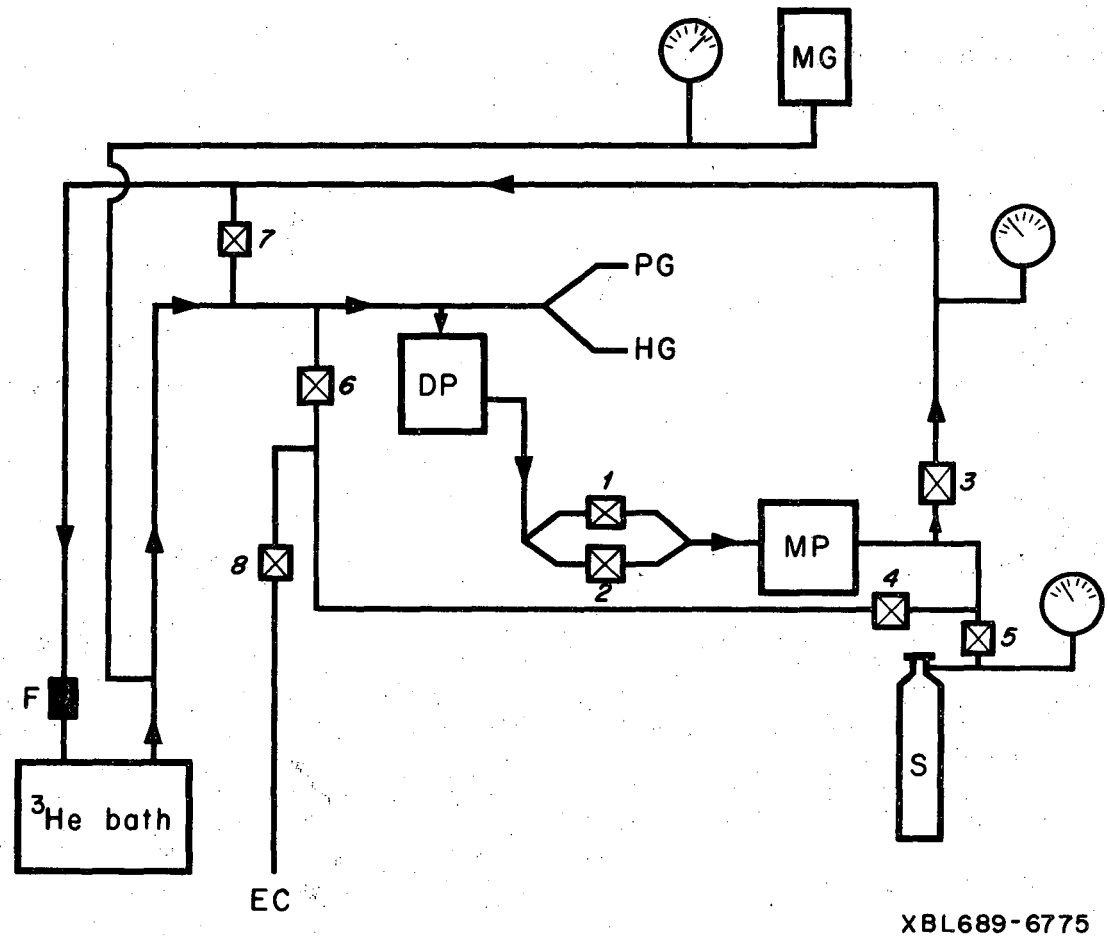

Fig. III.2.

bottom of the ^{3}He chamber to insure homogeneity in temperature and density throughout the liquid. The total volume of liquid ^{3}He in the bath at any one time is less than 10 cc.

The temperature of the ^{3}He bath is regulated by the speed of the pumping system. The minimum temperature of 0.3°K is attained with a Consolidated Vacuum Corporation[48] PMCS-2B two inch diameter oil diffusion pump (105 l/sec at 10^{-3}torr) in series with a Welch Duo-Seal 1402 KBG[49] mechanical pump (5 cubic per minute). A temperature of 0.5°K is achieved with the mechanical pump alone. Intermediate temperatures in the ranges 0.3° - 0.5°K and 0.5° - 1°K are obtained by throttling valves 1, 2 and 3 (c.f. Fig. III.2). The mechanical pump has been hermetically sealed and provided with an oil seal on the drive shaft to prevent loss of the ^{3}He. The ^{3}He exhaust gas from the mechanical pump may be either returned to the refrigeration system or shunted to a 2.5 liter storage cylinder. Slightly lower temperatures in the ^{3}He bath may be achieved if the ^{3}He is not recirculated.

B. Vapor Pressure Measurements

As was discussed in Section II.A the entropy removed during the magnetization is a function of the temperature of the paramagnetic crystal. In this work the temperature of the crystal was assumed to be equal to the temperature of the ^{3}He bath. The latter was determined by vapor pressure measurements. The precautions taken to insure that the paramagnetic salt was at the same temperature as the ^{3}He bath will be discussed in Sections III.C and III.F.

The vapor pressure of the ^{3}He bath was measured with a Consolidated Vacuum Corporation[48] GM-100A McLeod gauge. This gauge covers a pressure range from 10^{-5}torr to 10 torr and has a manufacturer's quoted accuracy of ±1.1% of the indicated pressure on the 0-10 torr scale, ±1.2% on the 0-1 torr scale, and ±1.5% on the 0-0.1 torr scale. The pressure may be read to $\pm 10^{-3}$torr at 0.2 torr and to $\pm 10^{-4}$torr for pressures less than 10^{-2}torr. The gauge is connected to a liquid nitrogen trap and in turn to the ^{3}He system through a 0.58cm i.d. stainless steel tube tapped into the ^{3}He pumping line just above the 1.1°K ^{4}He bath (c.f. Fig. III.1).

The vapor pressures measured in this way must be corrected for thermomolecular pressure differences resulting from the temperature difference between the gauge and the ^{3}He bath. This correction was obtained from the results of Roberts and Sydoriak[50] and is plotted in Fig. III.3. Recent measurements by Watkins et al.[51] and by Freddi and Modena[52] are in disagreement with the results of Roberts and Sydoriak. However, according to Watkins et al., the temperature determined from ^{3}He vapor pressure measurements with their pressure correction would be decreased by less than 0.005°K from the temperature determined with the Roberts and Sydoriak correction. Because of the smallness of the difference it was neglected in this work. The temperature of the ^{3}He bath can then be determined from the ^{3}He vapor pressure with the 1962 ^{3}He vapor pressure-temperature scale.[53]

The pressure fluctuation in the ^{3}He bath during the magnetization (after the paramagnetic salt had come into equilibrium with the ^{3}He bath) was about $\pm 3 \times 10^{-3}$torr when the bath temperature was 0.5°K.

Figure III.3. Thermomolecular Pressure Correction.

R is the radius in cm of the sensing tube. P_W is the pressure in microns measured at the room temperature (23°C) McLeod gauge. P_C is the actual pressure in microns of the ^{3}He bath.

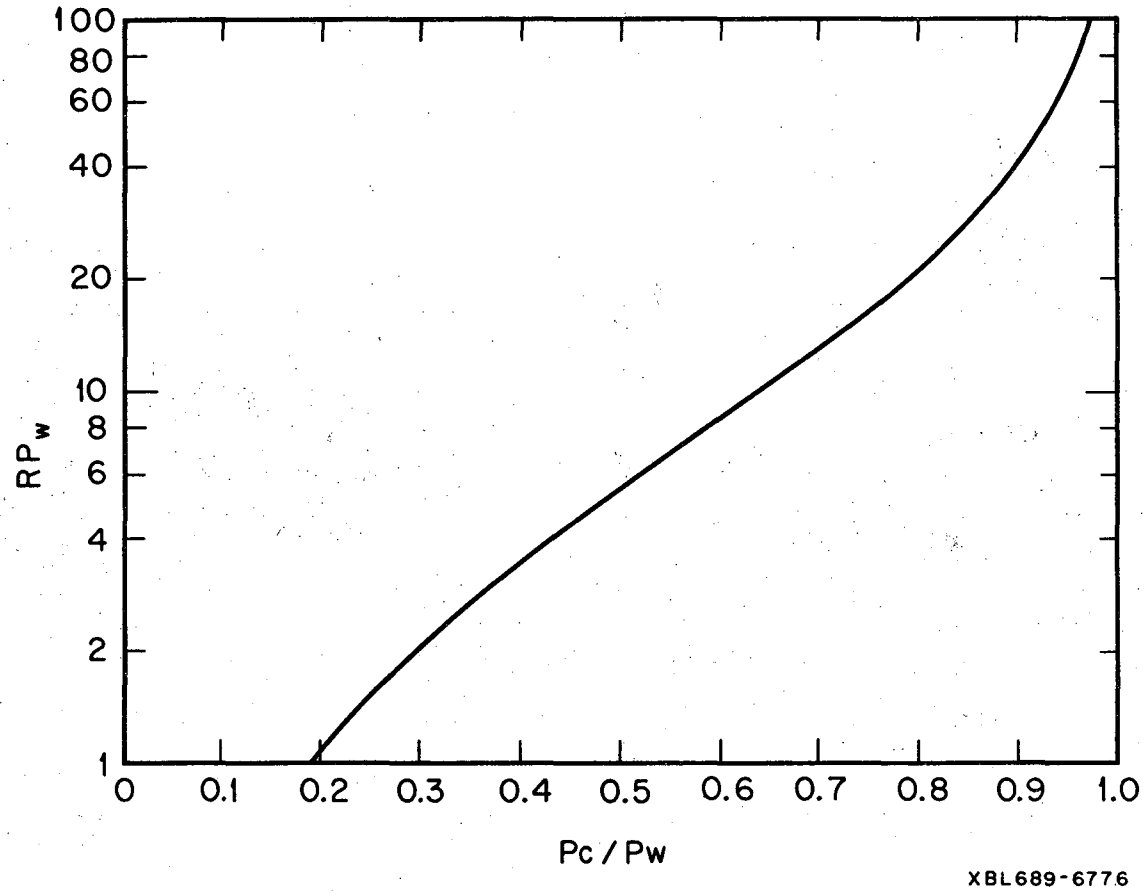
100
80
60
40
20
10
8
6
4
2
1
RPw
0
0.1
0.2
0.3
0.4
0.5
0.6
0.7
0.8
0.9
1.0
Pc / Pw
XBL689-6776

Fig. III.3.

This corresponds to a fluctuation of about 0.0015°K. At 0.3°K the bath pressure could be continuously monitored with a Phillips gauge (Model PHG-09).[48] No deviations larger than 2×10^{-4} torr (about 0.003°K) were observed.

C. The Experimental Chamber and its Contents

As has been discussed previously, it is essential for the measurement of entropy that the paramagnetic crystal attain thermal equilibrium with the ^{3}He bath during the magnetization. In addition the sample must be so positioned within the experimental chamber that any heat leak will have a small effect at the low temperatures. Early experiments in the developmental stage of this research indicated that great care was necessary to satisfy these requirements. In the course of time the following, rather elaborate arrangement was developed and was employed in all the experiments reported in this thesis.

The experimental chamber was a thin wall (0.010 inch) stainless steel right circular cylinder closed at the bottom and attached to the ^{3}He bath with Pb-Sn solder (c.f. Fig. III.1). Thermal contact between the sample and the bath was achieved by a small pressure (< 0.02 torr) of ^{3}He thermal exchange gas which could be both admitted and removed through the experimental chamber pumping tube. During the magnetization a considerable amount of heat was evolved, and it was discovered that the rate of heat exchange between the crystal and the ^{3}He bath was quite slow. This was primarily due to the fact that most of the surface area available to the ^{3}He exchange gas was stainless steel, which has a low

thermal conductivity at temperatures below 1°K. To overcome this difficulty and to insure a minimum heat leak at the lowest temperatures, the following "cage", which fitted snugly into the experimental chamber, was developed.

A diagram of the cage and its contents is shown in Fig. III.4. The various parts of the cage, denoted by the letters on the right side of the figure, are explained in the following discussion. The upper part of the cage was a hollow right circular cylinder (a) of OFHC copper, partially closed at the top. Three equally spaced vertical brass ribs (d) were hard soldered at the top to the copper cylinder and at the bottom to a brass ring (m). A horizontal circular brass rib (not shown) connecting the three vertical ribs was located at about the midpoint of the cage and added extra stability.

Tungsten rods (c,n) were hard soldered into both the top and the bottom of the cage, and 3mm thick pyrex rods (e) were joined to the tungsten rods by melting. The pyrex rods extended downward and upward to pyrex vessels (g,k) containing chromium potassium alum-glycerine slurries. This mixture was capable of cooling to 0.01°K by adiabatic demagnetization and prevented any large heat transfer through the pyrex rod to the sample at the low temperatures. Compressed tablets of manganous ammonium sulfate (f,ℓ) capable of cooling to about 0.1°K were glued to the pyrex rod above slurry holder (g) and below slurry holder (k). These tablets served as efficient cryopumps for any ^{3}He exchange gas remaining during the demagnetization. The slurry holders were joined by 2mm pyrex rods (h), which formed a stirrup-like holder

Figure III.4. Experimental Cage.

The letters are explained in the text.

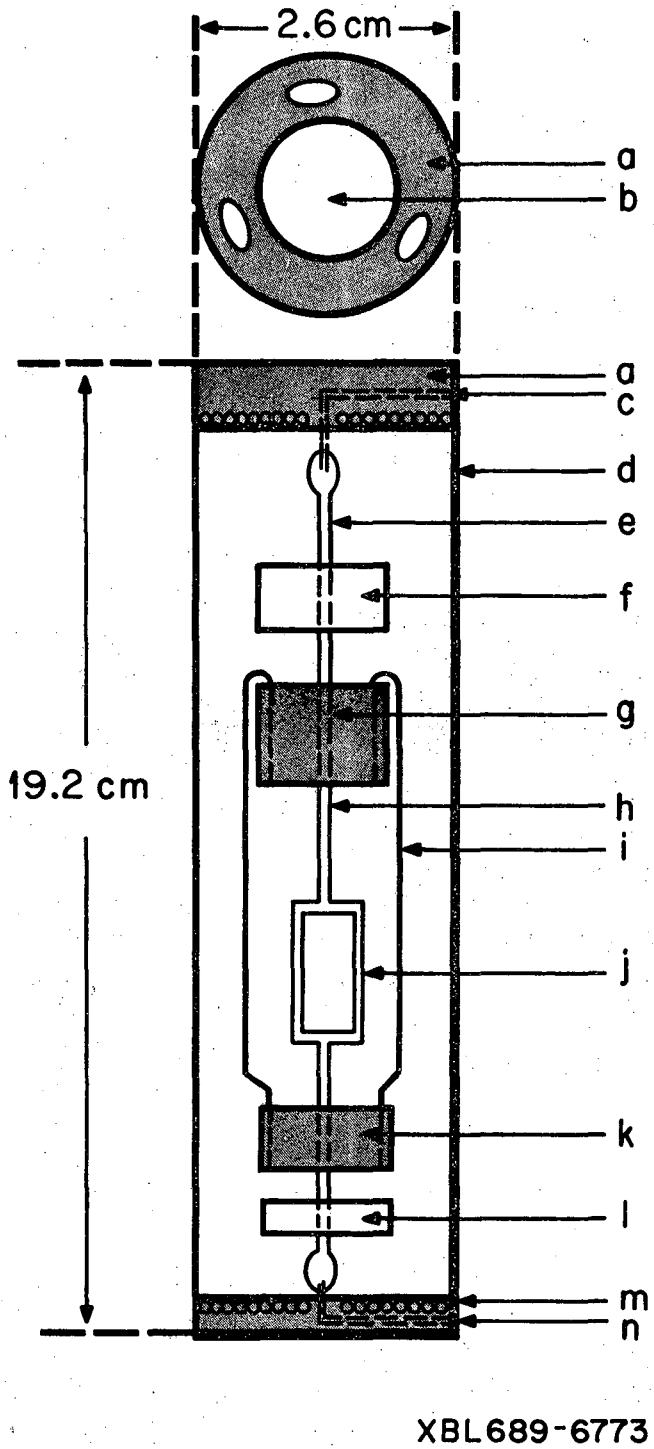

Fig. III.4.

(j) for the sample. When the sample was glued into the holder, it was prevented from undergoing any undesirable motion. Such motion might result either because of inhomogeneities in the magnetizing field which tend to pull the crystal toward the wall of the experimental chamber or because of room vibrations transmitted to the cryostat.

Two additional features of the cage deserve mention. First, two narrow, thin (0.005 inch) sheets (i) of high purity copper joined the upper and lower slurries and served as high surface area 0.01°K cryopumps for the ^{3}He exchange gas. The second feature was designed to promote more rapid thermal equilibrium between the paramagnetic crystals and the ^{3}He bath during the magnetization. Approximately 30 1/16-inch diameter holes were drilled in the bottom and the top of the cage, and six strands (about five feet in length) of formvar coated copper wire (AWG #30) were strung up and down the length of the cage. For the sake of clarity only the holes are shown in Fig. III.4. These wires were thermally anchored to the top of the cage by tightly winding each wire once around the copper cylinder (a). The cage was then bolted to the bottom of the ^{3}He bath, and both the cage and the wires were thermally anchored at the temperature of the bath. The wires thus presented a significant surface area of high thermal conductivity to the ^{3}He exchange gas and allowed thermal equilibrium with the ^{3}He bath to be reached in less than fifteen minutes. The hole (b) in the top of the cage provided access to the experimental chamber pumping tube.

D. Magnetic Field

Magnetic fields up to 21 kOe were produced across a 2-5/8 inch gap by a water cooled iron core solenoid with an iron yoke.[54] The magnet assembly was mounted on a carriage which could be rolled along a set of tracks in the laboratory. The power supply was capable of producing currents up to 300 A (60 KW) with a regulation of better than one part in 10^5 over the whole range. The current was determined by the voltage across a potentiometer and could be varied continuously from zero through the whole range. The potentiometer was driven by an appropriately geared electric motor, and thus the field could be raised and lowered automatically. At the operating speeds used the field was reduced from maximum to zero in about four minutes.

For the experiments of March 1967 and June 1967 a model 720 Rawson[55] rotating coil gaussmeter was used in conjunction with a model 203A George Associates[56] rotating coil gaussmeter. The former was a relatively crude instrument having a quoted accuracy of ±1% of the full scale reading which is equivalent to ±0.12 kOe for fields between 4 and 12 kOe and ±0.4 kOe for fields between 12 and 40 kOe. The reproducibility however, was much better, being ±0.05 kOe on the lower range and ±0.1 kOe on the upper range; this arises primarily from the uncertainty in aligning the probe with respect to the field direction. The linearity of the meter was found to be quite good below 20 kOe. Since the dewar was in the magnet during the experiment, the field could only be measured at the face of the pole piece and not at the location of the crystals. At the conclusion of the experiment the probe of the George

gaussmeter (accurate to about ± 10 Oe) was placed at the location of the crystals in the center of the gap and the Rawson probe at the point on the pole face where the experimental measurements had been made. The field was then re-measured with both meters for each current setting used in the experiment. A plot of the field values from the two meters for the runs of June 1967 is shown in Fig. III.5. A straight line was fitted through the points below 20 kOe by the least squares method and the experimental Rawson meter readings for each magnetization converted into "true" field values from the least squares coefficients. With this procedure the experimental error in a field measurement included a precision (not accuracy) error from the Rawson meter, the least squares error from the fit, and the ± 10 Oe from the George Associates meter.

Above 20 kOe the Rawson meter was no longer linear. All the measurements made in this field range were made at a magnetizing current of 275 A. The field was determined by taking the average of all the field readings from the George meter obtained during the calibration measurements at the end of each experiment. For the current equal to 275 A, the field was found to be 21.07 ± 0.02 kOe. Since the magnetic field is near its saturation value at this current, it is expected that this procedure gives a reliable measure of the field.

For all the remaining experiments a model 820 Rawson rotating coil gaussmeter with a quoted accuracy of ± 0.1% was used in conjunction with the George Associates meter. With the 820 Rawson meter the field is determined by balancing a bridge to give a null reading. The measurement procedure for these experiments was essentially the same as

Figure III.5. Magnetic Field Calibration for June 1967 Experiment.

H_G refers to readings from the George Associates gaussmeter and H_R to readings from the Rawson meter. The arrow indicates the point at 21 kOe which was not included in the fit to the data.

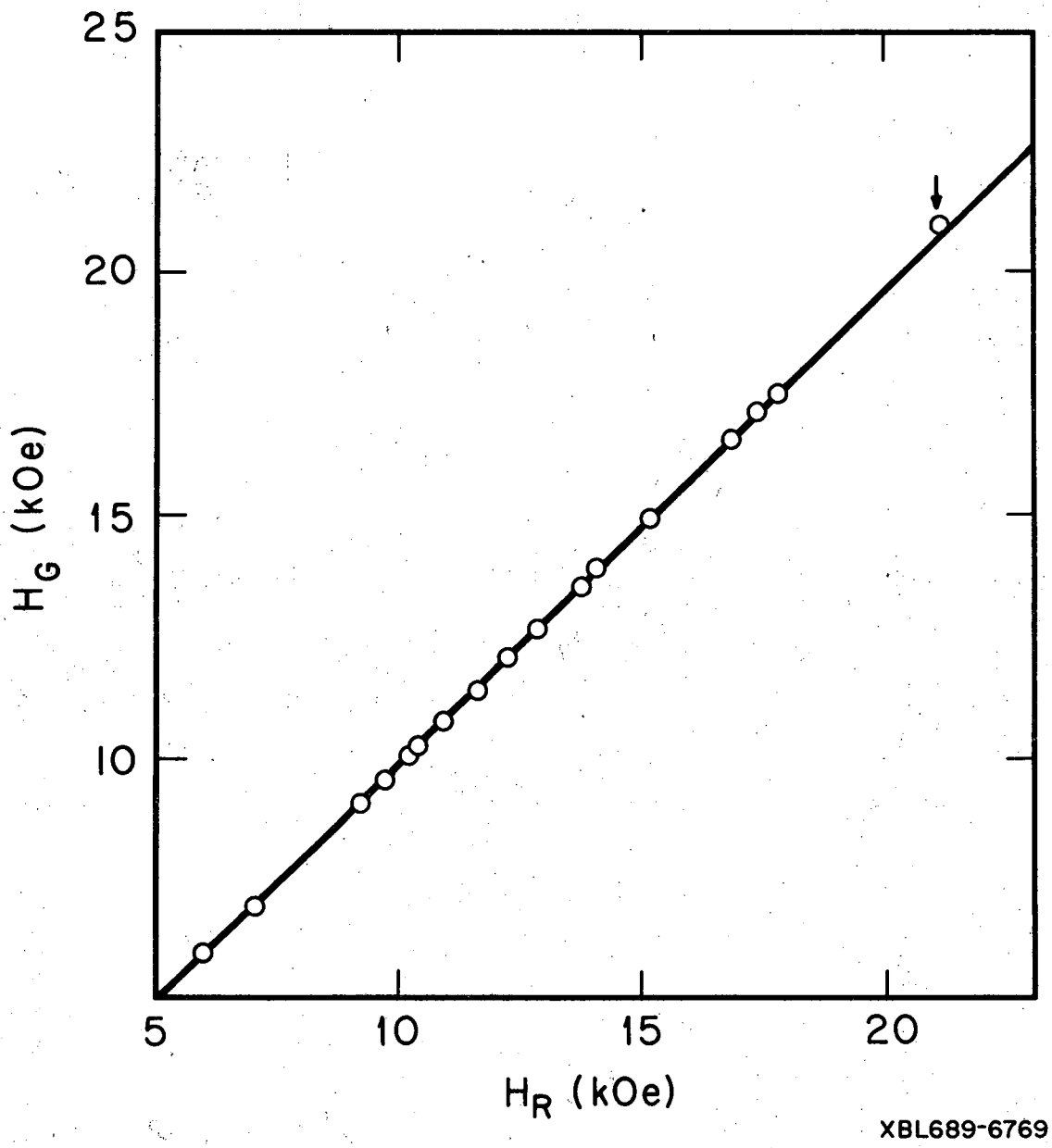

Fig. III.5.

described above except that the least squares fit was unnecessary because of the high accuracy of both meters. The difference between the two meter readings – a slowly varying function of field – was applied to the experimental field measurements with the Rawson meter to give "true" field values at the location of the crystals. The experimental error included ± 10 Oe from the George associates meter, ± 0.1% from the Rawson meter, and an additional ± 20 Oe from the Rawson meter because of uncertainty in aligning the probe properly with respect to the field direction.

E. Counting System

The γ-ray detection system used in this experiment consisted of two 3 × 3 inch NaI(Tl) scintillators, each with a resolution of about 7%. The scintillator and photomultiplier were purchased as a unit from the Harshaw Chemical Company.[57] The electronic amplification system consisted of standard transistorized units, and a block diagram is shown in Fig. III.6. The output from each biased amplifier was fed into a separate analogue to digital converter (ADC) which in turn transmitted the information to a PDP-7 computer[58] where the data was stored in two groups of 512 channels each.

The operation of the computer was controlled by a program called Twist[59] and employed several features worthy of mention. Any given "live time" counting period could be prescribed by a teletype command and the counting begun or terminated by a command delivered to a remote console at the experimental location. At the end of the prescribed live time the computer would store two identification records and one data record on magnetic tape, clear the data from memory, and recycle

Figure III.6. Counting System.

The components are: source (S); NaI(Tl) detector (D); photomultiplier (PM); preamplifier (PA); linear amplifier (LA); biased amplifier (BA); analogue to digital converter (ADC); teletype (TT); computer console (C); remote console (RC), magnetic tape unit (MT).

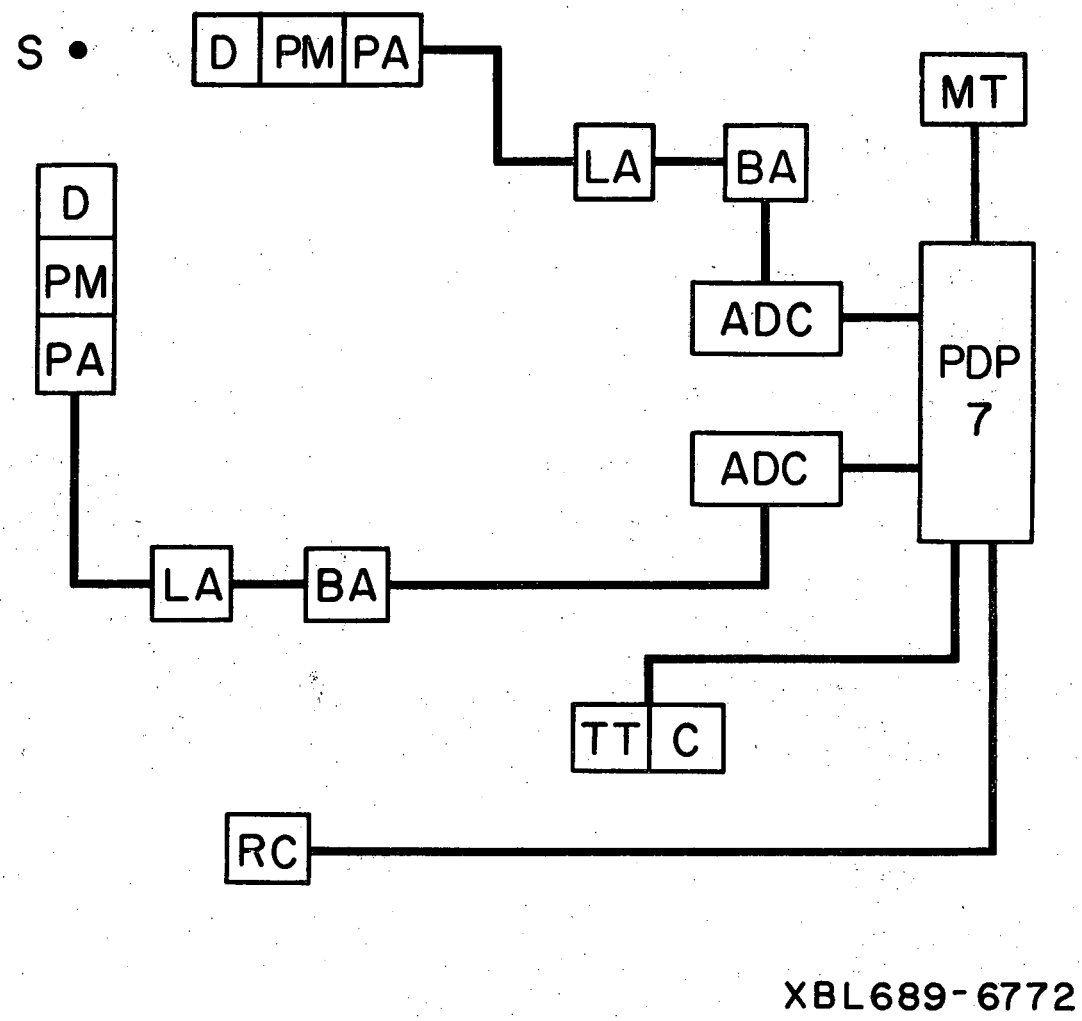

Fig. III.6.

until a stop command was received. The first identification record contained an alphanumeric title supplied by the experimenter through the teletype while the second identification record contained the prescribed live time, the actual live time, and the on and off times of the ADC's where time zero corresponds to the time when the computer was first turned on. The stop command writes an "end of file" on the magnetic tape, and a new identification and live time can be specified for the next file. Data can be recalled from the magnetic tape and analyzed at any time when the ADC's are not counting while more detailed analysis can be done in post-processing routines on the CDC-6600 computer.

F. Summary

To summarize this section a chronology of an experimental situation will be presented. After the crystal is mounted in the cryostat, it is precooled in stages to 77°K by liquid nitrogen, to 4.2°K by liquid ^{4}He, to 1.1°K by reducing the vapor pressure above the ^{4}He, and to temperatures below 1°K by ^{3}He refrigeration. During the liquid helium pre-cooling stages ^{3}He thermal exchange gas has been in the experimental chamber to equilibrate the paramagnetic crystals with their surroundings. At operating temperatures of about 0.5°K the exchange gas pressure is approximately 10-20 microns Hg while at 0.3°K the pressure is less than 5 microns Hg.

When the desired temperature is reached in the last pre-cooling stage, a magnetic field is applied to the crystals. The heat which is evolved is transferred to the ^{3}He bath by the exchange gas, and consequently the vapor pressure of the bath rises. The vapor pressure can

be monitored continuously either with a Hastings-Raydist Model VT-6 thermocouple gauge[60] or a Phillips[48] gauge and usually takes between 10-15 minutes to return to its equilibrium value. After an additional 15 minutes to insure thermal equilibrium between the crystals and the bath, the vapor pressure of the ^{3}He bath and the magnitude of the magnetic field are measured.

The exchange gas is pumped off by a Consolidated Vacuum Corporation[48] MCF-60 diffusion pump until the pressure is less than 10^{-5} torr at which point the magnetic field is turned slowly to zero field. When the zero field point is reached, a timer is started, the magnet rolled away, the counters rolled into position, and the counting begun. Several "cold" counts of 15 or 30 seconds live time duration are taken, and after approximately 5 minutes the crystals are warmed to the ambient temperature by admitting ^{3}He gas into the experimental chamber. A single "warm" count of 5 or 10 minutes duration is taken for normalization purposes. At the conclusion of the warm count the crystals are remagnetized and the process repeated until sufficient data are acquired.

IV. THE CERIUM MAGNESIUM NITRATE TEMPERATURE SCALE

This section is divided into five main parts: a summary of the properties of CMN and ^{137m}Ce, sample preparation, data reduction, the presentation of the results, and discussion. The first part of this section is devoted to a brief review of the electric and magnetic properties of CMN and the decay properties of ^{137m}Ce which will be relevant to the subsequent discussion.

A. Physical Properties of CMN and ^{137m}Ce

1. Crystal Structure

The crystal structure of CMN has been investigated by Zalkin *et al.*[61] using the x-ray diffraction technique. Their measurements indicated that the site symmetry for the Ce^{+3} ions is C_{3v} if only Ce and Mg atoms are considered. The nearest Ce neighbors (to a Ce) are three at 8.56 Å and three at 8.59 Å while the nearest Mg neighbors (to a Ce) are one at 6.17 Å, three each at 6.36 Å, 6.98 Å, and 8.31 Å, and one at 8.64 Å. The O atoms of the nitrate ions, however, are actually the nearest neighbors to the Ce atoms and are located at the twelve corners of an irregular icosahedron at an average distance of 2.64 Å. Thus the symmetry of the Ce^{+3} environment is not rigorously C_{3v} but is lowered to C_{3i}. In addition they found two types of Mg atoms (C_3 and C_{3i} symmetries) and confirmed the paramagnetic resonance results[62] which showed octahedral hydration of the Mg atoms. The remaining six waters of hydration are distant from the Ce atoms as was found by nuclear magnetic resonance.[63] Zalkin *et al.* concluded that the

most concise indication of the Ce and Mg coordination and the role of the waters is given in the formulation:

$$[Mg(H_2O)_6]_3[Ce(NO_3)_6]_2 \cdot 6H_2O \ .$$

2. Electric and Magnetic Properties

Ce^{+3} has a single 4f electron corresponding to a ^2F term which is split by the spin-orbit interaction into $^2F_{5/2}$ and $^2F_{7/2}$ terms. In the free ion the $^2F_{5/2}$ level is 2250 cm^{-1} below the $^2F_{7/2}$ level.[64] The crystalline electric field of the double nitrate lattice splits the $^2F_{5/2}$ level into three Kramers' doublets, and some important properties of these doublets are listed in Tables IV.1 and IV.2. In Table IV.1 Δ_{12}/k and Δ_{13}/k are the crystalline field splittings between the first and the second doublets and between the first and the third doublets respectively. In Table IV.2 $g_\perp$ refers to the direction perpendicular to the symmetry axis of the crystal, and $g_\parallel$ refers to the parallel direction. The measurements cited were performed on either pure CMN or Ce^{+3} in isomorphous, diamagnetic lanthanum magnesium nitrate, and the close agreement among the various values suggests that there is no substantial difference in the crystal field properties between the concentrated and dilute salts. For this research we have chosen $g_\perp = 1.84$ for the concentrated salt.

The crystal field properties of CMN have been investigated in detail by Judd[74] and by Leask et al.[65] The latter analyzed their susceptibility data in terms of a crystalline field of C_{3v} symmetry and showed that the ground Kramers doublet was primarily

Table IV.1. Crystal field splittings.

$\Delta_{1/2}/k\,°K$	$\Delta_{13}/k\,°K$	% Ce^{+3}	Ref.	Type of Measurement
37.6 ± 2.5	83.8	100	65	susceptibility
33.1	142.8	100	66	susceptibility
43	300 ± 50	100	67	susceptibility
36.25 ± 0.4		100	68	far infra-red spectroscopy
34		100	69	Casimir-du Pré relaxation
34		0.2	70	spin-echo relaxation
34		2 and 0.2	71	paramagnetic resonance relaxation

Table IV.2. Magnetic properties of ground doublet.

$g_{\perp}$	$g_{\parallel}$	$\%Ce^{+3}$	Ref.	Type of Measurement
1.84±.01	0.25	100	72	Electron Spin Resonance (ESR)
1.8264±.0013	0.032±.068	dilute	71	ESR
	<.03	100	63	Rotational Cooling
1.832	0.05±.05	100	65	Susceptibility
1.830±.003		2	73	ESR
1.838±.002		100	73	ESR

$|J = 5/2, J_z = \pm 1/2\rangle$ with an admixture of $|5/2, \mp 5/2\rangle$ and $|7/2, \pm 7/2\rangle$. Thus J is rigorously not a good quantum number for Ce^{+3} in CMN. In addition they found "anomalously" large values for the coefficients A_6^3 and A_6^6 in the crystalline field expansion and suggested that the simple crystal field model may not be strictly valid for CMN. Since the correct symmetry for the Ce^{+3} ion is C_{3i} - not C_{3v}, the interpretation of their data in terms of crystal field parameters will certainly be affected. For example, the following equalities are valid for C_{3v} symmetry but not for C_{3i}: $A_4^3 = A_4^{-3}$, $A_6^3 = A_6^{-3}$, and $A_6^6 = A_6^{-6}$. Interpretation of their susceptibility data in terms of C_{3i} symmetry is therefore highly desirable before drawing any conclusions about the validity of the crystal field model for CMN.

While this thesis was being written, the results of high field magnetization measurements on CMN were reported by Williamson and Cape.[75] They claimed that their data could not be explained by the simple ionic crystal field model, and therefore entropy calculations such as those described in Section II.A are incorrect. In Appendix A we present extensive calculations based on their paper and give a qualitative estimate of the effect of their findings on the calculation of entropy. For the reasons discussed in Appendix A we have retained the simple ionic model for the entropy calculations in this thesis. The effect of their results on the T-S relation for CMN is discussed in Section IV.E.

We have calculated entropy as a function of the magnetizing field (H) and the initial temperature (T) using Eq. (II.A.6) and the partition function:

$$Q = \left[\exp\left(\frac{-g_{\perp}\beta H}{2kT}\right) + \exp\left(\frac{g_{\perp}\beta H}{2kT}\right)\right]^{N} \qquad \text{(IV.A.1)}$$

where $g_{\perp} = 1.84$. This calculation is rigorously correct only for an ensemble of non-interacting Ce^{+3} ions populating only the lowest Kramers' doublet. This assumption has been used in all previous studies of the CMN temperature scale, and although the strictly ionic model is probably slightly deficient, it allows us to compare our results with the earlier studies. The lattice contribution to the entropy has been neglected in our calculations since the heat capacity measurements of Bailey[76] show that $S_{Lat}/R \approx 5 \times 10^{-5}$ at 0.5°K. Values of S/R calculated from (IV.A.1) have been tabulated as a function of H/T by Hull and Hull,[77] and a plot of S/R vs. H/T is shown in Fig. IV.1. In conclusion it should be noted that all stable Ce isotopes have zero nuclear spin, and thus there is no nuclear contribution to the entropy of CMN.

3. ^{137m}Ce

As was discussed in Section II.C the requisite properties for the choice of an isotope for nuclear orientation temperature measurements are: good thermal contact with the lattice and the electron spin system; nuclear and electronic properties which are well-understood; and a temperature sensitive angular distribution of radiation which does not saturate at even the lowest temperatures. Previous experiments[3,78-80] in this laboratory have indicated that 34 hour ^{137m}Ce satisfies all these requirements.

Figure IV.1. S/R vs. H/T for spin $\frac{1}{2}$ Ideal Paramagnet.

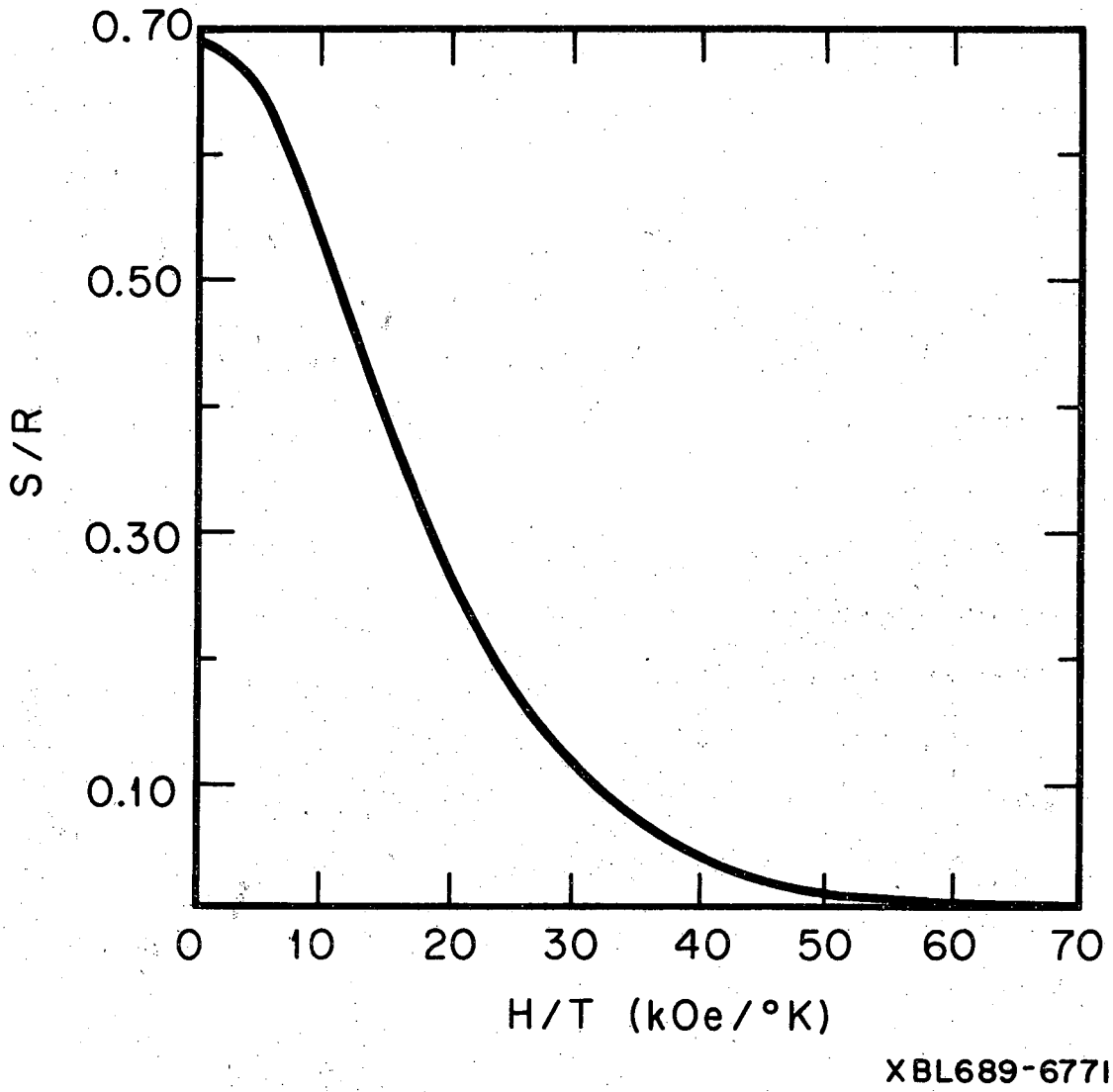

Fig. IV.1.

The decay properties of ^{137m}Ce have been investigated by Brosi and Ketelle[81] and most recently by Frankel et al.[80,82] The latter used a high resolution Ge(Li) detector, and the decay scheme resulting from their work is shown in Fig. IV.2. This figure was taken from Ref. 80. The transition of interest is the 255 keV γ-ray which de-excites the 11/2 - ^{137m}Ce level. Frankel et al.[83] have concluded that the multipolarity of this transition should be very pure M4. They say that "the lifetime (of ^{137m}Ce) is only a factor of three below the single particle estimates, and even if the E5 strength were enhanced by as much as a factor of 50 over single-proton estimates, which is extremely unlikely, the E5/M4 intensity mixing ratio would be only 2×10^{-4}."[83] Angular distribution studies[83] of conversion electrons from ^{137m}Ce oriented in neodymium ethyl sulfate support this conclusion. For this research we have therefore assumed that the 255 keV transition is pure M4. In addition Frankel[80] has shown that this transition is highly converted with $(e)_K/\gamma = 5.4$ and $(e)_K/(e)_{L+M} = 2.0$. This relatively high conversion coefficient places a limit on the amount of ^{137m}Ce which should be grown into the CMN because the conversion electron energy will be almost completely dissipated in the crystal. This will be an important source of heat leak at low temperatures.

The angular momentum properties of the nuclear decay are thus well known and the angular momentum coefficients described in Section II.C can be easily determined. Further discussion of this point, however, will be deferred until Section IV.D when the interpretation of the data will be presented. This section continues with a description of the method of sample preparation.

Table IV.2. $^{137m+g}Ce$ Decay Scheme.

This figure was copied from Reference 80.

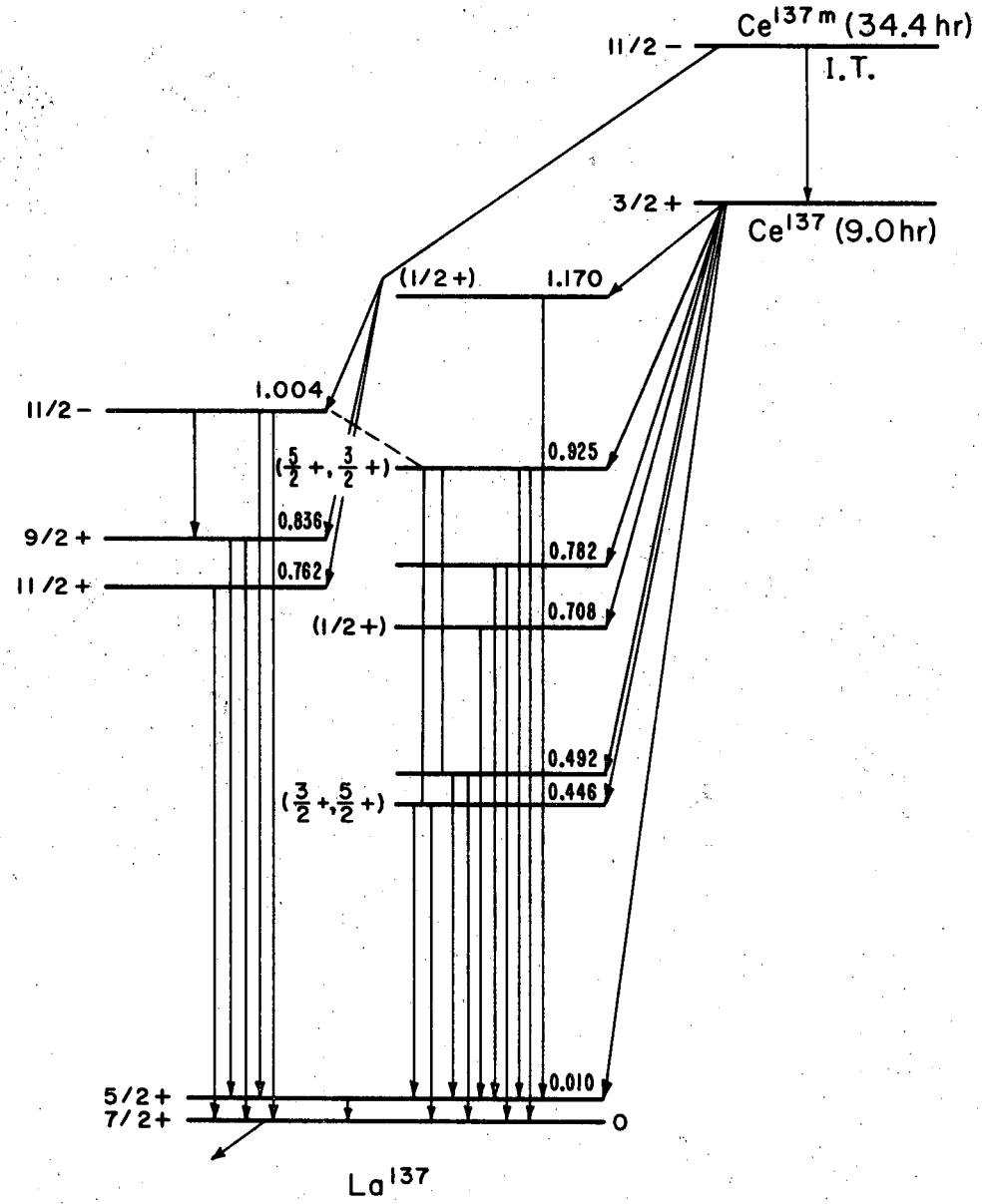
Ce137m (34.4 hr)
11/2 −
I.T.
3/2 +
Ce137 (9.0hr)
(1/2 +)
1.170
1.004
11/2 −
(5/2 +, 3/2 +)
0.925
0.836
9/2 +
0.782
0.762
11/2 +
(1/2 +)
0.708
0.492
(3/2 +, 5/2 +)
0.446
0.010
5/2 +
7/2 +
0
La137
MU-35181

Fig. IV.2.

B. Sample Preparation

^{137m}Ce was prepared in the Berkeley 88 inch cyclotron by a (p,3n) reaction on ^{139}La in high purity La_2O_3. At the bombarding energy of 30 MeV a small amount of ^{139}Ce was produced in the (p,n) reaction on ^{139}La but was not enough to hinder the experiment. Approximately 10^{12} - 10^{13} atoms of ^{137m}Ce were obtained for the bombardment times used in this experiment.

The Ce was separated from the La by a solvent extraction method described by Glendenin et al.[84] The target was first dissolved in a minimum amount of 16M HNO_3. The Ce^{+3} was then oxidized to Ce^{+4} by a solution of $KBrO_3$ in 8M HNO_3 (8.3g $KBrO_3$, 31.5 ml HNO_3, 18 ml H_2O) and transferred to a separatory funnel containing methyl-isobutyl ketone saturated with the oxidant. After a vigorous shaking for several minutes, the phases were allowed to separate and the lower aqueous phase containing the La^{+3} was drawn off and discarded. Approximately one milliter of 8M HNO_3 containing two drops of the oxidant was then added. The contents of the separatory funnel were again agitated vigorously and the lower aqueous layer drawn off. The purpose of this step was to remove any La^{+3} which remained after the first separation. Unfortunately a significant amount of the radioactive Ce^{+4} was always removed in this step possibly because the methyl isobutyl ketone had not been completely saturated with the oxidant. The Ce^{+4} "lost" at this point was saved for reclamation if necessary. The methyl isobutyl ketone containing the Ce^{+4} was pipetted into another separatory funnel containing a reducing solution (17 ml 30% H_2O_2, 50 ml HNO_3, 33 ml H_2O) and again vigorously

agitated. The lower aqueous phase, which now contained the Ce^{+3}, was drawn off and boiled to dryness. The organic phase was discarded. Invariably after the solution was boiled to dryness a dark residue – presumably from stop-cock grease dissolved by the methyl isobutyl ketone – remained. This could usually be destroyed by one or two boilings with the H_2O_2 - HNO_3 solution. The residue – a mixture of $La(NO_3)_3$ and $Ce(NO_3)_3$ – was converted to the respective chlorides by dissolution in 12M HCl and boiling to dryness several times.

As a final step in the separation procedure, the residue was redissolved in 0.1 M HCl and placed on a Dowex-50 cation exchange column for further purification. The column was washed throughly with 0.1 M HCl and the La-Ce mixture stripped off with 6M HCl. A spectrochemical analysis of the La_2O_3 target material, however, showed that it was of sufficient purity to forego this step (c.f. Appendix B). Nevertheless inertia perpetuated its inclusion until an interesting effect was discovered. Occasionally the solvent extraction was not very efficient and a considerable amount of La remained as was evidenced by a white powder when dry. If the ion exchange column were purposely made too small (generally a 2 mm i.d. column was used), it was found that most of the La would wash through in 0.1 M HCl along with some of the Ce while most of the Ce stuck on the column. The Ce could then be stripped off with 6M HCl, and when the solution was boiled to dryness only a clear transparent film containing practically all of the radioactive Ce and some La remained. The explanation for this effect presumably is due to the near equality of the equilibrium constants for the Ce^{+3} – resin and

La^{+3} – resin systems and the great initial excess of La (La/Ce) 10^8). In this way ^{137m}Ce sources of very small mass and high activity could be prepared. This last refinement (i.e. the "small column" effect) was used only for the ^{137m}Ce in cerium zinc nitrate experiment reported in Section V.

The Ce^{+3} - HCl solution from the ion exchange column was boiled to dryness, and the residue was dissolved in saturated CMN solution at 5°C. Clear, visibly faultless, single crystals of CMN between 10 and 15 mm in diameter and about 2 mm thick were placed in the solution. A photograph of one of the crystals is shown in Fig. IV.3. The light flecks on the surface of the crystal are due to reflection of light off surface imperfections. The solution was then placed in a 5°C refrigerator, and the radioactivity was allowed to grow into the crystals for 16-20 hours. Because of the incompleteness of the La-Ce separation some La was present in the solution and also grew into the crystals. A spectrochemical analysis[85] showed that the ratio of La to Ce was < 5/1000. The crystals were then removed from the radioactive solution, dried, and placed into a non-radioactive solution of CMN at 5°C. An inactive layer was allowed to grow for 16-24 hours. The CMN solution and crystals had been prepared in the usual way: i.e., by mixing stoichiometric amounts of $Ce(NO_3)_3$ and $Mg(NO_3)_2$ in H_2O to form a saturated solution, repeated recrystallization until the resulting crystals (and solution) were clear, and subsequent growth of the crystals from the saturated solution at 5°C. A spectrochemical analysis of the CMN used in this experiment is given in Appendix B.

Figure IV.3. Single Crystal of CMN.

This crystal in this photograph is magnified by a factor of about 2.5.

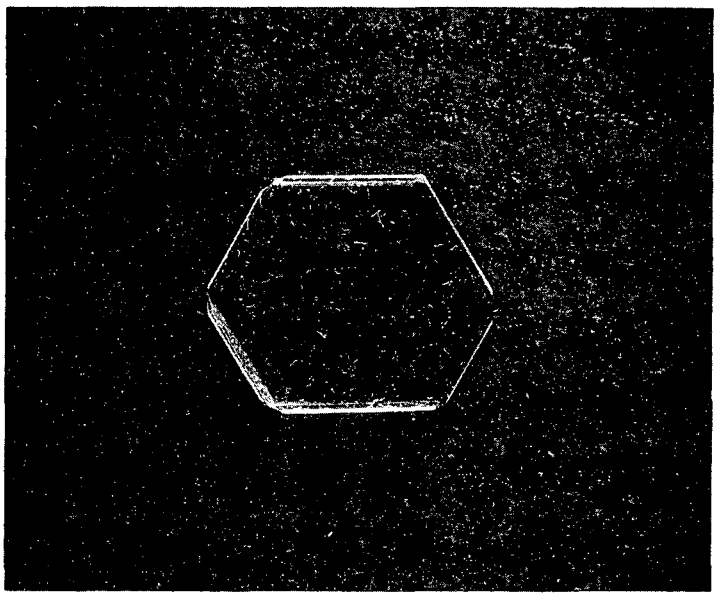

XBB 689-5407

Fig. IV.3.

After the inactive layer has been grown on the crystals, they were removed from the solution, dried and five or six of them weighing about 1.4 g total were glued together with Duratite[86] cement to form the experimental sample. The crystals were then mounted in the apparatus with great care being taken to insure that the c axes of the crystals were oriented properly with respect to the vertical plane and magnetic field direction (horizontal plane). The alignment in the vertical plane (i.e. perpendicular to the c axis) was checked with a level and was accurate to about ± 1.5°. A special procedure, however, was used to check alignment in the horizontal plane. The crystals were first aligned visually so that the c axis was oriented at 0° with respect to a set of angles marked off on the counting table. When all looked well, the crystals were glued into the holder and the apparatus was completely assembled. The first three runs were demagnetizations from $H/T_i \approx 43$ kOe/°K and were used to select the direction of the c axis. For these runs the γ-ray intensity $(W(\theta))$ was measured at six different angles (two per run), and the angular distribution in the horizontal plane was mapped. The centroid of the distribution could then be determined and the direction of the c axis was located at about ± 1°. A typical angular distribution is shown in Fig. IV.4 in which the points are uncorrected for background.

Figure IV.4. $W(\theta)$ vs. θ for the June 1967 Experiment.

The maximum and minimum, indicated by the arrows, are located at 182° and 92°, respectively. The detector positions were rotated to compensate for this slight misalignment.

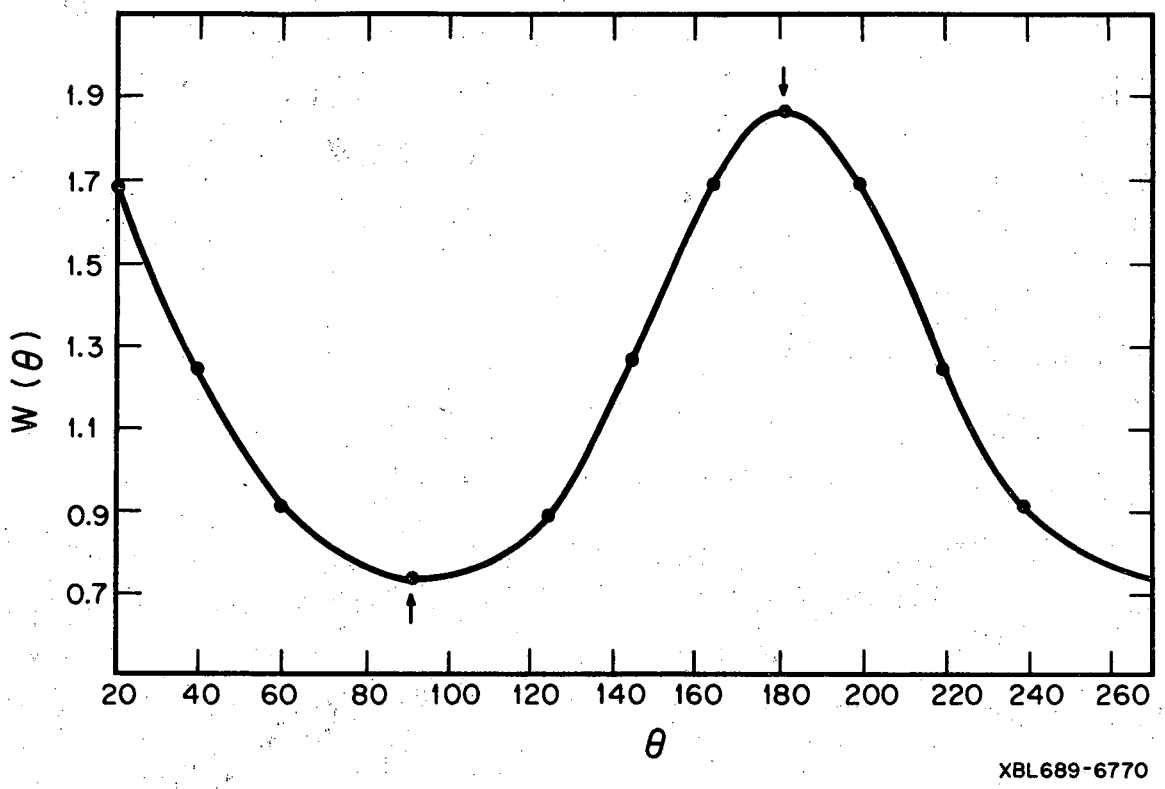
1.9
1.7
1.5
1.3
1.1
0.9
0.7
W (θ)
20
40
60
80
100
120
140
160
180
200
220
240
260
θ
XBL689-6770

Fig. IV.4.

C. Data Reduction

1. Background Correction

All the experiments utilized NaI(Tl) scintillation detectors, and a typical γ-ray spectrum is shown in Fig. IV.5. A high resolution Ge(Li) spectrum over the same energy region is shown in Fig. IV.6. This spectrum was taken ten days after the cyclotron bombardment, and consequently the relative intensity of the 166 keV γ-ray from 140-day ^{139}Ce is much larger than under normal running conditions. In actual practice it is usually about the same relative intensity as that of the 168 keV γ-ray of ^{137}Ce. The primary feature of interest in the Ge(Li) spectrum is the Compton edge at 284 keV, which falls under the 255 keV peak in the NaI(Tl) spectrum. This constitutes "background" and must be subtracted from the intensity of the 255 keV γ-ray to give correct intensities. In addition there is a room background which becomes increasingly large for energies below 280 keV and is due primarily to Compton scattered radiation from ^{40}K in the walls of the laboratory and various ^{60}Co sources in use elsewhere in the laboratory.

Because of the complexity of the background an empirical procedure was developed to make the necessary correction. The general slope of the background could be constructed by combining the room background spectrum with a spectrum of ^{22}Na. The latter has an annihilation quantum at 511 keV and so will have a Compton edge at 341 keV. By translating the photo peak downwards in energy until it coincided with the ^{137}Ce peak at 446 keV, the behaviour of the Compton background under the 255 keV peak could be qualitatively reproduced. Figure IV.7 illustrates the two components of the background. The correction was

Figure IV.5. NaI(Tl) Spectrum of $^{137m+g}Ce$.

The isotopic origins of the photopeaks are indicated in the plot with transition energies in parentheses. The peak at 446 keV is a composite peak consisting primarily of the 446 γ-ray but also including the following γ-rays: 433, 436, 479, 482, 492. The position of the Compton edge from the 446 keV is indicated by E_c.

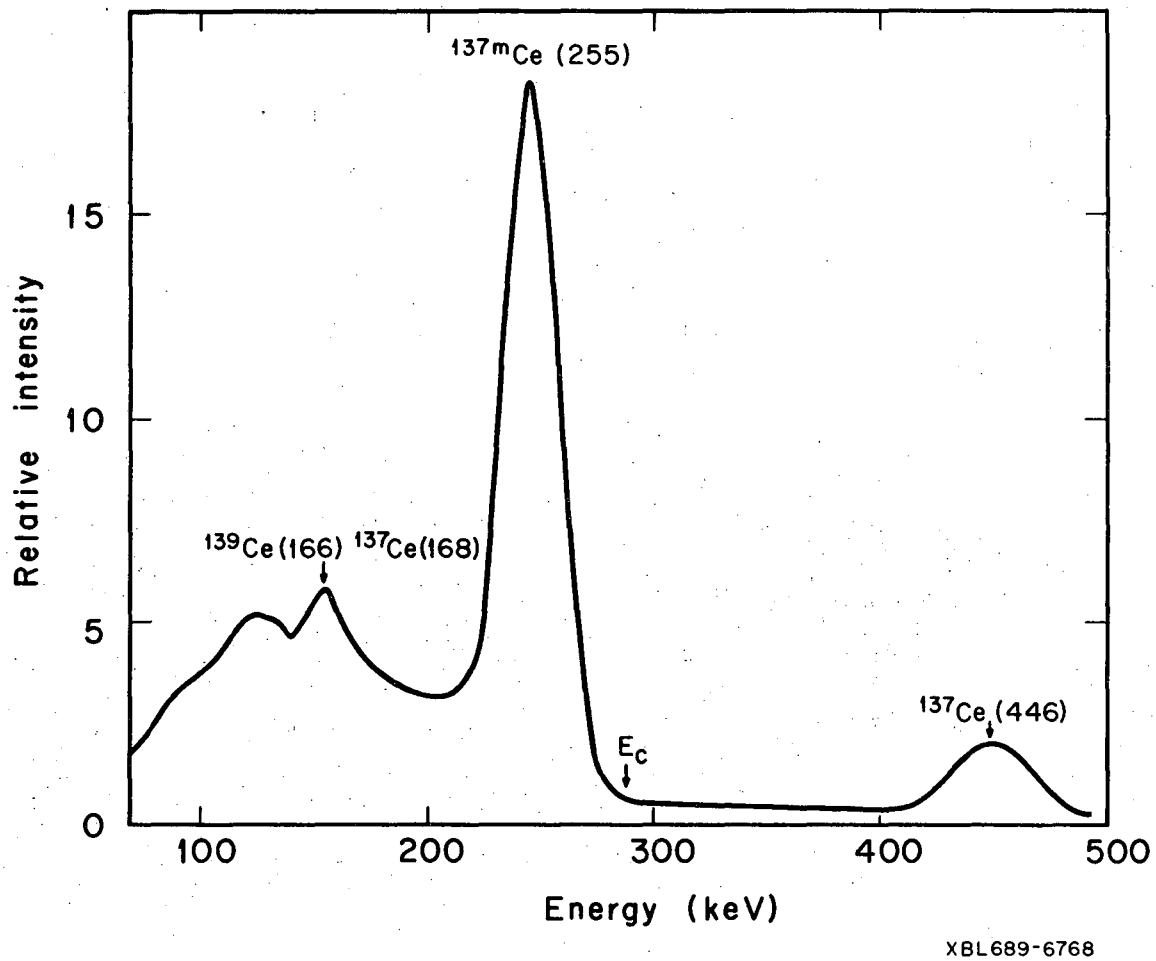
137mCe (255)
139Ce(166)
137Ce(168)
Ec
137Ce(446)
Relative intensity
0
5
10
15
100
200
300
400
500
Energy (keV)
XBL689-6768

Fig. IV.5.

Figure IV.6. Ge(Li) γ-Ray Spectrum of $^{137m+g}Ce$.

The isotopic origins of the γ-rays are indicated in the figure with the energies in parentheses. The small peak at about 265 keV was not identified but may correspond to a transition between the 708 and 446 keV levels in ^{137}La (c.f. Figure IV.2). The Compton edge from the 446 keV γ-Ray is indicated by E_c.

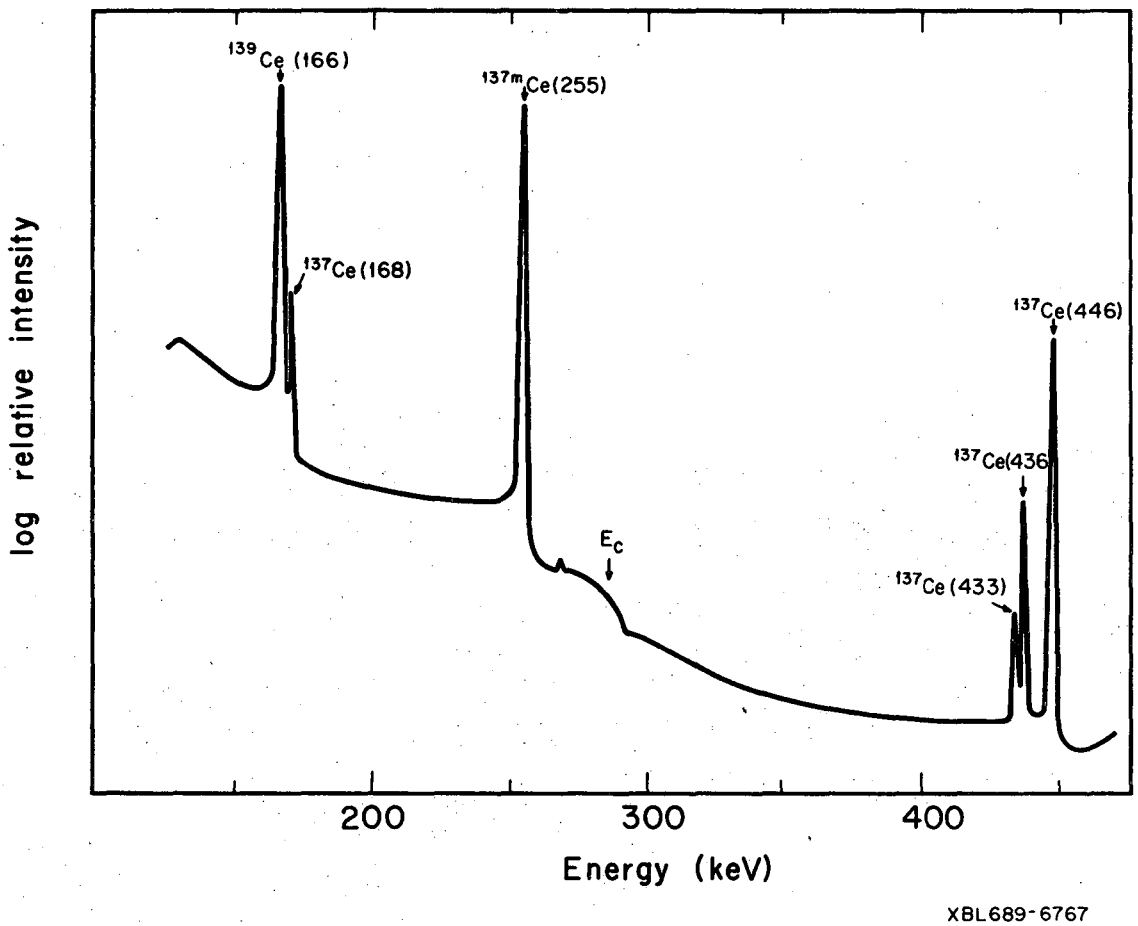
139Ce (166)
137mCe(255)
137Ce(168)
137Ce(446)
137Ce(436)
Ec
137Ce(433)
log relative intensity
200
300
400
Energy (keV)
XBL689-6767

Fig. IV.6.

Figure IV.7. Background Components.

The 511 keV peak of ^{22}Na has been translated to the position of the ^{137}Ce 446 keV peak and qualitatively shows the behaviour of the Compton background under the ^{137m}Ce 255 keV peak. The intensity of the 511 keV peak has not been normalized to the intensity of the 446 keV peak since the latter source was inside the stainless steel dewar while the former was not. This figure is designed only to show the shape of the background. The lowest line represents the room background.

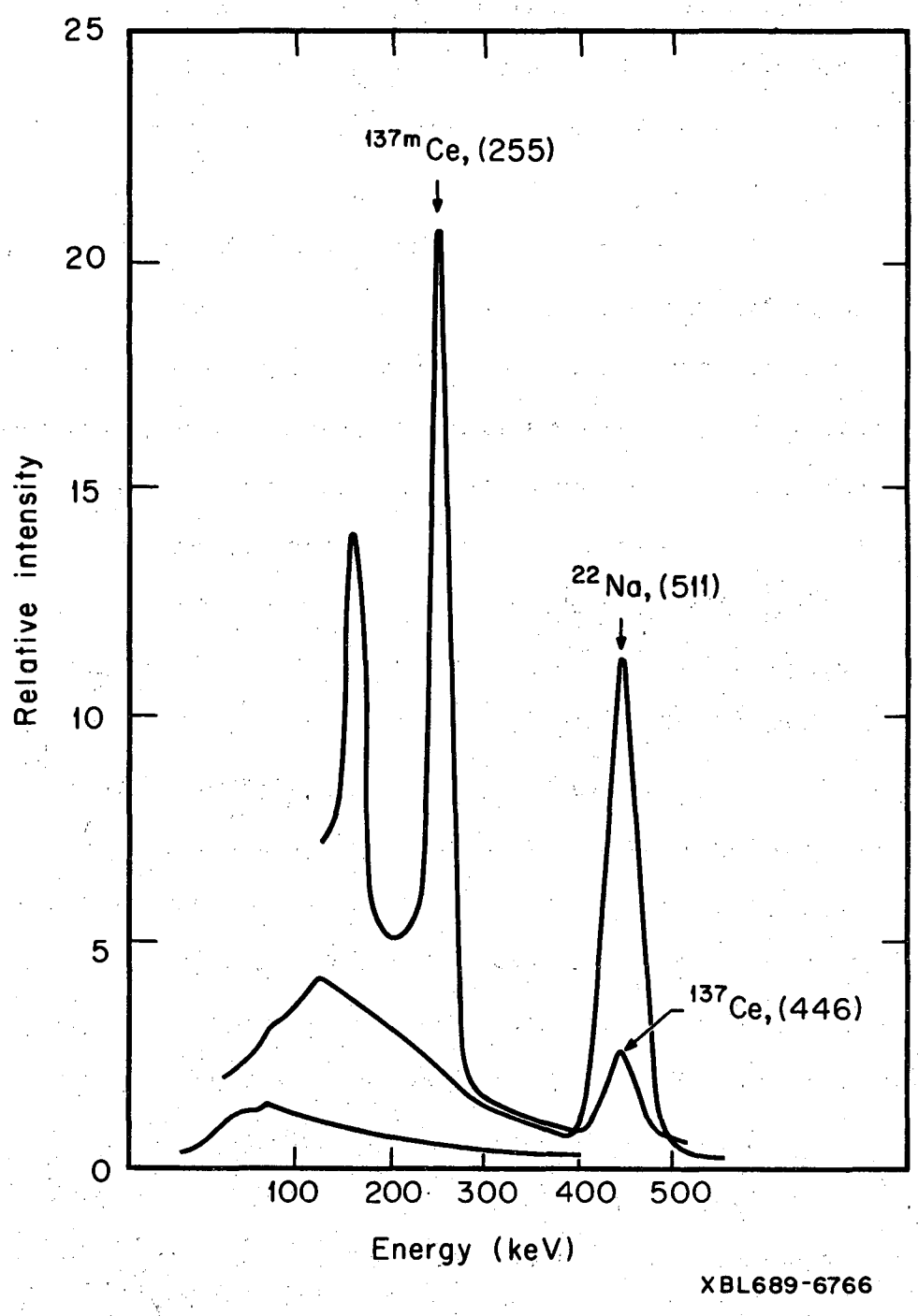
25
20
15
10
5
0
Relative intensity
137m Ce, (255)
22 Na, (511)
137 Ce, (446)
100
200
300
400
500
Energy (keV)
XBL689-6766

Fig. IV.7.

then estimated as is shown in Fig. IV.8, which is a plot of a "warm" count spectrum. Line (b_{ST}) is a linear extrapolation of the high energy background while lines (b_i) were drawn to approximate the effects shown in Fig. IV.7.

The selection of the best line (b_i) was the critical step and was performed in the following manner. The warm counts for a consecutive series of four or five runs were added together for each channel in the photopeak. The same was done for the cold counts, and the cold count channel values were multiplied by a factor accounting for any counting time difference between the cold and warm counts. The background was determined for each channel for the various lines (b_i) in Fig. IV.8 and subtracted from the corresponding values in the cold and warm counts. The function C-B/W-B (where C, W, and B refer to the cold count, warm count, and background correction respectively) was then calculated channel by channel for each line (b_i) and plotted as shown in Fig. IV.9. Because the cold and warm photopeaks are Gaussian in shape to first order and have the same full width at half maximum, the afore-mentioned function will be constant across the peak for the proper background correction. The background line (b_i) in Fig. IV.8 which best satisfied this condition was chosen as the appropriate correction. This correction was then used to calculate the cold and warm intensities over that part of the photopeak in which the constancy was observed.

Differences in the background for the cold and warm counts have not been explicitly taken into account. Such differences would arise from anisotropy in the Compton distribution from the 446 keV γ-ray.

Figure IV.8. Background Approximations.

Lines $b_i (1 \leq i \leq 4)$ were drawn to approximate the effects illustrated in Figure IV.6. Line b_{ST} is a straight line extrapolation of the high energy background.

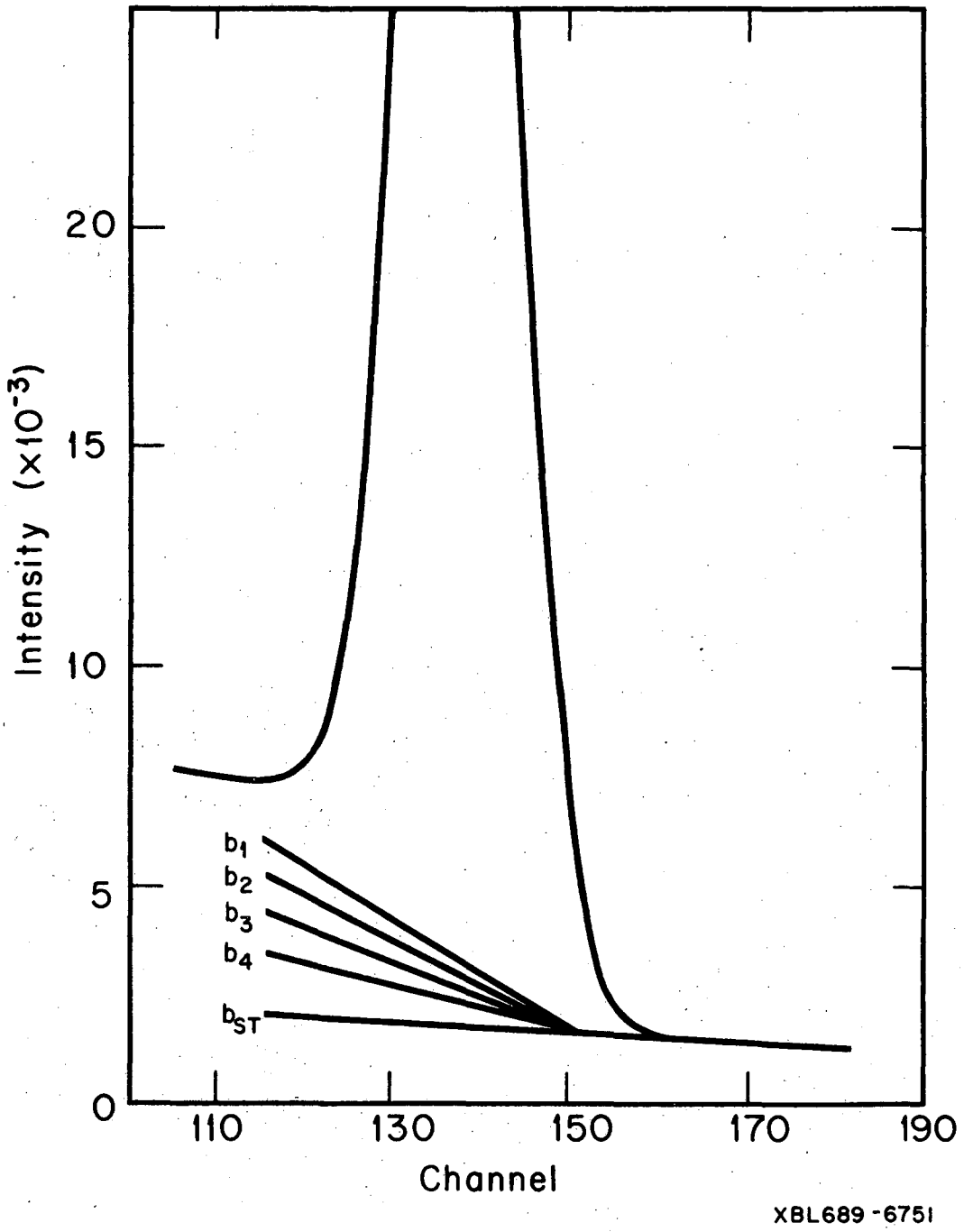
Intensity (x10^{-3})
20
15
10
5
0
110
130
150
170
190
Channel
b_1
b_2
b_3
b_4
b_{ST}
XBL689-6751

Fig. IV.8.

Figure IV.9. (C - B)/(W - B) vs. Channel.

B is the background correction per channel. The smoothed curves b_1, b_3, and b_{ST} refer to the corresponding background approximations in Figure IV.7. Line b_o corresponds to no background correction. Curve b_3 was selected as the best approximation to the actual background, and the cold and warm intensities were calculated for the photopeak from channel 132 to channel 150. The upward curl for channels > 150 is due to a slight over-correction in the background.

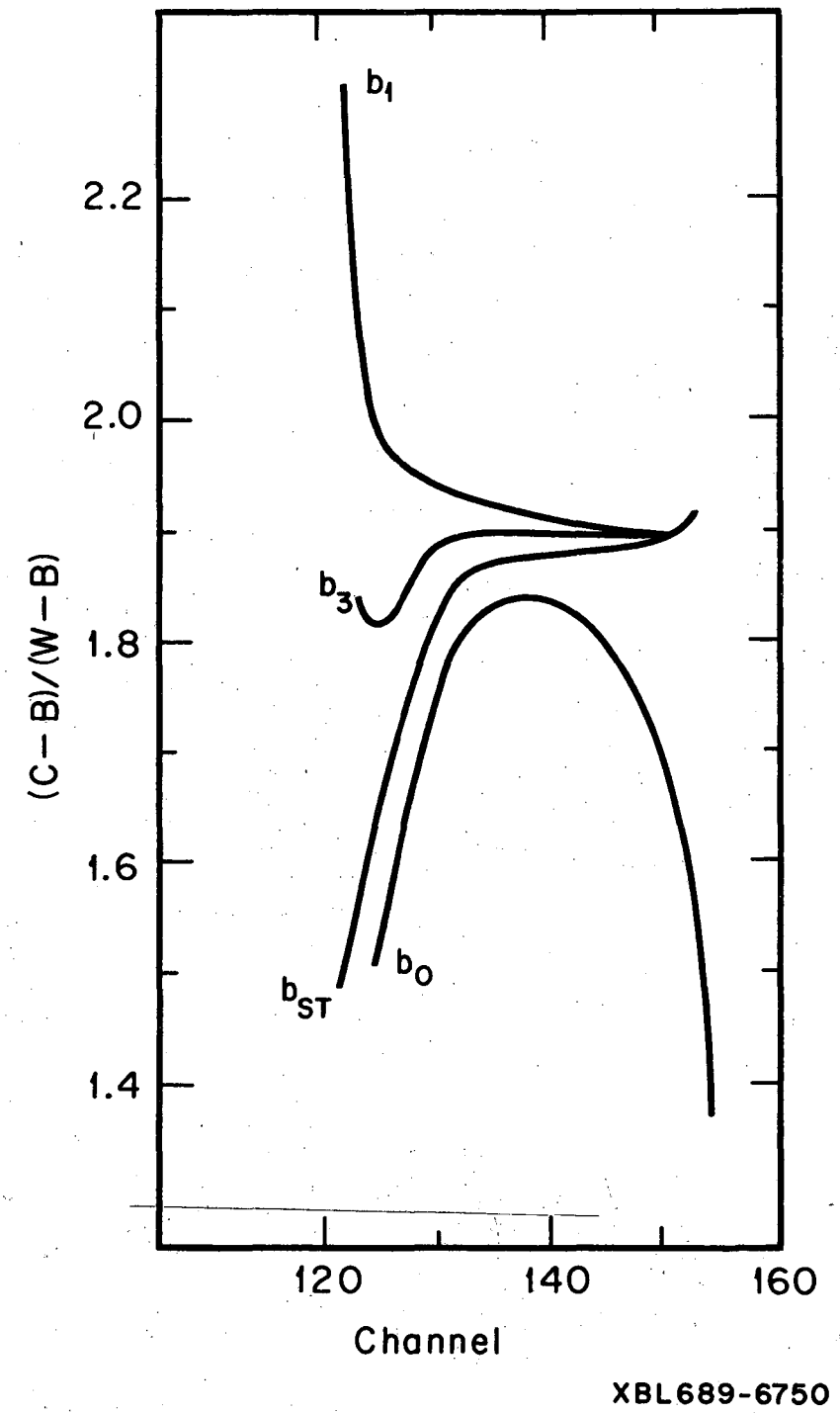

Fig. IV.9.

The procedure outlined above, however, serves to pick the best average background for the cold and warm counts. The internal consistency of the data over a wide range of γ-ray anisotropy does not indicate an empirical need for further refinement along these lines. Another effect associated with Compton scattering is the low energy tail on the 255 keV γ-ray. Because of the low energy of the γ-ray and the 7% resolution of the detectors, Compton-scattered radiation from this γ-ray falls under the low-energy side of its photopeak. The Compton tail has a different angular distribution than the γ-ray because the Compton scattering process is sensitive to the linear polarization of the γ-ray.[79] Figure IV.10 illustrates this feature. This tail, however, is automatically excluded from the calculation of intensities by the method outlined in the previous paragraph.

Because of the relatively short half life of ^{137m}Ce, the background contribution from the ^{137}Ce Compton distribution will decrease in time with respect to the constant room background. In a long series of runs extending over several days this effect should be taken into account. If we designate B as the total background, W_t as the warm count uncorrected for background, W as the intrinsic warm intensity of the ^{137m}Ce γ-ray, S as the Compton background from higher energy γ-rays in the source, and R as the room background, then

$$B = S + R \tag{IV.B.1}$$

$$W_t = W + B = W + S + R \tag{IV.B.2}$$

Figure IV.10. Cold and Warm Photopeak Intensities at $\theta = 0$.

The broken line delineates the region of the Compton "tail". This region was excluded in the calculation of $W(\theta)$.

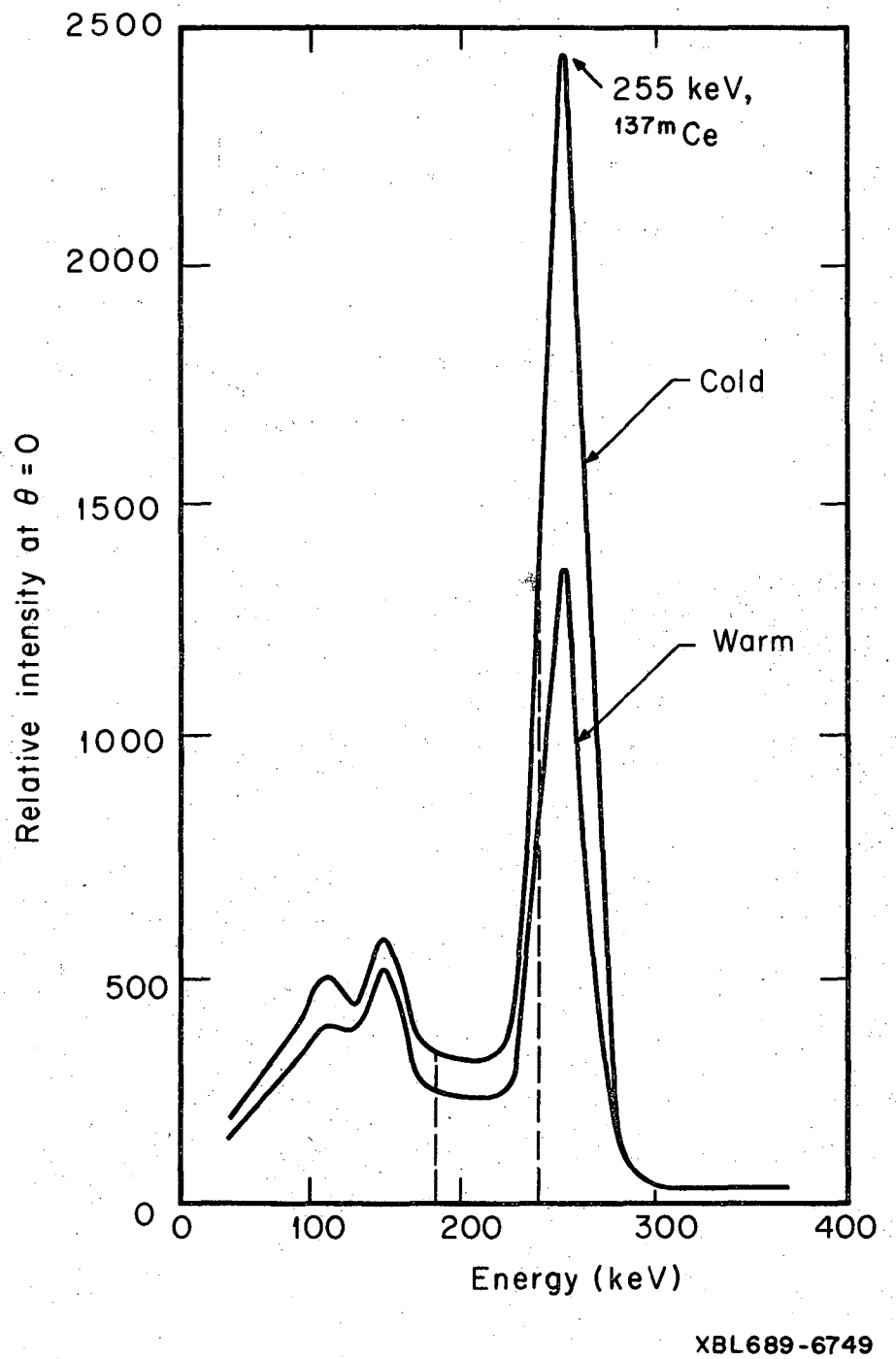
2500
2000
1500
1000
500
0
Relative intensity at θ = 0
0
100
200
300
400
Energy (keV)
255 keV,
137m Ce
Cold
Warm
XBL689-6749

Fig. IV.10.

and

$$\frac{B}{W_t} = \frac{S + R}{W + S + R} = \frac{\frac{S}{W} + \frac{R}{W}}{1 + \frac{S}{W} + \frac{R}{W}} \qquad \text{(IV.B.3)}$$

S/W depends only upon the geometrical set up of the experiment and should be constant for any one experiment, since both S and W have the same time dependence. R/W, however, varies in time since R remains constant while W decreases exponentially with time. If we let $S/W = a$ and $R/W = b\, e^{t/T}$ where t = time and T (mean lifetime) = $t_{1/2}/\ln 2$,* then

$$\frac{B}{W_t} = \frac{a + b\, e^{t/T}}{1 + a + b\, e^{t/T}} = \alpha \qquad \text{(IV.B.4)}$$

or

$$a + b\, e^{t/T} = \frac{\alpha}{1-\alpha} \quad . \qquad \text{(IV.B.5)}$$

Thus the time dependence of the background correction can be worked out by calculating the background as shown in Figs. IV.8 and IV.9 for several sets of runs at different points in time and fitting the results to Eq. (III.B.5). This formula can be converted to a simple linear equation merely by a change of variables, and the parameters a and b can be determined easily. The appropriate correction can then be calculated

*Because the half life of ^{137}Ce (9 hr) is shorter than the ^{137m}Ce half life (34 hr), the decays of ^{137}Ce and ^{137m}Ce are in secular equilibrium. The effective half life of ^{137}Ce is thus 34 hours.

at any time t. Figure IV.11 displays the background correction results as a function of time for the June 1967 experiment. Each of the points represents an average over a minimum of three runs. The background corrections determined in this way ranged between 7.6% to 11.6% of the total warm count depending on when the run came in the series. The estimated error in the correction is ± 6% (i.e. 6% of a 10% correction is equivalent to 10% ± 0.6%).

For the experiments of March 1967 and January 1968 the 90° data rather than the 0° data were used to calculate the background corrections. This was necessitated by very small electronic gain shifts in the 0° spectra. Presumably these gain shifts resulted from the large changes in the counting rate either just after demagnetization or upon warming the sample for the normalization count. An attempt was made to minimize the former by keeping a ^{137m}Ce source of appropriate intensity in front of the detectors during magnetization. Since the 0° and 90° corrections were quite similar for the June 1967 experiment, it was assumed that no additional uncertainty was introduced by using only the 90° data to make the corrections. Furthermore, because of the smallness of the gain shift and the difficulty in correcting for it, no attempt at correction was made.

2. Warm-up Corrections

Immediately after demagnetization a series of cold counts of either 15 or 30 second duration each were taken for about 5 minutes. For most of the demagnetizations in this experiment the counting rate did not change within statistics until several (between two and eight) of these

Figure IV.11. Time Dependence of Background (6/67 Experiment).

The data points represent summations over four or five runs. The circles correspond to 0° data and the squares to the 90° data. The solid line is the best straight line through the four points at the extrema of the plot. The intermediate points showed some evidence of a small electronic gain shift and were not used in the fit. The dashed lines represent ± 6% uncertainty in the background correction.

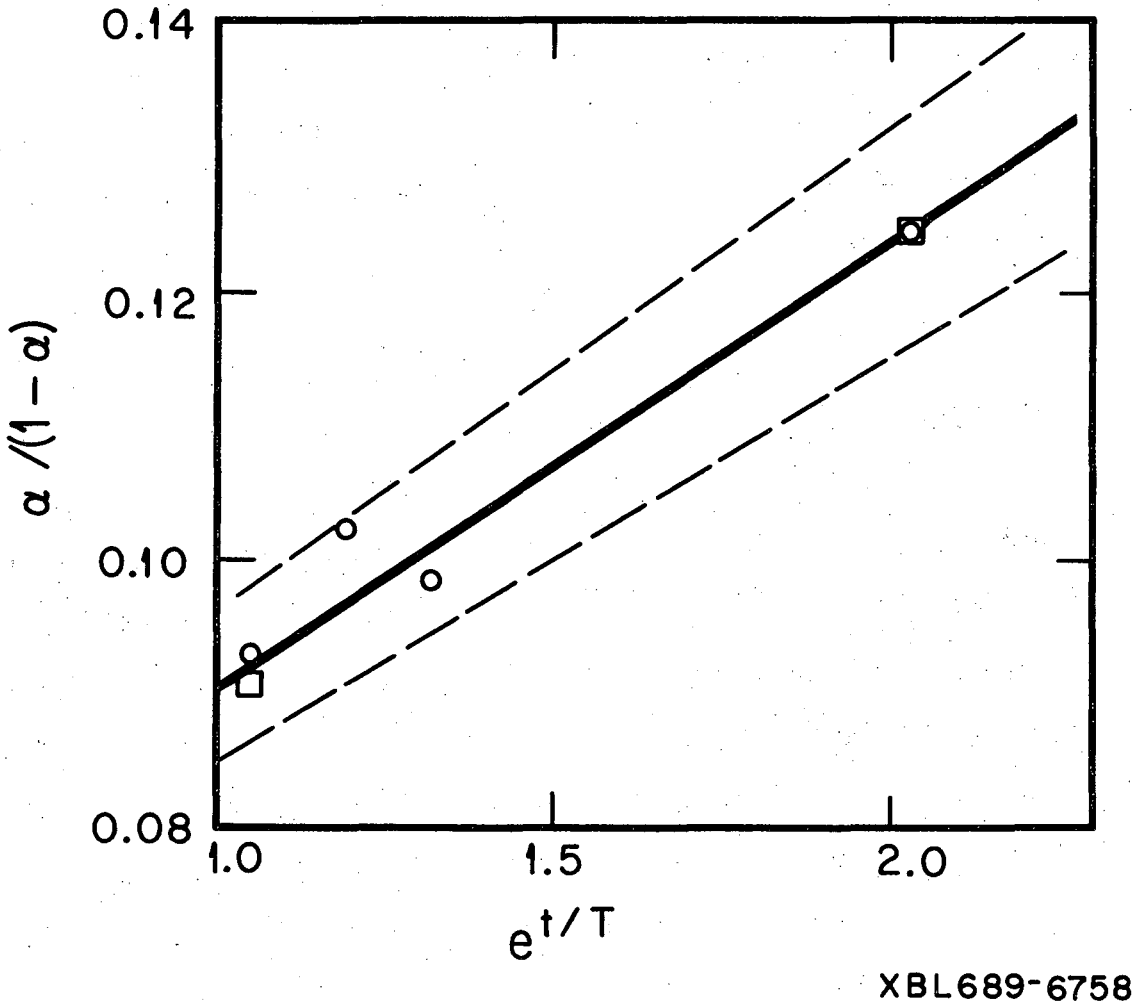

Fig. IV.11.

counting periods had elapsed. The total cold count was taken as a summation over the periods where the counting rates were essentially constant. For four of the demagnetizations into the high temperature region, however, the counting rate changed continuously as a function of time and had to be extrapolated back to the time of demagnetization. This was done empirically in the linear least squares sense.

D. Results

1. Data

The data from the various runs are listed in Tables IV.2, IV.3, and IV.4. The values of $W(\theta)$ have been corrected for source decay between the cold and warm counts but not for solid angle effects. The numbers in parentheses represent one standard deviation in the listed quantity and refer to the last significant figures of the experimental quantity. The errors in $W(\theta)$ were calculated in the usual way from the statistical errors in the cold and warm counts and the estimated 6% uncertainty in the background correction (e.g. see Reference 87). A sample calculation of $W(0)$ is given in Appendix C. The entropy values were determined from the values of H/T as discussed in Section IV.A. These entropies have not been corrected for radioactive heating effects during the isolation period of the magnetization since the change in entropy was found to be small. This point is discussed in detail in Appendix D. In Fig. IV.12 $W(0)$ is plotted against $\ln 2 - S/R$ (the entropy removed in the magnetization). T_H and T_o are explained later in Section IV.D (c.f. "Interpretation of Data Numerical"). The most

Table IV.2. ^{137m}Ce in CMN, March 1967.

$H/T\left(\frac{kOe}{°K}\right)$	S/R	W(0)	$W(\pi/2)$	T_H(m°K)	T_o(m°K)
27.9 (2)	.139 (3)	1.895 (14)	.6983 (75)	1.68 (9)	1.73 (9)
29.5 (2)	.120 (3)	1.923 (14)	.7172 (69)	1.49 (9)	1.55 (9)
31.7 (2)	.098 (2)	1.895 (15)	.7107 (55)	1.68 (10)	1.73 (10)
35.8 (2)	.065 (1)	1.940 (15)	.7055 (57)	1.38 (10)	1.45 (9)
21.6 (1)	.241 (3)	1.886 (17)	.7014 (93)	1.75 (12)	1.78 (11)
25.6 (2)	.172 (3)	1.870 (12)	.7105 (59)	1.86 (8,9)	1.89 (8)
68.2 (7)	.002 (0)	1.960 (18)	.6782 (79)	1.25 (11,12)	1.33 (10,11)
43.8 (6)	.029 (3)	1.937 (16)	.7081 (58)	1.40 (11)	1.46 (10)

The numbers in the parentheses indicate one standard deviation and refer to the last significant figures in the listed quantity. W(0) and $W(\pi/2)$ have not been corrected for solid angle effects. For $H/T < 45$ kOe/°K, $T \approx 0.5$°K; for $H/T > 45$ kOe/°K, $T \approx 0.31$°K.

Table IV.3. ^{137m}Ce in CMN, June 1967.

$H/T\left(\frac{kOe}{°K}\right)$	S/R	W(0)	W(π/2)	T_H(m°K)	T_o(m°K)
41.8 (1)	.036 (1)	1.936 (15)	.7076 (51)	1.41 (9,10)	1.47 (9)
34.7 (2)	.072 (1)	1.918 (11)	.7054 (48)	1.53 (7)	1.58 (7)
29.6 (2)	.118 (3)	1.932 (14)	.7045 (49)	1.43 (9)	1.49 (9)
27.1 (2)	.150 (3)	1.915 (12)	.7060 (55)	1.55 (8)	1.60 (8)
17.9 (1)	.324 (2)	1.879 (14)	.7028 (73)	1.80 (9)	1.83 (9)
11.7 (1)	.489 (3)	1.721 (13)	.7367 (76)	3.04 (13)	3.05 (12)
10.2 (1)	.529 (3)	1.703 (20)	.7601 (62)	3.22 (19,20)	3.22 (19)
13.7 (1)	.434 (3)	1.804 (16)	.7168 (77)	2.34 (12)	2.36 (12,13)
20.0 (1)	.276 (2)	1.857 (11)	.7211 (53)	1.95 (8)	1.98 (8)
22.9 (1)	.217 (2)	1.879 (11)	.7050 (53)	1.80 (7)	1.83 (7,8)
25.4 (2)	.175 (3)	1.897 (12)	.7050 (56)	1.67 (8)	1.71 (8)
21.5 (1)	.244 (2)	1.899 (13)	.7177 (65)	1.66 (9)	1.70 (8)
66.3 (7)	.003 (1)	1.936 (15)	.6877 (71)	1.41 (10)	1.47 (9)
53.9 (6)	.009 (1)	1.932 (16)	.7148 (62)	1.43 (11)	1.49 (10)
33.2 (2)	.084 (2)	1.936 (19)	.7015 (66)	1.41 (12)	1.47 (12)
68.0 (7)	.002 (0)	1.933 (16)	.6998 (58)	1.43 (10,11)	1.49 (10)
44.6 (6)	.027 (2)	1.937 (15)	.6989 (65)	1.40 (10)	1.46 (9)
66.9 (7)	.002 (1)	1.941 (14)	.7003 (59)	1.37 (9)	1.44 (8,9)
32.8 (2)	.088 (2)	1.933 (18)	.7048 (66)	1.43 (12)	1.49 (11)
23.9 (2)	.199 (4)	1.890 (17)	.6986 (74)	1.72 (11)	1.75 (11)
20.4 (1)	.268 (3)	1.871 (15)	.7068 (71)	1.85 (10)	1.88 (10)
18.9 (1)	.301 (3)	1.873 (17)	.7215 (73)	1.84 (11,12)	1.87 (11)

The numbers in the parentheses indicate one standard deviation and refer to the last significant figures in the listed quantity. W(0) and W(π/2) have not been corrected for solid angle effects. For $H/T < 45$ kOe/°K, $T \approx 0.5$°K; for $H/T > 45$ kOe/°K, $T \approx 0.31$°K.

Table IV.4. ^{137m}Ce in CMN, January 1968.

$H/T \left(\frac{kOe}{°K}\right)$	S/R	W(0)	W(π/2)	T_H(m°K)	T_o(m°K)
25.74 (10)	.170 (2)	1.894 (12)	.7187 (47)	1.69 (8)	1.73 (8)
35.55 (13)	.067 (1)	1.924 (15)	.7194 (51)	1.49 (10)	1.54 (9)
30.18 (11)	.112 (1)	1.919 (15)	.7232 (66)	1.52 (10)	1.57 (9)
23.13 (9)	.213 (2)	1.887 (12)	.7255 (57)	1.74 (8)	1.78 (8)
21.89 (9)	.235 (2)	1.885 (11)	.7245 (46)	1.75 (8)	1.79 (7)
16.41 (7)	.362 (2)	1.838 (12)	.7205 (52)	2.08 (9)	2.11 (9)
13.13 (6)	.450 (2)	1.797 (15)	.7456 (59)	2.40 (12)	2.42 (12)
17.48 (7)	.334 (2)	1.901 (19)	.7041 (67)	1.64 (13)	1.69 (12)
9.28 (5)	.554 (2)	1.655 (17)	.7563 (70)	3.69 (17)	3.69 (18)
8.10 (5)	.584 (2)	1.551 (12)	.7726 (71)	5.00 (18)	5.00 (18)
7.27 (5)	.603 (1)	1.518 (13)	.7838 (66)	5.49 (21)	5.49 (22)
5.94 (5)	.630 (1)	1.479 (17)	.7766 (119)	6.17 (32)	6.17 (30)
6.57 (5)	.618 (1)	1.464 (12)	.8053 (86)	6.45 (22,24)	6.45 (22,24)
7.80 (5)	.591 (1)	1.536 (12)	.7944 (70)	5.22 (18)	5.22 (18)
8.84 (5)	.565 (1)	1.633 (14)	.7656 (73)	3.94 (16)	3.94 (16)
11.84 (7)	.485 (2)	1.745 (15)	.7282 (84)	2.83 (13)	2.84 (13)
15.07 (7)	.397 (2)	1.831 (26)	.7081 (78)	2.14 (19)	2.16 (19)
8.48 (5)	.574 (2)	1.614 (24)	.7570 (88)	4.17 (29)	4.17 (29)

The numbers in the parentheses indicate one standard deviation and refer to the last significant figures in the listed quantity. W(0) and W(π/2) have not been corrected for solid angle effects. For $H/T < 45$ kOe/°K, $T \approx 0.5$°K; for $H/T > 45$ kOe/°K, $T \approx 0.31$°K.

Figure IV.12. W(0) as a function of $\ell n2 - S/R$ for the three sets of runs. The solid curve represents the smooth curve through the present data and the broken curve the smoothed results of Frankel, Shirley, and Stone. These curves are discussed in Section IV.E.

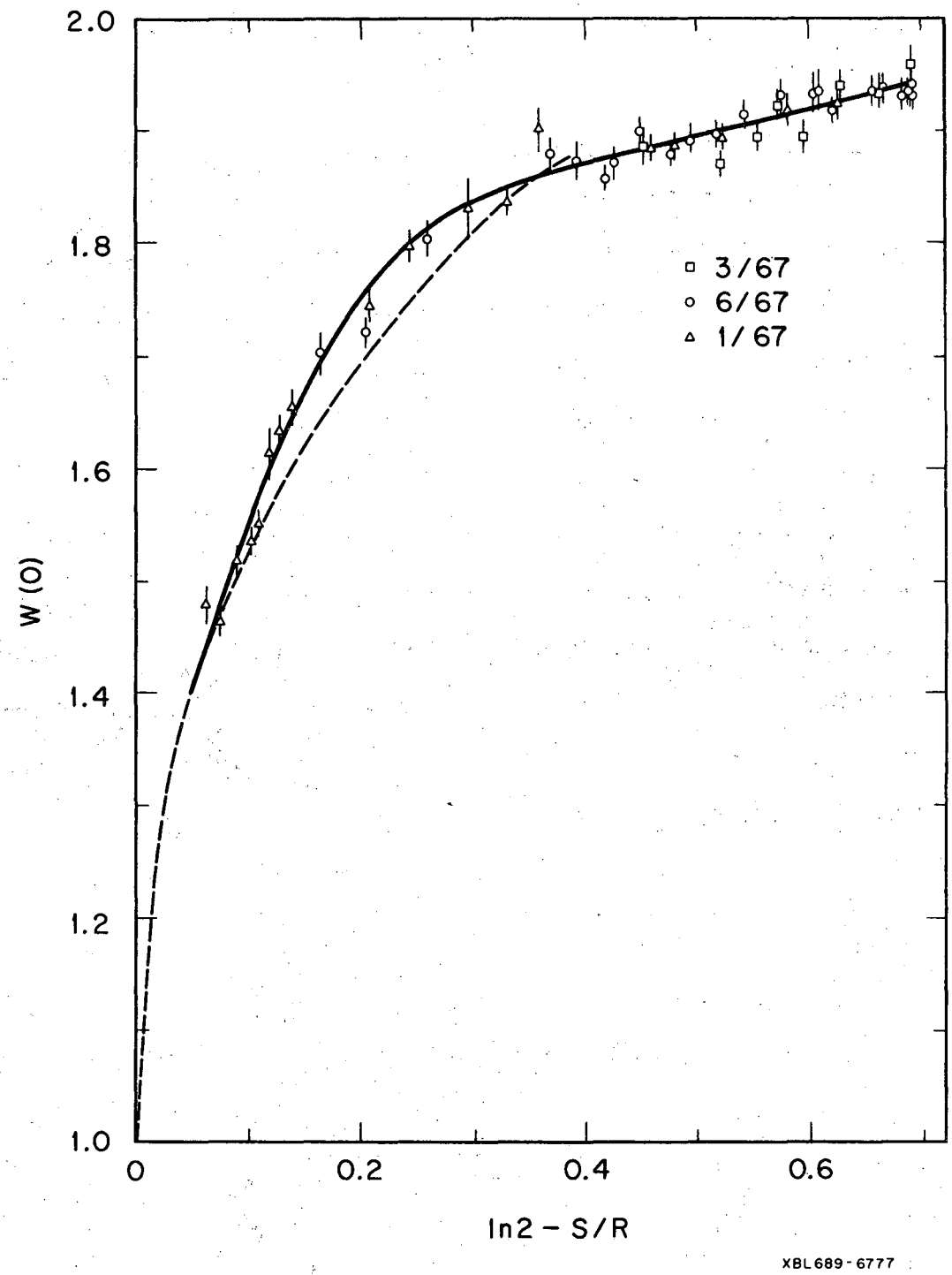

Fig. IV.12.

notable feature of this plot is that $W(0)$ continues to increase over practically all of the entropy range which indicates that there is no region where the temperature becomes constant.

2. Interpretation of Data, Theoretical

To interpret the $W(\theta)$ data in terms of temperature one must know the parameters $B_k(T)$, U_k, F_k, g_k, and $P_k(\cos\theta)$ (c.f. Eq. (II.C.1)). For an M4 transition from an 11/2 level the maximum value of k is 8. Since there are no transitions preceding the one of interest, all the U_k are equal to one. The F_k (4,4,11/2,3/2) can be determined from the tabulation of Ferentz and Rosenzweig.[32] Values of g_2 and g_4 for the photopeak have been calculated by Yates[88] as a function of γ-ray energy and experimental geometry. For our experimental geometry (the center of the source is 10 cm from the face of 3" × 3" NaI(Tl) detector), g_2 and g_4 for a 255 γ-ray were obtained by interpolation from Yates' tabulation. Culvahouse[89] has suggested that g_6 and g_8 may be calculated from the formula given by Rose.[90]

$$g_k = \frac{P_k(\cos\theta) - \cos\theta\, P_k(\cos\theta)}{(k+1)(1-\cos\theta)} \quad . \qquad \text{(IV.D.1)}$$

The value of $\cos\theta$ is chosen so as to reproduce the photopeak values of g_2 and g_4 given by Yates and is found to be 0.9464.[89] The values of the various g_k and F_k are tabulated in Table IV.5. The angular distribution can then be written:

$$W(\theta, T) = 1 - 0.8191\, B_2(T)\, P_2(\cos\theta) + 0.3346\, B_4(T)\, P_4(\cos\theta)$$
$$+ 0.0169\, B_6(T)\, P_6(\cos\theta) - 0.0774\, B_8(T)\, P_8(\cos\theta) \; . \qquad \text{(IV.D.2)}$$

Table IV.5. F Coefficients and solid angle factors for ^{137m}Ce.

k	F_k	g_k
2	- 0.88902	0.9214
4	+ 0.44341	0.7545
6	+ 0.03197	0.5297
8	- 0.26243	0.2948

The minimum requirement for determining the $B_k(T)$ factors is that the form of the spin Hamiltonian be known. Kedzie et al.[91] have observed the electron spin resonance absorption of $^{141}Ce^{+3}$ $(I = 7/2)$ in the isomorphous, diamagnetic salt, lanthanum magnesium nitrate, and found hyperfine structure which they interpreted in terms of the spin Hamiltonian:

$$\mathcal{H}_o = g_{\parallel} \beta H_z S_z + g_{\perp} \beta(H_x S_x + H_y S_y) + A S_z I_z + B(S_x I_x + S_y I_y) \tag{IV.D.3}$$

where $B \gg A$. In the concentrated cerium salt spin-spin interactions will be present and should be included in the Hamiltonian. The spin-spin Hamiltonian $(\mathcal{H}_{ss})$ includes both dipolar $(\mathcal{H}_{dip})$ and interatomic exchange $(\mathcal{H}_{exc})$ terms and can be written:

$$\mathcal{H}_{ss} = \mathcal{H}_{exc} + \mathcal{H}_{dip} \tag{IV.D.4}$$

where

$$\mathcal{H}_{exc} = \sum_k J_{ik} \vec{S}_i \cdot \vec{S}_k \tag{IV.D.5}$$

and

$$\mathcal{H}_{dip} = \sum_k \left[\frac{\vec{\mu}_i \cdot \vec{\mu}_k}{r_{ik}^3} - \frac{3(\vec{\mu}_i \cdot \vec{r}_{ik})(\vec{\mu}_k \cdot \vec{r}_{ik})}{r_{ik}^5} \right]. \tag{IV.D.6}$$

In these equations the subscript i designates the ion of interest. J_{ik} is the exchange integral between ions i and k and r_{ik} the distance between them. In Eq. (IV.D.6) $\vec{\mu}$ is the magnetic moment of the atom and

$$\vec{\mu} = -\beta[g_{\perp}(S_x\,\hat{i} + S_y\,\hat{j}) + g_{\parallel}\,S_z\,\hat{k}]\ . \qquad \text{(IV.D.7)}$$

All the available calculations of spin-spin effects have neglected the exchange interaction and have considered only dipolar effects. This is a good approximation for CMN in the temperature region above 0.006°K where Daniels[23] has shown that the heat capacity of CMN is adequately explained by considering only dipolar interactions. The dipolar field has been calculated classically by Felsteiner[92] who finds an effective field of 60.67 Oe acting on the Ce^{+3} ions. Culvahouse et al.[93] have performed a quantum mechanical calculation using the density matrix formalism and find that the dipolar effects can be approximated by a weighted superposition of local fields at the Ce site for the high temperature region (i.e. above 0.006°K). This reduces to a local field of 58 Oe at the lower temperatures.

Because of the large distance (8.56 Å) between the Ce ions, the exchange interaction is small. We have therefore neglected the effects of exchange and have chosen the following spin Hamiltonian for the purpose of analysis:

$$\mathcal{H} = B(S_x\,I_x + S_y\,I_y) + g_{\perp}\,\beta\,H_x\,S_x \qquad \text{(IV.D.8)}$$

where we have set $A = 0$ and represented the dipolar interaction by a magnetic field $H_x = 60.67$ Oe.

3. Interpretation of Data, Numerical

The value of the hyperfine structure constant B was determined by normalizing our data to the results of Hudson and Kaeser[4] in the entropy range $0.063 \leq (\ln 2 - S/R) \leq 0.164$. The region was

arbitrarily chosen as the region over which there was substantial agreement between the two sets of results. The (T, S) results of Hudson and Kaeser were converted to (W(0), S) points with the aid of a computer program employing Eqs. (II.C.6), (II.C.7), (IV.D.2) and (IV.D.8) for various values of B. A smooth curve was drawn through these points and was compared to the W(0), S/R data in the above-mentioned entropy range. The best value of B was selected by the least squares criterion and was found to be: $B/k = 0.00820 \pm 0.00042\,°K$. For comparison purposes B was also determined for the case when $H_x = 0$ (i.e. no spin-spin interactions) and was found to be: $B/k = 0.00814 \pm 0.00043\,°K$. This is somewhat smaller than the value $B/k = 0.00864\,°K$ ($H_x = 0$) found by Frankel et al.[3] after normalization to the calorimetric results of Daniels and Robinson.[1]

With these values of B, W(0, T) was calculated by computer for values of 1/T in the range $0 \leq 1/T \leq 1000$. A plot of the results of these calculations is shown in Fig. IV.13. The values of W(0) in this figure have been corrected for the solid angle effects of the experimental geometry. The upper curve (a) refers to the case $H_x = 0$ and the lower curve (b) to $H_x = 60.67$ Oe. The two important features of this plot are that: W(0) is sensitive to temperature over the whole range of interest; and $H_x \neq 0$ lowers W(0) for a given value of 1/T.

The importance of the P_6 and P_8 terms in Eq. (IV.D.2) is indicated in Fig. IV.14. The abcissa represents the temperature determined from the k = 2 and k = 4 terms in the W(0) expansion. The ordinate denotes the (additive) change in 1/T when the k = 6 and k = 8 terms are included.

Figure IV.13. W(0) vs. 1/T.

The solid angle corrections are included in W(0). Curve (a) corresponds to $H_x = 0$ and curve (b) to $H_x = 60.67$ Oe.

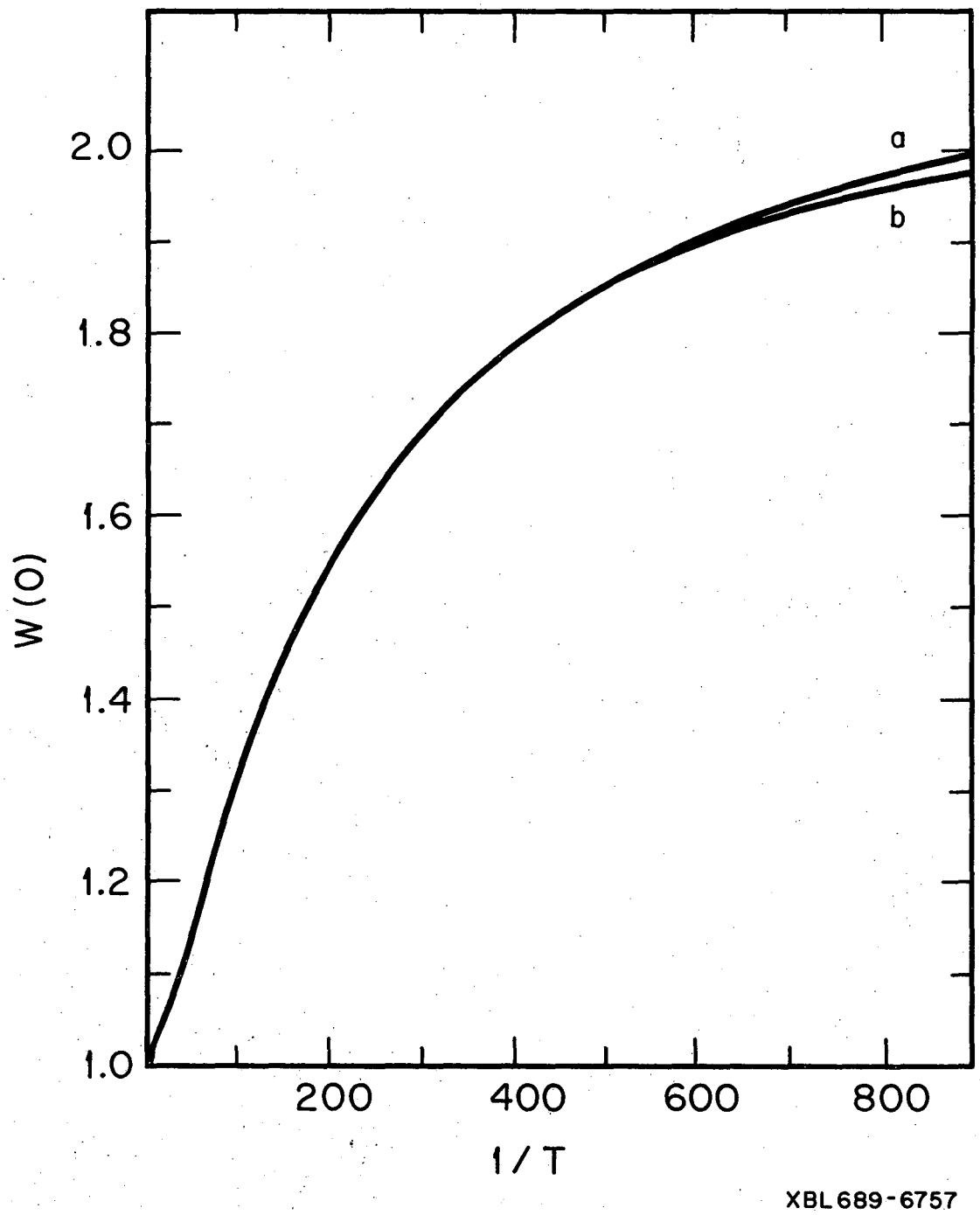

Fig. IV.13.

Figure IV.14. P_6 and P_8 Contribution ($B/k = 0.00820°K$; $H_x = 60.67$ Oe).

$(1/T)'$ is the temperature determined from the $k = 2$ and $k = 4$ terms in the $W(0)$ expansion. $\Delta 1/T$ is the (additive) change in $1/T$ when the $k = 6$ and $k = 8$ terms are included.

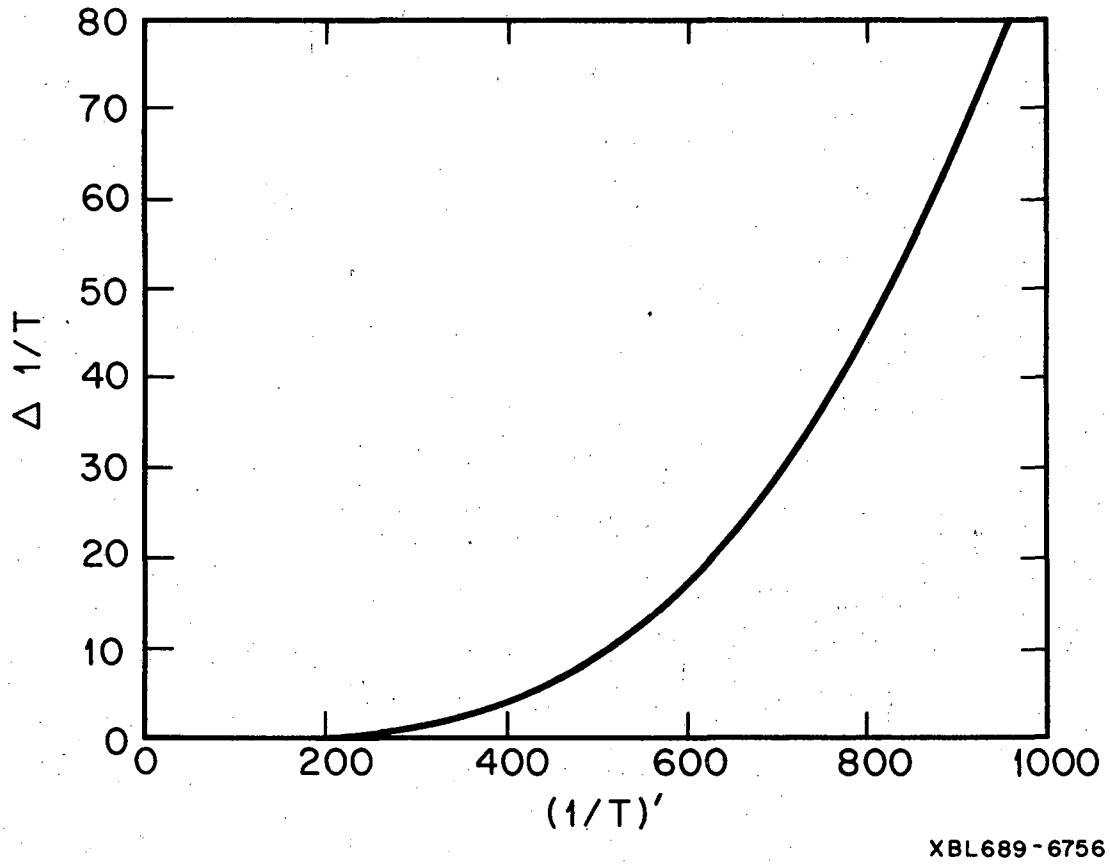

Fig. IV.14.

From the $W(0)$, T correlation established above, the $W(0)$ values in Tables IV.2, IV.3, and IV.4 were converted to absolute temperatures and are listed in the last two columns of those tables. In these tables T_H is a temperature (in millidegrees K) determined from the $W(0)$, T relation corresponding to $H_x = 60.67$ Oe and T_o the temperature for $H_x = 0$. In cases where there are two numbers in the error parentheses, the value $T(t_1, t_2)$ is to be read $T + t_1$ or $- t_2$. The error bars are not symmetric about T because $W(0)$ is not a linear function of T.

In Fig. IV.15, the temperature (T_H) is plotted as a function of S/R. The broken line corresponds to the calorimetric results of Hudson and Kaeser while the solid line is the best least squares computer fit to the data. For the $(T_H, S/R)$ data the fit was performed in two parts: a cubic equation for $0.002 \leq S/R \leq 0.312$ and a sixth order polynomial for $S/R > 0.312$. These equations joined smoothly with equal first derivatives at $S/R = 0.312$. In the upper region the following $(T, S/R)$ points from the Hudson and Kaeser results were included with a weight of ten to insure consistency between the smoothed results and the normalization procedure described previously: (2.93, 0.5063), (3.37), 0.5333), (3.90, 0.5595), (4.65, 0.5844), (5.14, 0.5963), (5.66, 0.6077), (6.18, 0.6185), (6.69, 0.6289). The same procedure was followed for the $(T_o, S/R)$ results and the smooth curves for the two sets of results are shown in Fig. IV.16. The largest difference between the two curves occurs at the lowest temperatures $(S/R = 0.002)$ and is approximately 0.06 m°K. The computer generated equations for the $(T, S/R)$ fits are given below.

Figure IV.15. S/R vs. T_H.

- - - - - - Hudson and Kaeser results

_____ computer generated curve to the present data (Eqs. IV.D.9 and IV.D.10).

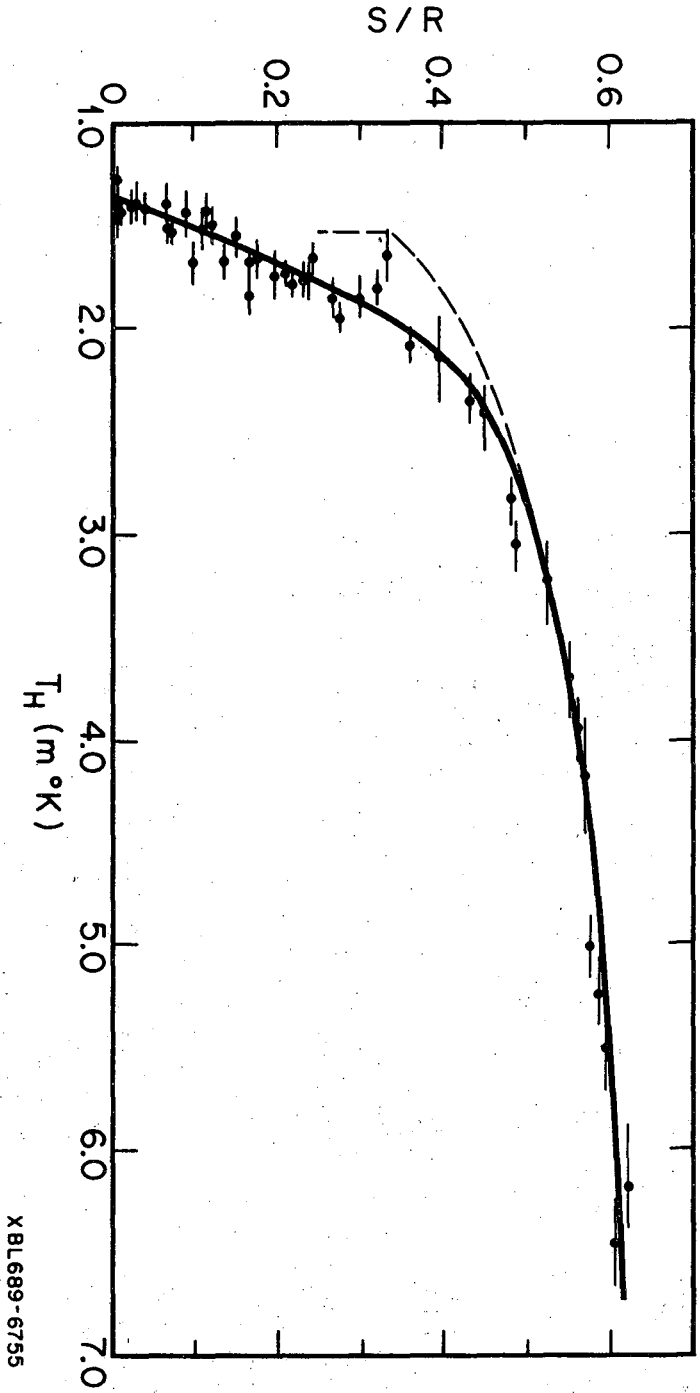

Fig. IV.15.

Figure IV.16. T_H and T_o vs. S/R.

a) T_H vs. S/R

b) T_o vs. S/R.

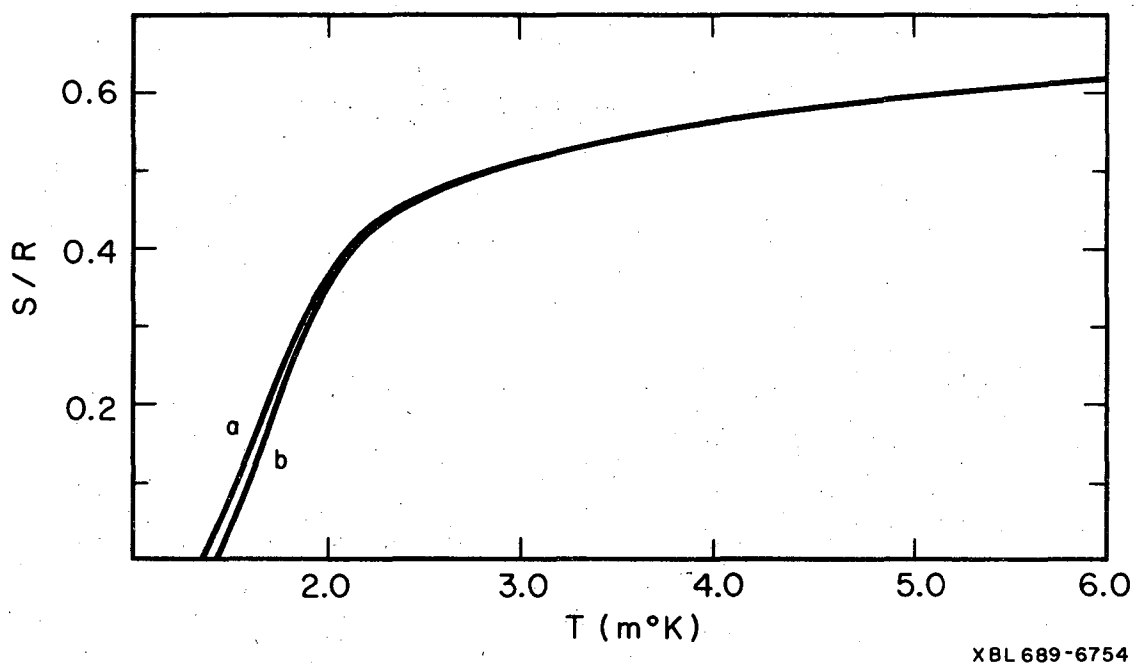

Fig. IV.16.

$$H_x = 60.67 \text{ Oe}$$

$$T_H = 1.3492 + 2.1458(S/R) - 3.2667(S/R)^2 + 5.8891(S/R)^3$$
$$\text{for} \quad 0.002 \leq S/R \leq 0.312 \qquad \text{(IV.D.9)}$$

$$T_H = 1.3768 - 0.31721(S/R) + 34.679(S/R)^2 - 228.58(S/R)^3$$
$$+ 721.32(S/R)^4 - 1145.6(S/R)^5 + 784.30(S/R)^6$$
$$\text{for} \quad 0.312 \leq S/R \leq 0.640 \qquad \text{(IV.D.10)}$$

$$H_x = 0$$

$$T_o = 1.4160 + 2.0082(S/R) - 3.3578(S/R)^2 + 6.3913(S/R)^3$$
$$\text{for} \quad 0.002 \leq S/R \leq 0.317 \qquad \text{(IV.D.11)}$$

$$T_o = 1.4402 - 0.071287(S/R) + 27.827(S/R)^2 - 184.32(S/R)^3$$
$$+ 595.02(S/R)^4 - 981.22(S/R)^5 + 704.53(S/R)^6$$
$$\text{for} \quad 0.317 \leq S/R \leq 0.640 \ . \qquad \text{(IV.D.12)}$$

Tables IV.6 and IV.7 list values of T_H and T_o calculated for various values of S/R from Eqs. (IV.D.9-12). The column labelled "SIGT" lists the computed standard deviations in T resulting from the curve fitting only; it does not include the uncertainty in the hyperfine structure constant B. The uncertainty in T_H and T_o resulting from uncertainty in B is tabulated in Table IV.8. In addition the heat capacity (C/R) and the enthalpy (H'/R) were calculated from Eqs. (IV.D.9-10) and are tabulated in Tables IV.6 and IV.7. H'/R is the function $(1000/R)[H(S/R) - H(S/R = 0.002)]$; i.e., the enthalpy curve

Table IV.6. Thermodynamic Functions for CMN; H_x = 60.67 Oe.

S/R	T_H	SIGT	C/R	H'/R
.002	1.354	.041	.635	0.
.004	1.358	.039	.640	.005
.006	1.362	.038	.646	.008
.008	1.366	.036	.652	.011
.010	1.370	.035	.658	.014
.020	1.391	.030	.688	.027
.030	1.411	.027	.718	.041
.040	1.430	.026	.748	.056
.050	1.449	.025	.778	.070
.060	1.467	.026	.807	.085
.070	1.485	.027	.837	.099
.080	1.503	.027	.866	.114
.090	1.520	.028	.894	.129
.100	1.537	.028	.921	.145
.110	1.554	.028	.947	.160
.120	1.570	.027	.971	.176
.130	1.586	.027	.994	.192
.140	1.602	.026	1.015	.207
.150	1.617	.026	1.035	.224
.160	1.633	.025	1.052	.240
.170	1.649	.025	1.067	.256
.180	1.664	.025	1.079	.273
.190	1.679	.025	1.089	.290
.200	1.695	.025	1.096	.306
.210	1.710	.026	1.101	.323
.220	1.726	.027	1.104	.341
.230	1.742	.028	1.104	.358
.240	1.757	.030	1.102	.375
.250	1.774	.031	1.097	.393
.260	1.790	.032	1.090	.411
.270	1.806	.032	1.082	.429
.280	1.823	.033	1.072	.447
.290	1.840	.034	1.060	.465
.300	1.858	.034	1.046	.484
.310	1.876	.034	1.032	.503

(continued)

Table IV.6. Continued

S/R	T_H	SIGT	C/R	H'/R
.320	1.898	.056	.985	.521
.330	1.918	.058	.928	.541
.340	1.939	.058	.870	.560
.350	1.962	.059	.812	.579
.360	1.988	.059	.754	.599
.370	2.015	.058	.697	.619
.380	2.046	.057	.643	.639
.390	2.079	.056	.590	.660
.400	2.116	.054	.541	.681
.410	2.157	.052	.495	.702
.420	2.203	.050	.453	.724
.430	2.255	.047	.413	.746
.440	2.313	.045	.377	.769
.450	2.378	.043	.345	.793
.460	2.451	.041	.315	.817
.470	2.534	.039	.289	.842
.480	2.627	.037	.265	.868
.490	2.732	.035	.244	.894
.500	2.851	.033	.226	.922
.510	2.985	.030	.209	.951
.520	3.137	.028	.195	.982
.530	3.308	.026	.182	1.014
.540	3.501	.024	.171	1.048
.550	3.719	.022	.161	1.084
.560	3.964	.021	.152	1.123
.570	4.240	.021	.145	1.164
.580	4.550	.022	.139	1.208
.590	4.898	.022	.133	1.255
.600	5.287	.022	.128	1.306
.610	5.723	.021	.124	1.361
.620	6.210	.019	.121	1.420
.630	6.753	.019	.118	1.485
.640	7.359	.028	.115	1.556

Table IV.7. Thermodynamic Functions for CMN; $H_x = 0$.

S/R	T_o	SIGT	C/R	H'/R
.002	1.420	.038	.712	0.
.004	1.424	.037	.719	.006
.006	1.428	.035	.725	.009
.008	1.432	.034	.732	.011
.010	1.436	.033	.739	.014
.020	1.455	.028	.773	.029
.030	1.473	.025	.808	.043
.040	1.491	.024	.842	.058
.050	1.509	.024	.877	.073
.060	1.526	.024	.911	.088
.070	1.542	.025	.945	.104
.080	1.558	.026	.978	.119
.090	1.574	.026	1.010	.135
.100	1.590	.026	1.040	.151
.110	1.605	.026	1.069	.167
.120	1.620	.026	1.096	.183
.130	1.634	.025	1.120	.199
.140	1.649	.025	1.142	.215
.150	1.663	.024	1.161	.232
.160	1.678	.023	1.178	.249
.170	1.692	.023	1.191	.266
.180	1.706	.023	1.201	.283
.190	1.720	.023	1.208	.300
.200	1.734	.024	1.211	.317
.210	1.749	.025	1.212	.334
.220	1.763	.026	1.209	.352
.230	1.778	.027	1.203	.370
.240	1.793	.028	1.195	.388
.250	1.808	.029	1.184	.406
.260	1.823	.030	1.170	.424
.270	1.839	.031	1.155	.442
.280	1.855	.031	1.137	.460
.290	1.872	.031	1.119	.479
.300	1.889	.032	1.099	.498
.310	1.906	.032	1.078	.517

(Continued)

Table IV.7. Continued.

S/R	T_o	SIGT	C/R	H'/R
.320	1.930	.056	1.046	.536
.330	1.949	.057	.989	.556
.340	1.970	.058	.929	.575
.350	1.992	.058	.868	.595
.360	2.016	.058	.806	.615
.370	2.042	.057	.745	.635
.380	2.071	.056	.685	.656
.390	2.103	.055	.627	.677
.400	2.138	.053	.573	.698
.410	2.177	.051	.522	.720
.420	2.222	.049	.475	.742
.430	2.271	.047	.432	.764
.440	2.327	.045	.392	.787
.450	2.390	.043	.357	.811
.460	2.462	.041	.325	.835
.470	2.542	.039	.296	.860
.480	2.634	.037	.271	.886
.490	2.738	.035	.248	.913
.500	2.855	.032	.229	.941
.510	2.988	.030	.211	.970
.520	3.139	.028	.196	1.000
.530	3.309	.025	.183	1.033
.540	3.501	.023	.171	1.067
.550	3.719	.022	.161	1.103
.560	3.964	.021	.153	1.141
.570	4.239	.021	.145	1.182
.580	4.549	.022	.139	1.226
.590	4.897	.022	.133	1.273
.600	5.287	.022	.128	1.324
.610	5.723	.020	.124	1.379
.620	6.210	.018	.121	1.439
.630	6.754	.019	.118	1.503
.640	7.359	.028	.115	1.574

Table IV.8. HFS Error in T.

T_H(m°K)	$+\Delta T_H$	$-\Delta T_H$	T_o(m°K)	$+\Delta T_o$	$-\Delta T_o$
6.67	0.34	0.35	6.67	0.35	0.35
5.0	0.27	0.25	5.0	0.27	0.26
4.0	0.22	0.20	4.0	0.21	0.21
3.33	0.18	0.16	3.33	0.18	0.17
2.86	0.15	0.15	2.86	0.15	0.15
2.50	0.14	0.13	2.50	0.14	0.13
2.22	0.12	0.11	2.22	0.12	0.11
2.00	0.11	0.10	2.00	0.11	0.11
1.82	0.10	0.09	1.82	0.10	0.10
1.67	0.09	0.09	1.67	0.09	0.09
1.54	0.09	0.08	1.54	0.08	0.08
1.43	0.09	0.07	1.43	0.08	0.07
1.33	0.09	0.06	1.33	0.08	0.06
1.25	0.08	0.06	1.25	0.08	0.06

was not extrapolated to $S/R = 0.0$. C/R and H'/R are plotted as a function of T_H in Figs. IV.17 and IV.18. The maximum in the heat capacity presumably indicates the onset of antiferromagnetism.[94] Only qualitative significance should be placed on the heat capacity values however since they result from differentiation of the $T(S)$ function and are very sensitive to the curve fitting. The apparent failure of the heat capacity to obey the third law of thermodynamics results from the fact that the empirical $T(S)$ function does not approach zero with zero slope. This, however, is only an artifact of the curve fitting and has no physical significance. The enthalpy function, which results from an integration of the $T(S)$ function, should be much more reliable.

E. Discussion

The various temperature scales for single crystal CMN are plotted in Fig. IV.19. In this figure the present work (curve b) is represented by the $(T_H, S/R)$ data. Two curves are given for the Frankel, Shirley, and Stone[3] results, one of which (curve c) has been renormalized to the calorimetric results of Hudson and Kaeser[4] for $T > 0.006°K$. The normalization yielded a value of $B/k = 0.00826°K$ for $H_x = 60.67$ Oe. The value of B is slightly higher than reported in this work because of a difference in the high temperature nuclear orientation results for the two sets of data. Despite the renormalization of the earlier nuclear orientation results, a systematic discrepancy between this work and that of Frankel *et al.* still exists.

Figure IV.17. C/R vs. T_H.

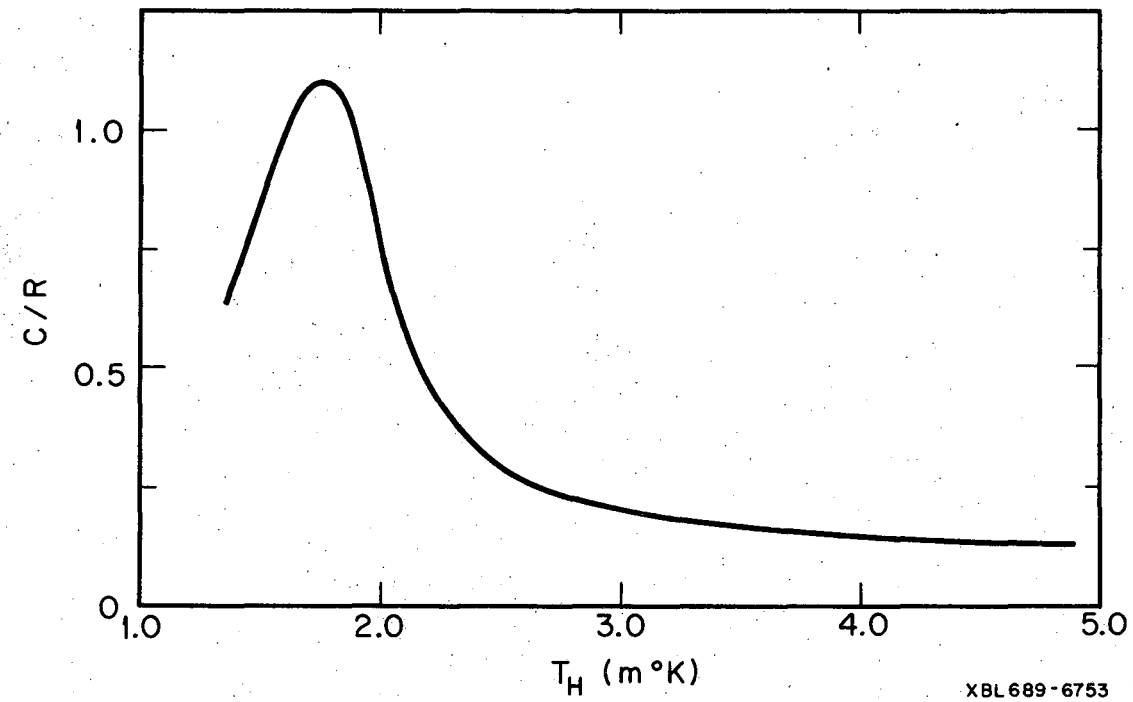

Fig. IV.17.

Figure IV.18. H'/R vs. T_H.

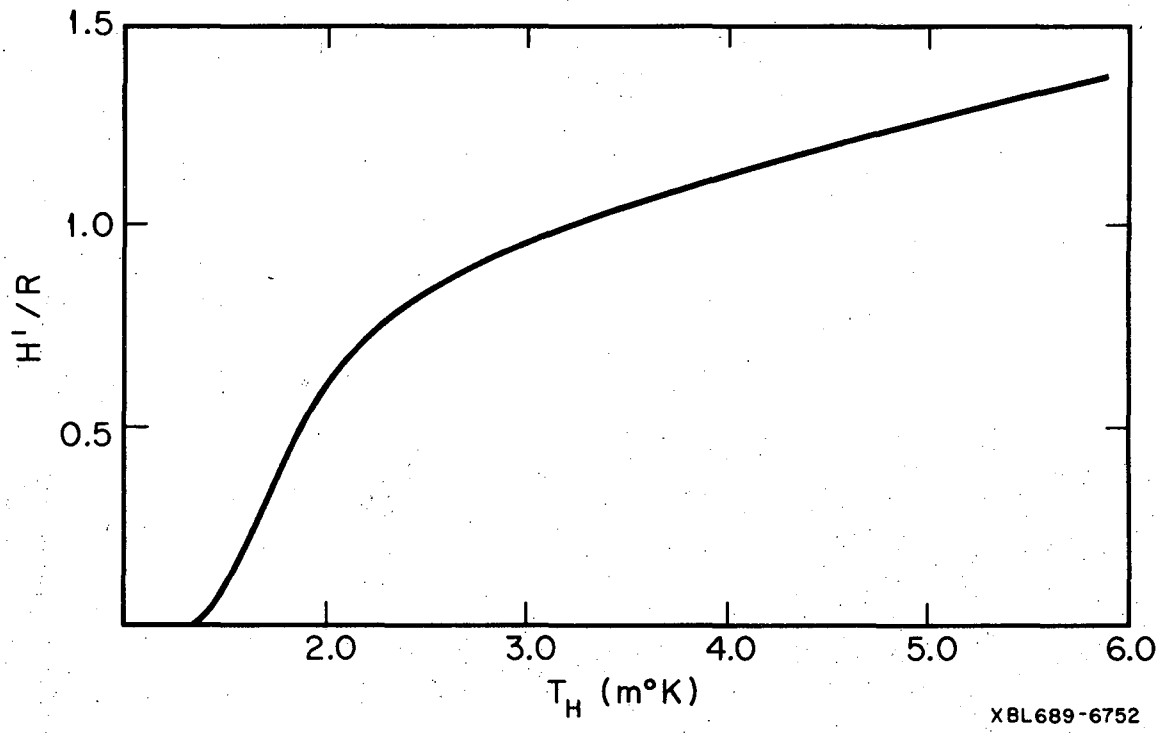

Fig. IV.18.

Figure IV.19. S/R vs. T.

a) Hudson and Kaeser[4].

b) This work (T_H vs. S/R).

c) Frankel, Shirley, and Stone (modified to $B/k = 0.00826°K$ and $H_x = 60.67$ Oe).

d) Frankel, Shirley, and Stone[3] (as published).

e) de Klerk[2].

f) Daniels and Robinson[1].

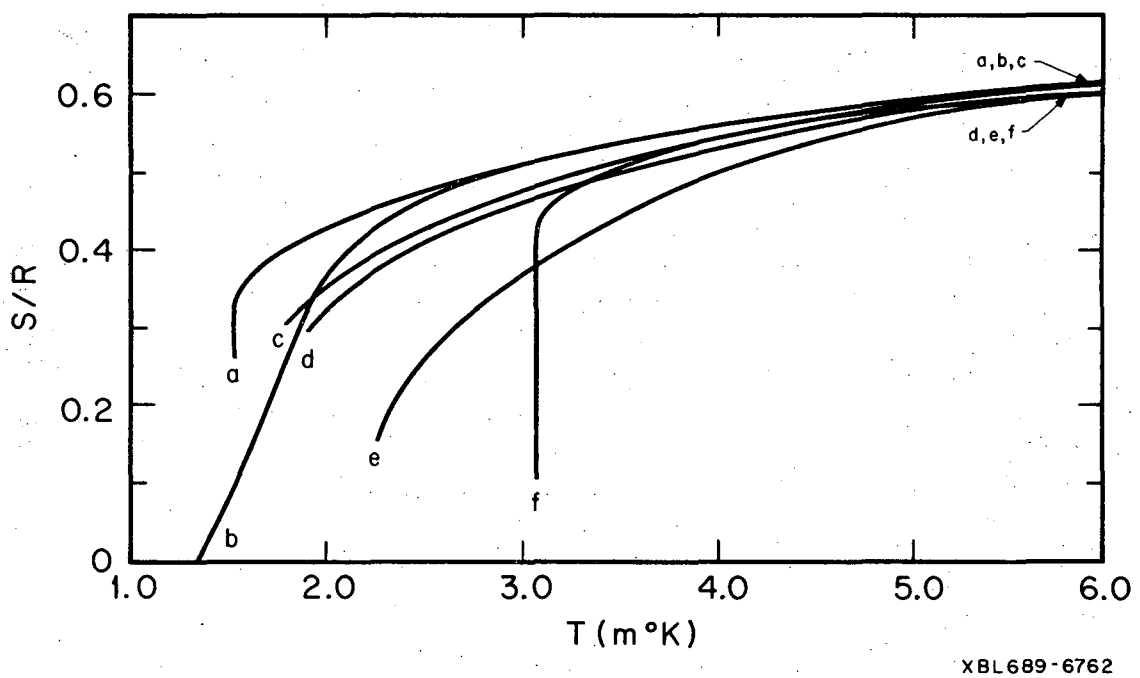

Fig. IV.19.

The two sets of data are compared on a more basic level in Fig. IV.12 where the smoothed $W(\theta)$ vs. $\ln 2 - S/R$ curves are shown along with the data points from the present experiment. The curve representing these data was derived from the computer generated entropy – temperature correlation resulting from the best fit to the $(T_H, S/R)$ data (c.f. Eqs. (IV.D.9) and (IV.D.10)). The temperatures were then converted to $W(0)$ values from the $W(0)$, T correlation illustrated in Fig. IV.13. It should be noted that our smooth curve in Fig. IV.12 is heavily weighted to the Hudson and Kaeser data for $\ln 2 - S/R \leq 0.187$. Inspection of the data of Frankel et al. reveals that the scatter in their data is somewhat greater than in the present work. As is evident from Fig. IV.12, the Frankel, Shirley, and Stone results fall systematically below the present results for most of the common entropy range. Most of this discrepancy presumably arises in the calculation of γ-ray intensities. As was discussed in Section IV.C, great care was taken in calculating the background corrections in this work, and the chances of serious error in this research appear to be less than in that of Frankel, Shirley, and Stone. In light of the difficulty of making measurements at these low temperatures, however, the disagreement between the two sets of results cannot be considered serious.

The close agreement between our work and that of Hudson and Kaeser above 2.8 m°K is due primarily to our normalization procedure for determining the hyperfine structure constant B and does not test the validity of their data. The two sets of data are compared in somewhat more detail in Fig. IV.20. The lightly-shaded area indicates the

Figure IV.20. Comparison of Experimental Errors.

Lightly shaded area - error limits on the Hudson and Kaeser curve.

Darkly shaded area - error limits due to uncertainty in B for present work.

Inner unshaded (or lightly shaded area) - statistical curve fitting error in present work.

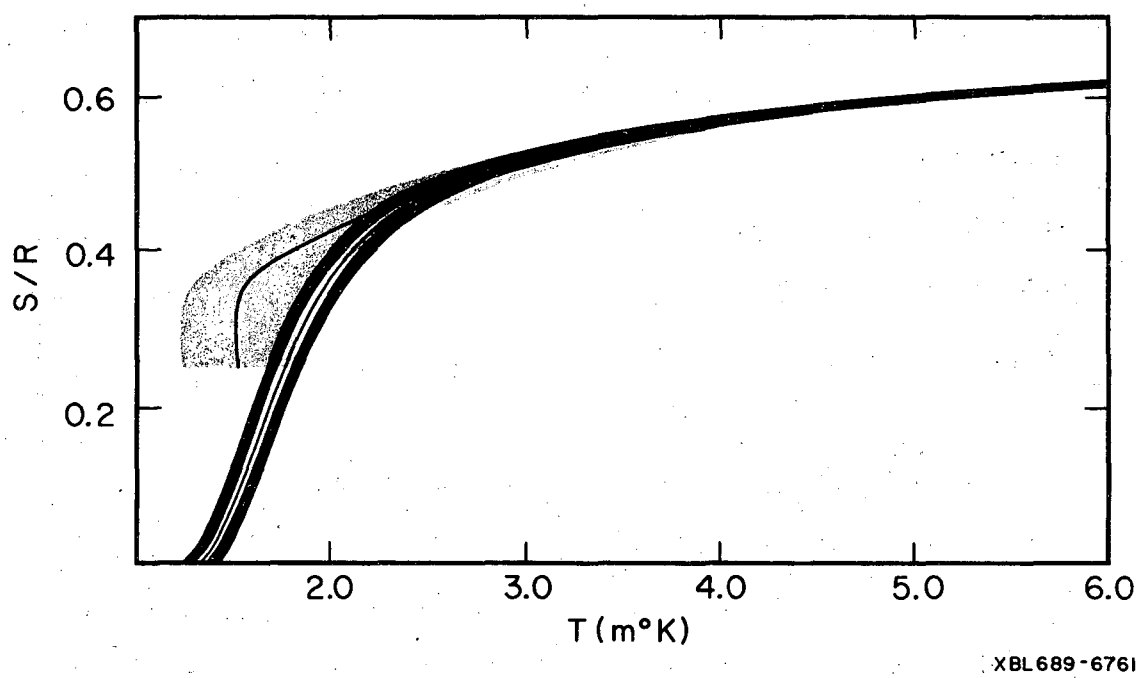

Fig. IV.20.

error range which Hudson and Kaeser assigned to their data. The darkly shaded area around the smooth curve from this work represents the uncertainty in T_H resulting from the uncertainty in B, and the inner unshaded (or lightly shaded) area is the statistical curve-fitting error. The two sources of error in this work are represented separately since error arising from an uncertainty in B is – in a sense – a systematic error with respect to the (T, S) curve. As is evident, the two curves agree within overlapping error bars over the common range of entropies and below 2 m° K the error bars associated with the present work are smaller by more than a factor of two.

Although there is agreement within overlapping error bars, there is still a systematic disagreement between the two curves for temperatures less than 2.8 m°K. In the calorimetric method the temperature is obtained by differentiating the experimental Q, S relation as was discussed in Section II.B. Further insight can be gained by comparing the calorimetric Q, S relation with the H, S relation found by integration of the present T_H, S results. In curve (b) of Fig. IV.21 values of $Q''/R = (1000/R)[Q(S/R) - Q(S/R = 0.043)]$, which have been read from Fig. 5 of Hudson and Kaeser's[4] paper are plotted. The shaded area represents an r.m.s. error for Q''/R of 0.02 which probably slightly overestimates the error at any given point. Curve (a) corresponds to the computed values of enthalpy from the present work: $H''/R = (1000/R) \times [H(S/R) - H(S/R = 0.043)]$. The error bars on this curve are statistical curve-fitting errors only and do not take into account uncertainties in the hyperfine structure constant. Inclusion of this uncertainty

Figure IV.21. Heat Content vs. T.

a) $\frac{H''}{R} = \frac{1000}{R} [H(S/R) - H(S/R = .043)]$

from the present work.

b) $\frac{Q''}{R} = \frac{1000}{R} [Q(S/R) - Q(S/R = .043)]$

from Figure 5 of Hudson and Kaeser's paper.

The shaded areas represent the limits of error for the two curves. The solid circles represent data points read from Figure 5 of Hudson and Kaeser's paper.

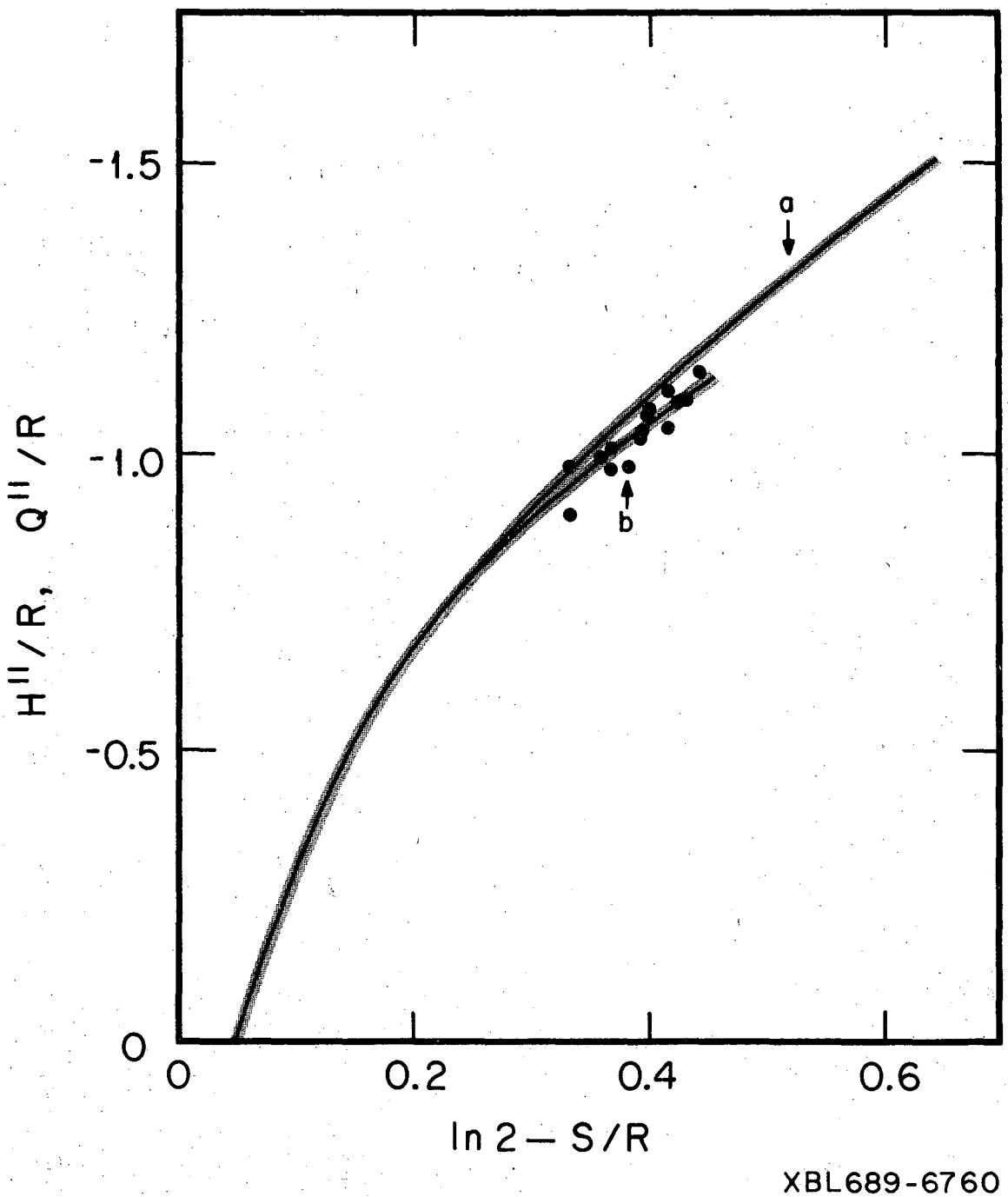

Fig. IV.21.

would lengthen the error bars by about 40% at $\ln 2 - S/R = 0.45$.

The two curves correspond almost exactly until $\ln 2 - S/R \approx 0.275$, but the derived temperatures are somewhat different. At this entropy Hudson and Kaeser report 1.94 m°K while our results give $T_H = 2.19$ m°K. It is reasonable to assume that the difference arises primarily from difficulty in measuring the derivative dQ/dS in the calorimetric work. At $\ln 2 - S/R \approx 0.45$, the deviation between the two curves appears to be outside experimental error. Hudson and Kaeser report that the actual differentiation of their Q, S curve yielded a T, S curve which curled toward higher temperatures at the lowest entropies. Although this is physically impossible, it would be equivalent to the fitted Q, S curve curling upward for $\ln 2 - S/R > 0.40$. This would have the effect of bringing curves (a) and (b) closer together. Any experimental scatter near the end point of the calorimetric data will cause rather large statistical (curve-fitting) errors both in the Q, S curve and in the slope (i.e. T). The conclusion to be drawn is that the calorimetric method probably breaks down at the lowest temperatures and that the nuclear orientation results provide a more reliable picture of the physical situation.

Two alternative explanations for the discrepancy at the lowest temperatures should be considered. The first concerns the possibility of significant systematic errors in the data reduction methods of this research. As mentioned earlier in this discussion, the method of background correction is the most likely candidate. Any systematic error in this correction, however, would effectively shift the T, S curve

along the temperature axis and would not change the general shape of the curve. The change in the background correction necessary to bring the two sets of data into agreement appears to be unreasonably large and does not seem justified with respect to the criteria of Section IV.C. The other possibility concerns a radical change (not unusual in Berkeley) of the spin Hamiltonian as the antiferromagnetic Neél point is approached. It is more likely, however, that the onset of antiferromagnetism can be approximated by a continuous increase in H_x as the temperature is lowered. The net effect of this would be to move the T_H, S curve toward lower temperatures; this is somewhat analogous to the situation depicted in Fig. IV.15. The general shape of the T_H, S curve, however, would be maintained.

One final point should be considered. If Williamson and Cape[75] are correct in their assertion that the simple ionic model is no longer valid for $H/T > 7$ kOe/°K, then all the temperatures below 5.8 m°K in the calorimetric work are incorrect. In our experiment S/R would become merely a parameter related to H/T, and the temperature would be known as a function of H/T. Since the value of the hyperfine structure constant B was determined by normalizing the present nuclear orientation results to the calorimetric results of Hudson and Kaeser[4] in the range 6 kOe/°K $\leq$ H/T $\leq$ 10 kOe/°K, a re-adjustment in B would be expected. However, the close agreement between the hyperfine structure constant found in this work and that derived by renormalizing the results of Frankel et al.[3] for $H/T \leq 7$ kOe/°K suggests that the present value of B is satisfactory. Thus the temperatures reported here are not affected.

The effect of Williamson and Cape's magnetization measurements on the calculation of entropy is discussed in Appendix A. From the values given there, an adjusted (T_H, S/R) relation is shown in Fig. IV. 22 where curve (a) is based on Williamson and Cape's measurements and curve (b) is based on the simple ionic model. As was emphasized in Appendix A curve (a) should be regarded as only qualitatively correct because of the difficulty in calculating the "non-ideal" contribution to the entropy. As is evident, the two curves differ only slightly over the whole entropy range. From the calculations of Appendix A the Hudson and Kaeser data were also adjusted to the measurements of Williamson and Cape. The results of this modification (which also is only qualitatively correct) are depicted in Fig. IV. 22 where (d) is Hudson and Kaeser's original curve and (c) is the modified curve. As is apparent, the effect of the modification is small but in the direction which reduces the disagreement between the calorimetric and nuclear orientation results.

Although the resultant changes in the T-S relations are small for both cases, it seems imperative that a complete study of the magnetic properties of CMN along the lines of the Williamson and Cape experiment be undertaken. Measurements of the magnetization as a function of both T and H would be highly desirable. These measurements should be extended at least to 0.3°K so that the H/T measurements in this work can be given a rigorous thermodynamic interpretation.

Figure IV.22. T vs. S/R.

Curve a Present results with entropy calculated on the basis of Williamson and Cape's results.

Curve b Present results with entropy calculated on the basis of the simple ionic model.

Curve c Modified Hudson and Kaeser results.

Curve d Original Hudson and Kaeser results.

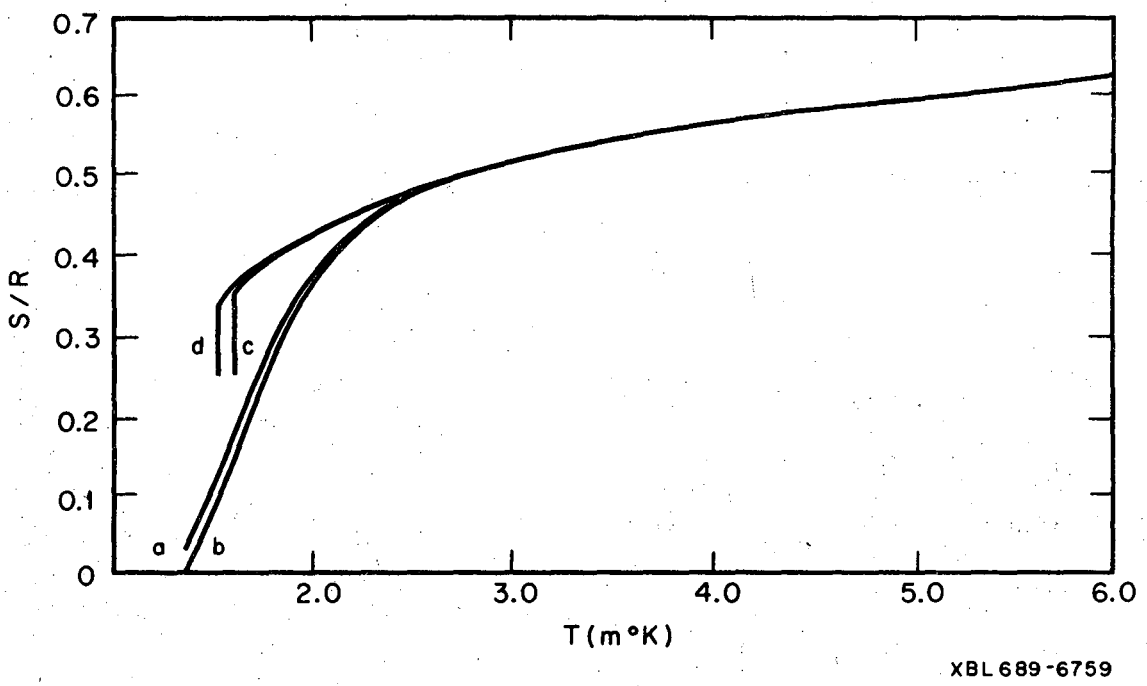

Fig. IV.22.

V. THE NUCLEAR ORIENTATION OF ^{137m}Ce IN CERIUM ZINC NITRATE: PRELIMINARY RESULTS

In this section the preliminary results of a nuclear orientation experiment for ^{137m}Ce in cerium zinc nitrate (CZN) are presented. This salt has also been used in low temperature experiments, but its thermodynamic properties have never been investigated. It therefore seemed worthwhile to use the ^{137m}Ce thermometer to study the low temperature behaviour of CZN.

A. Theoretical

CZN has been primarily studied by Culvahouse, Sapp, and colleagues at the University of Kansas. They have measured the electronic g-factors of a CZN crystal with a small amount of Co substituted for the Zn and have found $g_{\perp} = 1.823 \pm 0.007$[95] and $g_{\parallel} = 0.125$.[96] Thornley[68] has measured the far infrared spectrum of CZN and has determined the splitting between the two lowest Kramers' doublets to be $\Delta_{12}/k = 30.2 \pm 0.4°K$. These values are quite similar to the values found for CMN (c.f. Table IV.1) and seem to indicate that CMN and CZN have similar crystal field properties.

Culvahouse *et al.*[96] have investigated the crystal structure of CZN by the x-ray powder diffraction technique and find unit cell dimensions similar to those of Zalkin *et al.*[61] A Laue photograph of single crystal CZN with the x-ray beam along the trigonal axis indicated C_{3v} symmetry in contradiction with the C_{3i} symmetry found by Zalkin *et al.* for CMN. Furthermore, investigation of the divalent sites in CZN by

paramagnetic resonance[96] gave results which are in disagreement with the findings of Zalkin et al. for CMN. It seems unlikely that the structures of CMN and CZN are significantly different, but only a thorough crystallographic study will decide this question.

CZN has previously been used in nuclear orientation experiments, but the absence of a temperature scale for this salt has hampered the interpretation of the data. Levi et al.[95] have studied the nuclear orientation of ^{60}Co in CZN and found a considerably larger anisotropy than found for ^{60}Co in CMN.[97,98] They interpreted the CZN results in terms of a temperature dependent local magnetic field set up at the Co X sites and zero magnetic field at the Co Y sites with the ratio Co in X/Co in Y = 1.6. (There are two types of divalent sites; c.f. Section IV.A. and Ref.61.) The limiting field was found to be 165 Oe in contrast with the 66.71 Oe field calculated at a Mg site in CMN by Daniels and Felsteiner.[94] Carboni and Sapp,[99] however, have pointed out that the paramagnetic Co^{+2} ion will perturb the Ce long range order and that the spatial reversal of one nearest neighbor Ce dipole would more than compensate for the difference. Carboni and Sapp also suggested that the ^{60}Co in CMN results could be explained by a local field of 165 Oe, (Co in X)/(Co in Y) = 2, and a lowest temperature of 1.05 m°K.

The temperature invoked by Carboni and Sapp for CMN is inconsistent with the results presented in Section IV.D, and the temperatures in the CZN experiments were not well known. The data which is presented below suggests a high degree of similarity in the thermal properties of the two salts, but because of the unfortunate lack of data, especially at the lowest temperatures, no firm conclusions can be drawn.

B. Experimental and Results

The experimental technique and method of data reduction were identical to that described in Sections III and IV of this paper. A spectrochemical analysis[85] of the CZN crystal indicated a 1% Mg impurity - presumably as a substitutional impurity for Zn. Analysis of the solution from which the CZN crystals were grown, however, showed only 0.07% Mg. The apparent conclusion is that the double nitrate lattice exhibits a large preference for the smaller Mg^{+2} ion.

The results are listed in Table V.1 where the values of S/R have been calculated from H/T and $g_{\perp} = 1.823$ on the basis of the simple ionic model. The values of $W(\theta)$ are corrected for radioactive decay between the cold and warm counts but not for solid angle effects. The background correction in the calculation of $W(\theta)$ amounted to about 11% of the warm count. In Fig. V.1 $W(0)$ is plotted with respect to $\ln 2 - S/R$. The scarcity of data for $\ln 2 - S/R > 0.50$ is due to a failure in the apparatus. The solid curve through the data represents the $(W(0), \ln 2 - S/R)$ correlation derived from the smoothed T_H, S/R curve for CMN. The solid angle corrections, which were identical for the two experiments, are incorporated into the curve. The shaded area around the curve denotes the statistical curve fitting error from the CMN data.

Table V.1. ^{137m}Ce in CZN.

H/T	S/R	W(0)	W(π/2)
41.52	.037	1.953 (15)	.7045 (76)
14.22	.420	1.821 (15)	.7298 (66)
12.84	.460	1.768 (15)	.7216 (89)
10.60	.518	1.715 (23)	.7407 (80)
8.839	.565	1.610 (17)	.7731 (93)
6.797	.613	1.496 (22)	.7716 (156)
16.10	.369	1.879 (25)	.7218 (75)
17.86	.325	1.871 (15)	.7156 (76)
19.98	.276	1.884 (13)	.7237 (60)
22.79	.218	1.877 (14)	.7107 (72)

The numbers in the parentheses indicate one standard deviation and refer to the last significant figures in the listed quantity. W(0) and W(π/2) have not been corrected for solid angle effects. For $H/T < 45$ kOe/°K, $T \approx 0.5$°K.

Figure V.1. ^{137m}Ce in CZN vs. $\ell n2$ - S/R.

The solid curve represents the (W(0), $\ell n2$ - S/R) correlation derived from the smoothed T_H, S/R curve for CMN.

The shaded area represents the statistical curve fitting error.

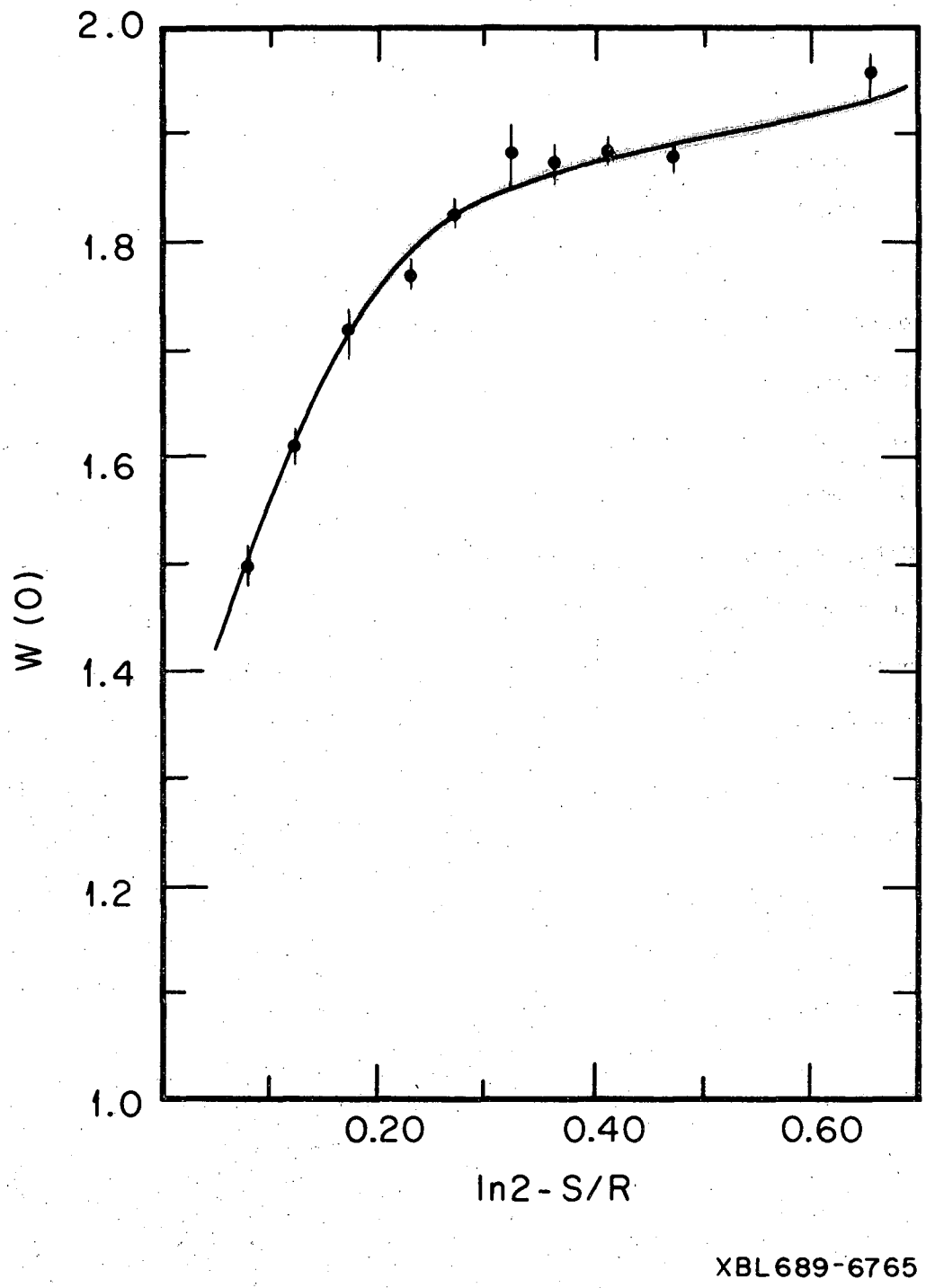

Fig. V.1.

C. Discussion

Despite the small number of data points it is evident that the thermal behaviour of CZN and CMN are quite similar. No reliable data was obtained in the entropy range $0.50 \leq \ln 2 - S/R \leq 0.60$, and so "anomalous" behaviour in this region cannot be ruled out. The point at $\ln 2 - S/R = 0.656$, however, was confirmed in other experiments but difficulties with the apparatus prevented the acquisition of any further data. The additional points at $\ln 2 - S/R = 0.65$ are not included in this data. The lack of any calorimetric work on CZN prevents the determination of the hyperfine structure constant B for ^{137m}Ce in CZN, and therefore actual temperatures for CZN cannot be derived from this data. However, from the similarity in the nuclear orientation data for ^{137m}Ce in CZN and CMN, it can be concluded that the hyperfine structure constants for the two cases must be very nearly the same. If this is the case, then the minimum temperature obtainable with CZN is about 1.35 m°K.

In light of the results presented here, the early nuclear orientation work on CZN should probably be re-interpreted. For example, as was mentioned earlier, Levi *et al.*[95] derived a dipolar field of 165 Oe acting on a $^{60}Co^{+2}$ ion in a CZN X site from their nuclear orientation data. They based their interpretation on a minimum $T^* \approx 3.3$ m°K after demagnetization from $H/T \approx 26.8$ kOe/°K. If the CZN and CMN T-S relations are identical, then the thermodynamic temperature for this value of H/T is 1.67 m°K. With this temperature, however, the results of Levi *et al.* are reasonably well explained by the calculations

of Daniels and Felsteiner[94] who derive a dipolar field of 66.71 Oe at the Co site. Furthermore the disagreement between the ^{60}Co in CMN results and the ^{60}Co in CZN results are difficult to understand since the thermal properties of the two salts seem so similar. If the dipolar fields acting on the Co^{+2} ions are equal for the two salts, then the only remaining variable is the ratio (Co in X/Co in Y). Since the X and Y sites have quite different hyperfine structure constants,[99] a large difference in the X/Y ratio between the two salts would have a significant effect on the nuclear orientation results and could account for the disagreement. To resolve these questions, it is clear that further nuclear orientation, calorimetric, and magnetic resonance work is required before the properties of CZN are well understood.

APPENDICES

A. The Magnetization of CMN as a Function of Magnetic Field

High field magnetization measurements on CMN have recently been reported by Williamson and Cape.[75] From their data they concluded that the ionic crystal field model is not valid for CMN and that entropy calculations based upon this model are incorrect. The purpose of this appendix is to examine their conclusion and calculate the effect on our results.

Williamson and Cape have measured the magnetization of CMN in fields up to 52 kOe and at temperatures between 1.2°K and 4.2°K. They have interpreted their data according to the following expression:

$$\frac{M}{N} = \frac{g_\perp \beta}{2} \tanh(x) + [\beta^2 H(|a'|^2 + |b'|^2)/2\Delta_{12}] \times \left[1 - \left(3\frac{g_\perp \beta H}{4\Delta_{12}}\right) \tanh(x)\right] + \frac{\beta^2 H}{2\Delta_{13}}(|c'|^2 + |d'|^2) \tag{A.1}$$

where $x = g_\perp \beta H/2kT$

Δ_{12}, Δ_{13} are the energy splittings between the lowest Kramers' doublet and the two excited doublets.

N is Avogadro's number.

a' is the matrix element of $\mathcal{H} = \beta H(L_x + 2S_x)$ connecting one of the correct zero-order ground states with one of the first excited states.

b' is the matrix element between the same ground state and the other first excited state.

c',d' are the matrix elements between this ground state and the second two excited states.

This equation is valid to a high precision for the following three conditions which are satisfied for Ce^{+3} in CMN:

1) $g_{\perp} \beta H/2 \ll \Delta_{12}$
2) the g-factor of the first excited doublet ≈ 0.
3) the matrix elements c and d are less than the larger of a or b.

The terms in Eq. (A.1) which are linear in H correspond to the second order temperature independent contirubtion to the susceptibility.*

*The temperature independent contribution to the susceptibility is defined by Eq. (A.2)

$$\chi = \frac{M}{H} = \frac{C'M}{T} + \alpha_o \qquad (A.2)$$

From Eq. (A.1)

$$\alpha_o H = \frac{\beta^2 H}{2\Delta_{12}} \left(|a'|^2 + |b'|^2\right) + \frac{\beta^2 H}{2\Delta_{13}} \left(|c'|^2 + |d'|^2\right) \qquad (A.3)$$

The third order effect of the first excited doublet is accounted for in the multiplicative term $[1 - (3g_\perp \beta H/4\Delta_{12}) \tanh(x)]$, while third order effects from the second excited doublet are neglected.

Williamson and Cape obtained C'_M from their magnetization data and took the value of α_o/C'_M from the data of Leask, et al.[65] To test the ionic crystal field model, they subtracted the quantity $\alpha_o H\left[1 - \frac{3g_\perp \beta H}{4\Delta_{12}} \tanh(x)\right]$ from their magnetization data. The modified data (defined by them as M'/N) should be expressed by Eq. (A.4)

$$\frac{M'}{N} = \frac{g_\perp B}{2} \tanh(x) \quad . \tag{A.4}$$

From Eqs. (A.1) and (A.2) it can be seen that the third order effects are slightly overemphasized. Detailed calculations show that this discrepancy is insignificant.

Williamson and Cape presented data for two samples designated CMN #3 and CMN #4. In Fig. 1 of their paper they plot $(2M/Ng_\perp B)$ vs. H for CMN #3 and in Fig. 2 $(2M'/Ng_\perp B)$ vs. H/T for both samples. In the second figure the data for CMN #4 are systematically less (~1%) than for CMN #3 for $H/T > 15$ kOe/°K. We have read points off the smooth curve in Fig. 1 (from an enlarged version in a preprint kindly sent to us by Dr. Williamson) and will compare detailed calculations which we have made with these points.

We have calculated the magnetization of CMN by perturbation theory through third order and have included effects from both excited doublets. The perturbation Hamiltonian is $\mathcal{H} = \beta H_x(L_x + 2S_x)$, and

we have used the crystal field splittings and the zero order wave functions derived by Leask et al.[65] from magnetic susceptibility data. These wave functions are given in L_z, S_z quantization and are linear combinations of $|M_L, M_S\rangle$ where $-3 \leq M_L \leq +3$ and $M_S = \pm 1/2$. If we designate Leask's wave functions as $|a\rangle$, $|b\rangle$, $|c\rangle$, $|d\rangle$, $|e\rangle$, $|f\rangle$, then it is easy to show that the correct zero-order functions to use in the perturbation theory are:

$$\psi_1^o = \frac{1}{\sqrt{2}} \left(|a\rangle + |b\rangle\right)$$

$$\psi_2^o = \frac{1}{\sqrt{2}} \left(-|a\rangle + |b\rangle\right)$$

$$\psi_3^o = |c\rangle$$

$$\psi_4^o = |d\rangle$$

$$\psi_5^o = \frac{1}{\sqrt{2}} \left(|e\rangle + |f\rangle\right)$$

$$\psi_6^o = \frac{1}{\sqrt{2}} \left(|e\rangle - |f\rangle\right)$$

The effect of the first order perturbation is depicted in Fig. A.1. In first order the degeneracy between $|c\rangle$ and $|d\rangle$ is not removed. Leask et al. give the values of Δ_{12}/k and Δ_{13}/k as 37.6°K and 83.8°K respectively.

Using the third order perturbation formula given by Powell and Craseman[100] the energies of the levels in the lowest Kramers doublet were calculated to be:

Figure A.1. First Order Zeeman Diagram for Ce^{+3} in CMN.

The splittings are not drawn to scale.

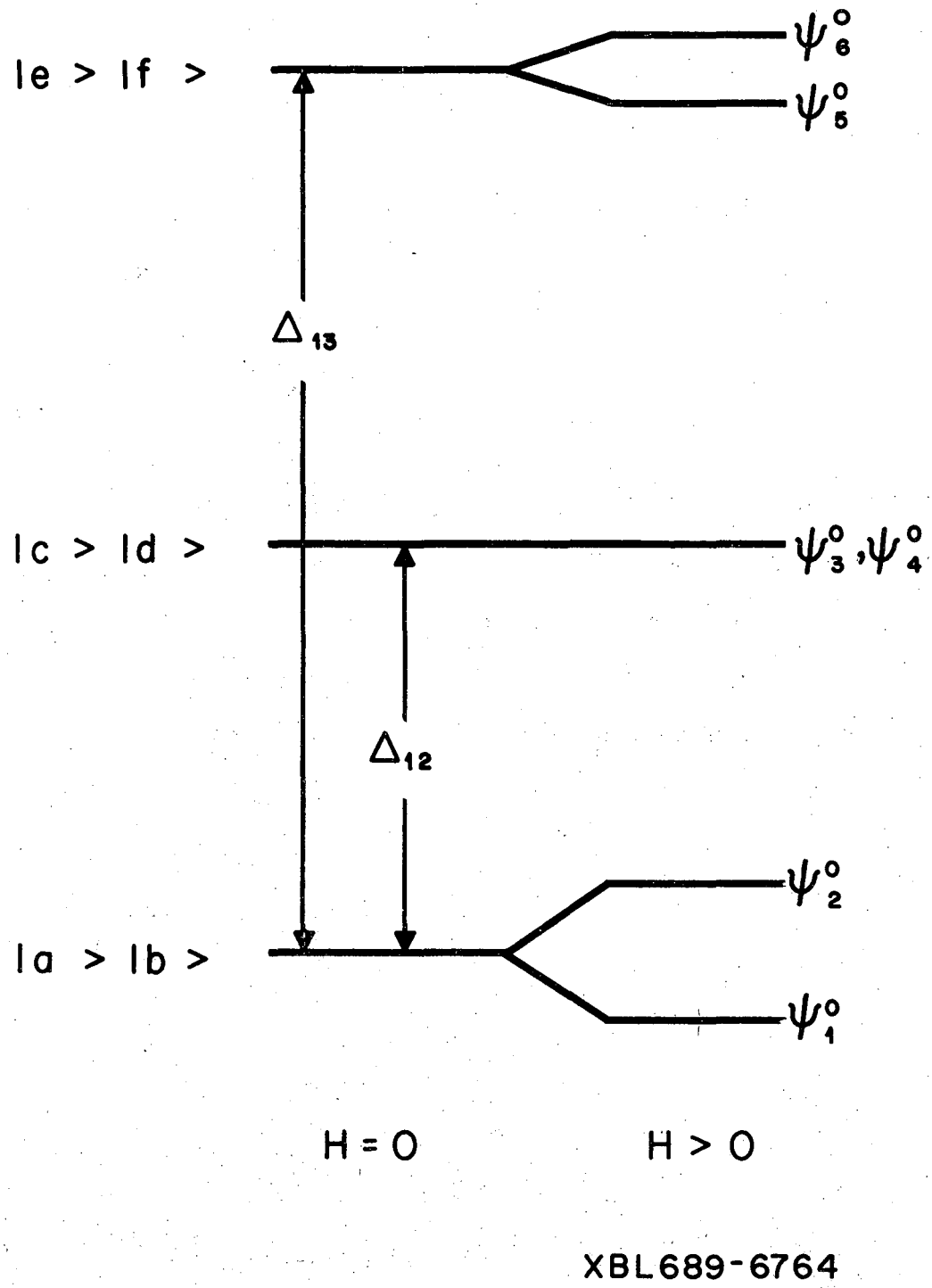
|e > |f >
ψ_6^0
ψ_5^0
Δ_{13}
|c > |d >
ψ_3^0, ψ_4^0
Δ_{12}
ψ_2^0
|a > |b >
ψ_1^0
H = 0
H > 0
XBL689-6764

Fig. A.1.

$$E_1 = -\frac{g_\perp}{2}\beta H - B\frac{\beta^2 H^2}{k} + C\frac{\beta^3 H^3}{k^2} \tag{A.5}$$

$$E_2 = \frac{g_\perp}{2}\beta H - B\frac{\beta^2 H^2}{k} - C\frac{\beta^3 H^3}{k^2} \tag{A.6}$$

where $g_\perp = 1.8356$ (calculated)

$B = 0.02958$

$C = 7.095 \times 10^{-4}$.

The calculations necessary for the derivation of Eqs. (A.3) and (A.4) were thoroughly checked for arithmetic errors. In addition the calculations were cross checked by an exact computer diagonalization of the Hamiltonian matrix for various values of the magnetic field. The very close agreement is shown in Table A.1 where E_1 and E_2 refer to the values calculated from Eqs. (A.5) and (A.6) and E_{1D} and E_{2D} refer to the values calculated by the computer diagonalization.

The magnetization is then obtained from the partition function Q.

$$Q = \left[\exp\left(-E_1/kT\right) + \exp\left(-E_2/kT\right)\right]^N \tag{A.7}$$

$$M = kT\left(\frac{\partial \ln Q}{\partial H}\right)_T \quad \text{or}$$

$$\frac{M}{N} = \left(\frac{g_\perp}{2} - 3C\frac{\beta^3 H^2}{k^2}\right)\tanh\left[\left(\frac{g_\perp}{2} - \frac{C\beta^3 H^2}{k^2}\right)\frac{\beta H}{kT}\right] + 2B\frac{\beta^2 H}{k} . \tag{A.8}$$

Table A.1. Eigenvalues of $\mathcal{H} = \beta H_x(L_x + 2S_x)$ for Ce^{+3} in CMN in °K.

H(kOe)	E_1	E_{1D}	E_2	E_{2D}
5	-0.3117	-0.31169	0.3051	0.30501
10	-0.6300	-0.62990	0.6032	0.60319
15	-0.9545	-0.95437	0.8943	0.89428
20	-1.2851	-1.28513	1.1783	1.17829
25	-1.6219	-1.62193	1.4549	1.45499
30	-1.9643	-1.96430	1.7239	1.72397
35	-2.3130	-2.31302	1.9858	1.98580
40	-2.6668	-2.66689	2.2394	2.23954
45	-3.0261	-3.02628	2.4851	2.48543
50	-3.3912	-3.39150	2.7232	2.72359

In addition there is a diamagnetic contribution[101] to the magnetization equal to

$$(M/N)_{dia} = -\ 5.463 \times 10^{-8}\ H \quad . \tag{A.9}$$

The magnetization has been calculated from Eqs. (A.8) and (A.9) and is listed in Table A.2 under the heading $(2M/Ng_{\perp}\beta)_{PER}$. For comparison purposes the magnetization has also been calculated from the equation

$$\left(\frac{M}{N}\right)_L = \frac{g_{\perp}\beta}{2} \tanh\left(\frac{g_{\perp}\beta H}{2kT}\right) + \alpha_o H \left[1 - \frac{3g_{\perp}\beta H}{4\Delta_{12}} \tanh\left(\frac{g_{\perp}\beta H}{2kT}\right) \right] \tag{A.10}$$

where we have taken $g_{\perp} = 1.835$ and $\alpha_o = 0.02235$ from the data of Leask et al.[65] Equation (A.10) is just the combination of Eqs. (A.1) and (A.3) used by Williamson and Cape to test their data. The numbers calculated from (A.9) and (A.10) are listed under the heading $(2M/Ng_{\perp}\beta)_{A.10}$. Magnetization values read from Fig. 1 of Williamson and Cape's paper are listed under the heading $(2M/Ng_{\perp}\beta)_{WC}$. The column labelled "% Deviation" refers to the difference between Williamson and Cape's experimental curve and the magnetization calculated from Eqs. (A.8) and (A.9) (i.e. $(2M/Ng\ \beta)_{PER}$).

The close agreement between the columns $(2M/Ng_{\perp}\beta)_{A.10}$ and $(2M/Ng_{\perp}\beta)_{PER}$ indicates that there are no serious mistakes in the calculated values. For the calculations at $T = 1.270°K$ the deviations between calculation and experiment are very close to the $\pm$ 1% experimental error limits quoted by Williamson and Cape while for $T = 4.194°K$ the agreement is almost exact. Unfortunately the only available raw

Table A.2. Comparison of calculated and experimental values of the magnetization.

H	H/T	$(2M/Ng_{\perp}\beta)_{A.10}$	$(2M/Ng_{\perp}\beta)_{PER}$	$(2M/Ng_{\perp}\beta)_{WC}$	% Deviation
T = 1.270°K					
5	3.937	.2595	.2595	.270	-3.70
10	7.874	.4932	.4929	.500	-1.40
15	11.811	.6851	.6844	.681	0.44
20	15.748	.8320	.8311	.822	1.09
25	19.685	.9398	.9385	.927	1.20
30	23.622	1.0175	1.0160	1.006	0.99
35	27.559	1.0737	1.0721	1.059	1.23
40	31.496	1.1154	1.1138	1.100	1.27
45	35.433	1.1475	1.1460	1.133	1.15
50	39.370	1.1734	1.1720	1.161	0.95
T = 4.194°K					
5	1.192		.0948	.093	+1.93
10	2.384		.1887	.189	0.
15	3.577		.2806	.278	+1.08
20	4.769		.3698	.370	0.
25	5.961		.4558	.460	-0.87
30	7.153		.5379	.543	-0.92
35	8.345		.6155	.621	-0.80
40	9.537		.6884	.692	-0.58
45	10.730		.7566	.756	+0.13
50	11.922		.8199	.821	-0.12

% Deviation = (PER - WC)/100 WC .

data were those shown in their Fig. 1 which is systematically the larger of the two sets. In Fig. 2 of their paper where they plot $(2M'/Ng_{\perp}\beta)$ vs. H/T for all the data, Williamson and Cape drew a smooth curve through the data. This curve fell a maximum $2.5\% \pm 1\%$ below the expected value, and they based their conclusion on this deviation. It seems dangerous (to this author) to draw an average curve through two sets of data which are systematically different. Rather one might speculate on which set of data more closely represents the properties of CMN. Because of the large magnetic anisotropy $(g_{\perp} = 1.84,\ g_{\parallel} = 0.02)$ of CMN, any misalignment of the crystal in the magnetic field would reduce the magnetization. Perturbation calculations taking misalignment into account are possible, but very complicated, and we have not performed them. Thus we cannot give a numerical estimate of this effect.

It does seem reasonable, however, to suggest that the systematically higher set of data are more representative of CMN. If, indeed, this is the case, then our calculations show that the ionic crystal field model is a reasonable one for CMN. Thus the entropy can be calculated from the partition function of Eq. (A.7). In this calculation it is easy to show that the second order Zeeman effect will not contribute to the magnetic entropy of CMN. The third order contribution to the magnetization, however, reduces the effective H/T as shown in Eq. (A.8) for the magnetization. Our calculations show that at the maximum field used in our experiments (21 kOe) the effective H/T is reduced by less than 0.2%. Thus we have neglected third order effects and have calculated entropy in terms of the first order Zeeman effect for the treatment of our data.

If, however, the smooth curve given by Williamson and Cape in their Fig. 2 is representative of CMN, then the effect on the entropy can be estimated in the following manner. The magnetization M' consists of two contributions

$$M' = M_{CF} + M'' \tag{A.11}$$

where M_{CF} is the magnetization of an ideal spin 1/2 paramagnet with $g = 1.84$ and M'' is the (negative) contribution to the magnetization arising from any non-ideality. (M'' corresponds to $-2\Delta m'/N_g\beta$ in Williamson and Cape's paper.) The entropy may be calculated as follows:

$$\Delta S = \int_{H=0}^{H_f} (\partial M'/\partial T)_H \, dH = \int_{H=0}^{H_f} (\partial M_{CF}/\partial T)_H \, dH + \int_{H=0}^{H_f} (\partial M''/\partial T)_H \, dH. \tag{A.12}$$

The contribution from M_{CF} is shown in Fig. IV.1. The values of M'' for various H/T may be obtained from the insert in Fig. 2 of Williamson and Cape's paper. If we assume that M'' is a function of H/T, then we can fit the M'' (or $\Delta m'$) data to the empirical function

$$\frac{M''}{R} = \sum_i a_i \, (H/T)^{i-1} \quad . \tag{A.13}$$

Then

$$\frac{\Delta S''}{R} = \left[\sum_i a_i [(1-i)/i] \, (H/T)^i \right]_{H=0}^{H=H_f} \quad . \tag{A.14}$$

A satisfactory fit to the M" values (read from Fig. 2 of Williamson and Cape's paper) was obtained for $i_{max} = 8$ in Eq. (A.13) and the results are listed in Table A.3. It should be emphasized that the values of $\Delta S''/R$ in this table are only approximate since it was necessary to differentiate the fitted $M''(H/T)$ function in the calculation. The effect of these calculations on the nuclear orientation T-S relation for CMN is discussed in Section IV.E.

The last column in Table A.3 lists a multiplicative factor (F) to be applied to temperatures determined by calorimetry. The factor is derived in the following manner:

$$S = S_{CF} + \Delta S'' \tag{A.15}$$

$$T = dQ/dS = (dQ/dS_{CF})\,(dS_{CF}/dS) = (dQ/dS_{CF}) \cdot F \tag{A.16}$$

where dQ/dS_{CF} is the "temperature" derived by Hudson and Kaeser. [Here Q = "heat".]

$$1/F = \frac{dS}{dS_{CF}} = 1 + \frac{d(\Delta S'')}{dS_{CF}} = 1 + \frac{d(\Delta S'')}{d(H/T)} \cdot \frac{d(H/T)}{dS_{CF}} \,. \tag{A.17}$$

From Eq. (A.14) it follows that

$$\frac{d(\Delta S''/R)}{d(H/T)} = \sum_i a_i\,(1-i)\,(H/T)^{i-1} \,, \tag{A.18}$$

and from Eqs. (II.A.6) and (IV.A.1) it is easy to show that

Table A.3. Entropy corrections.

H/T(kOe/°K)	$(S/R)_{CF}$	$\Delta S''/R$	$(S/R)_{CF} + \Delta S/R$	F
5	0.648	0.002	0.650	1.025
10	0.534	0.004	0.538	1.027
15	0.399	0.009	0.408	1.044
20	0.276	0.015	0.291	1.054
25	0.181	0.019	0.200	1.049
30	0.114	0.022	0.136	1.040
35	0.070	0.024	0.094	1.048
40	0.043	0.025	0.068	1.031

$$\frac{d(H/T)}{d(S_{CF}/R)} = \frac{\left[\cosh\left(\frac{g_\perp \beta H}{2kT}\right)\right]^2}{\left(\frac{g_\perp \beta}{2k}\right)^2 (H/T)} \tag{A.19}$$

then

$$1/F = 1 - \left[\sum_i a_i \, (1-i) \left(\frac{H}{T}\right)^{i-1}\right] \left\{\frac{\left[\cosh\left(\frac{g_\perp \beta H}{2kT}\right)\right]^2}{\left(\frac{g_\perp \beta}{2k}\right)^2 (H/T)}\right\} . \tag{A.20}$$

It should be emphasized here that the tabulated values of F are only approximate because of the double differentiation involved in the calculation. The effect of these calculations on the Hudson and Kaeser T-S relation is discussed in Section IV.E.

B. Spectrochemical Analysis

1. La_2O_3 (Bryant Laboratory, Inc., Berkeley, California)

The only element detected was Ca; the ratio of Ca to La was 0.005. The following elements were searched for but were not detected. The numbers in parentheses indicate the percentage limits of detection with respect to La equal to 100%.

Al (0.01), Bi (0.05), Ce (0.1), Cr (0.01), Dy (0.1), Er (0.05), Eu (0.01), Fe (0.01), Gd (0.05), Ho (0.05), K (1.0), Lu (0.05), Mg (0.01), Mn (0.01), Mo (0.01), Na (1.0), Nb (0.01), Nd (0.1), Ni (0.05), Pb (0.1), Pr (0.1), Sc (0.01), Si (0.01), Sm (0.05), Sn (0.1), Ta (0.1), Tb (0.5), Ti (0.01), Tm (0.05), W (0.1), Yb (0.01), Y (0.01), Zn (0.1), Zr (0.01).

2. CMN: $Ce_2Mg_3(NO_3)_{12} \cdot 24H_2O$

The CMN was prepared from 99.9% $Mg(NO_3)_2 \cdot 6H_2O$ (J. T. Baker Chemical Co., Phillipsburg, N. J.) and "purified" $Ce(NO_3)_3 \cdot 6H_2O$ (Allied Chemical Co., Morristown, N. J.). A separate analysis of the $Ce(NO_3)_3 \cdot 6H_2O$ is given in Appendix B.3.

The sample size of CMN was chosen to yield about 50 μg of Ce as the metal. Cu, Al, and Ca were observed at the limits of detection, all of which were 0.01 μg. Approximately 0.03 μg of Na were detected. The following impurity elements were searched for but were not detected. The limits of detection are indicated in parentheses.

Bi (0.05), Co (0.05), Cr (0.01), Dy (0.1), Er (0.05), Eu (0.01), Fe (0.05), Gd (0.05), Ho (0.05), La (0.05), Li (0.01), Lu (0.05), Mn (0.01), Nb (0.01), Nd (0.1), Ni (0.01), Pb (0.1), Pr (0.1), Sc (0.05),

Si (0.01), Sm (0.05), Sn (0.1), Tb (0.5), Th (0.5), Ti (0.01), Tl (0.5), Tm (0.05), V (0.01), Zn (0.1), Zr (0.01).

3. $Ce(NO_3)_3 \cdot 6H_2O$ (Allied Chemical Co., Morristown, N. J.)

The results are listed in percentage with respect to Ce as the metal. The following elements were detected: Ca (0.1%), Mg (0.5%), and Na (0.05%). The following elements were searched for but not detected. The limits of detection (percentage) are given in parentheses. Ag (0.01), Al (0.01), As (0.5), Au (1.0), Bi (0.05), Cd (0.5), Co (0.05), Cr (0.01), Dy (0.1), Er (0.05), Eu (0.01), Fe (0.01), Ga (0.05), Gd (0.05), Ge (0.05), Hf (0.05), Ho (0.05), In (0.05), Ir (0.5), K (0.5), La (0.01), Li (0.01), Lu (0.05), Mn (0.01), Mo (0.01), Nb (0.01), Nd (0.1), Ni (0.05), Pb (0.1), Pr (0.5), Re (0.1), Rh (0.5), Sb (0.5), Sc (0.01), Si (0.01), Sm (0.05), Sn (0.1), Sr (0.01), Ta (0.1), Th (0.5), Ti (0.01), U (0.5), V (0.01), W (0.5), Yb (0.01), Y (0.01), Zn (0.1), Zr (0.01).

C. Sample Calculation of W(0)

In Table C.1 the intensity values for three cold counts [C (1), C (2), and C (3)] and one warm count (W_t) are listed for the channels covering the photopeak. These values are for the first run in Table IV.3 (June 1967). The numbers in the brackets list the counting time in seconds for the respective counts. Then W(0) is calculated as follows:

(Note the distinction between W(0) and the abbreviation for the warm count W_t)

$$W(0) = \left[\frac{C\ (1) + C\ (2) + C\ (3) - aB}{aW_t - aB}\right] \times e^{-\frac{t'\ell n2}{t'_{1/2}}} \qquad (C.1)$$

where a is a factor accounting for the counting time difference between the warm count and the sum of the cold counts and B is the background correction. The factor $e^{-t'\ell n2/t'_{1/2}}$ corrects for source decay between the cold and the warm counts; here t' is the elapsed time between the midpoints of the cold and warm counts and $t'_{1/2}$ is the half-life (34.4 hr) of ^{137m}Ce. For this run t' = 8.20 minutes and $e^{-t'\ell n2/t'_{1/2}} = 0.9972$. From Table C.1 the constant a is seen to be (30 + 30 + 30)/300 = 0.3. From the method described in Section IV.B, B/W_t is found to be 0.0820 or $B = 0.0820\ W_t = 5083$. Therefore

$$W(0) = \left[\frac{11581 + 11545 + 11540 - (0.3 \times 5083)}{0.3 \times (61984 - 5083)}\right] (.9972)$$

$$= (33141/17070) \times .9972 = 1.936\ .$$

Table C.1. Raw data for the first run in the June 1967 experiment.

Channel	C (1)[30]	C (2)[30]	C (3)[30]	W_t[300]
132	675	631	646	3592
133	713	705	711	4022
134	766	820	807	4318
135	886	864	936	4395
136	841	892	852	4535
137	925	859	915	4620
138	914	887	870	4675
139	848	888	868	4536
140	826	810	826	4332
141	767	741	717	4070
142	662	648	677	3744
143	571	615	591	3258
144	512	544	484	2779
145	397	445	408	2336
146	391	346	366	1960
147	301	303	315	1567
148	233	239	213	1337
149	204	181	178	1044
150	149	127	160	864
SUM	11581	11545	11540	61984

D. Calculation of Heating Effects During the Magnetization

1. Heating by Conversion Electrons

The 255 keV γ-ray of ^{137m}Ce is highly converted; $e_K/\gamma = 5.4$ and $K/L + M + \ldots = 2.0$. The energy of the K electrons is 214.6 keV, and the remainder of the conversion electrons will be assumed to have an energy of 249 keV, the energy of the L electrons. It will be assumed that all the energy of the conversion electrons is dissipated in this sample; this will give a maximum energy input.

Under the experimental conditions described in Sections III and IV, a 3" × 3" NaI(Tl) detector (of right circular cylindrical shape) is 10 cm from a source. For simplicity the source will be assumed to be a point source. Thus the problem is simply one of counting the conversion electrons or γ-rays emitted in the solid angle of the detector and making the appropriate solid angle correction. From simple goemetrical considerations we see that

$$\frac{\text{Counts (total)}}{\text{Counts (solid angle)}} = \frac{2}{1 - \cos\alpha} \qquad \text{(D.1)}$$

where α is shown in Fig. D.1. Then $\tan\alpha = 3.81/10 = .381$ and $\cos(\tan^{-1}\alpha) = .935$. If we assume a γ-ray counting rate of 20,000 per minute and unit efficiency, then the number of K electrons in the solid angle is 108,000 per minute and the number of L + M conversion electrons is 54,000 per minute. The total number of K conversion electrons per minute is then 3.32×10^6 and for L + M electrons 1.66×10^6. This corresponds in energy to 1.8 erg/min.

Figure D.1. Solid Angle Diagram.

S indicates the radioactive source and D indicates a 3 inch × 3 inch NaI(Tl) detector.

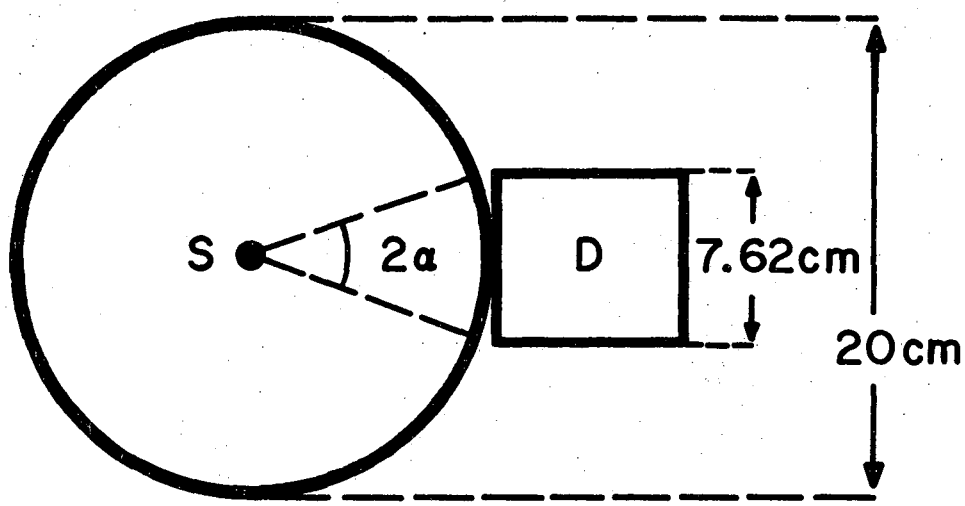

XBL689-6763

Fig. D.1.

2. Heating During Magnetization

After the salt pill has come into thermal equilibrium with the ^{3}He bath, the exchange gas is pumped out of the experimental chamber. During this period the sample will be subjected to an energy input from the ^{137m}Ce conversion electrons and will warm slightly. The amount of warming can be estimated in the following manner.

The heat capacity (C_H) of a spin 1/2 system at constant field can be expressed in terms of the partition function Q.

$$C_H = T\left(\frac{\partial S}{\partial T}\right)_H \quad \text{where} \quad S = kT\left(\frac{\partial \ln Q}{\partial T}\right)_H + k\ln Q$$

and

$$Q = \left[\exp\left(\frac{g\beta H}{2kT}\right) + \exp\left(\frac{-g\beta H}{2kT}\right)\right]^N$$

$$= \left[2\cosh\left(\frac{g\beta H}{2kT}\right)\right]^N \quad . \qquad \text{(D.2)}$$

After some simple manipulation it is found that

$$C_H = N\left(\frac{g\beta H}{2T}\right)^2\left(\frac{1}{k}\right)\left\{1 - \left[\tanh\left(\frac{g\beta H}{2kT}\right)\right]^2\right\} . \qquad \text{(D.3)}$$

Table C.1 lists values of the heat capacity for a 1.4 g crystal of CMN at various H/T's. For small heat inputs $\Delta Q \approx C_H \Delta T$ where C_H is assumed constant over ΔT. On the average, the pump out time was 15 minutes, but the effective time of isolation was probably only about 10 minutes or less. This corresponds to a maximum heat input of 18 ergs (c.f. preceding section). The last two columns in Table C.1 list the temperature rise in millidegrees and the associated change in entropy. Because of the smallness of the change, this effect was neglected.

Table C.1. Radioactive heating effects.

H/T_i	C_H(erg/1.4 g, m°K)	ΔT_i(m°K)	$\delta(\Delta S)$
5.0	13.2	1.4	0
6.0	18.3	1.0	0
10.0	40.5	0.4	0
20.0	66.5	0.3	0
30.0	101.4	0.2	0
40.0	26.0	0.7	0
50.0	11.6	1.5	+0.001
60.0	5.0	3.0	<0.001
70.0	2.1	8.6	<0.001

For $H/T_i \leq 40$ kOe/°K, $T_i = 0.5$°K and for $H/T_i \geq 50$ kOe/°K, $T_i = 0.31$°K.

ACKNOWLEDGMENTS

The most enjoyable part of any thesis is acknowledging the many people who have helped to bring the work to fruition. This thesis is no exception.

I would first like to thank Professor David A. Shirley, who not only initiated and directed this research but who also allowed me sufficient independence of action to profit from my own experience. Many helpful discussions -- especially with respect to the interpretation of this work -- helped to form the content of this thesis. I am also grateful to Dr. Nicholas J. Stone and Dr. Richard B. Frankel for the valuable guidance which they generously gave me in the early stages of my graduate career. Dr. Eckart Matthias also deserves my thanks for his constant support and for the direction which he provided during my fourth year as a graduate student.

I take great pleasure in acknowledging the friendship of Mr. Stephen S. Rosenblum, who was always willing to listen and to discuss my questions -- whether scientific, social, or political. He deserves special credit for surviving five years in the same office with me -- which, as he will testify, was no small fete. It is also my pleasure to thank Mr. John A. Barclay, a fellow graduate student, room-mate, and "mountain man," for his friendship and his interest in my problems -- both scientific and otherwise. In addition I am indebted to all the graduate students and postdoctoral fellows in our research group for their friendship and helpfulness.

Many people provided excellent technical assistance, but four people deserve special mention: Mrs. Wini Heppler for her aid in growing single crystals; Mr. Dimitri "Ed" Voronin for his unfailing mechanical help; Mrs. Gertie Bolz for her skill as a health chemist in handling radioactive materials; and Mr. Clint Ward for his assistance with electronics problems.

Finally I would like to thank my parents and grandparents for their faith in me and for their constant encouragement. Most important of all, however, I am grateful to my wife Patty, who personally shared in the trauma of writing this thesis, but who nevertheless was a source of strength for me. Her assistance in typing the first draft of this thesis and her critical evaluation of the manuscript were invaluable.

I also wish to acknowledge the financial support of the United States Atomic Energy Commission.

REFERENCES

1. J. M. Daniels and F. N. H. Robinson, Phil Mag. 44, 630 (1953).
2. D. deKlerk, Handbuch der Physik 15, 38 (Springer - Verlag, Berlin, 1956).
3. R. B. Frankel, D. A. Shirley, and N. J. Stone, Phys. Rev. 140, A 1020 (1965).
4. R. P. Hudson and R. S. Kaeser, Physics 3, 95 (1967).
5. W. R. Abel, A. C. Anderson, W. C. Black, and J. C. Wheatley, Phys. Rev. 147, 111 (1966).
6. W. R. Abel, A. C. Anderson, W. C. Black, and J. C. Wheatley, Physics 1, 337 (1965).
7. J. C. Wheatley, Ann. Acad. Sci. Fennicae: Ser. A VI No. 210, 15 (1966).
8. B. M. Abraham and Y. Eckstein, Phys. Rev. Letters 20, 649 (1968).
9. W. C. Black, Phys. Rev. Letters 21, 28 (1968).
10. A. C. Anderson, Phys. Letters 20, 1474 (1968).
11. W. F. Giauque, J. Am. Chem. Soc. 49, 1864 (1927).
12. P. Debye, Ann. Phys. 81, 1154 (1926).
13. W. F. Giauque and D. P. MacDougall, Phys. Rev. 43, 768 (1933).
14. E. Ambler and R. P. Hudson, Rept. Prog. Phys. 18, 251 (The Physical Society, London, 1955).
15. D. deKlerk and M. J. Steenland, Progress in Low Temperature Physics 1, ed. by C. J. Gorter (North Holland Publishing Comp., Amsterdam, 1957) Chap. XIV.
16. N. Kurti, Nuovo Cimento, Suppl. Ser. 10, 6, 1101 (1957).
17. J. H. Van Vleck, The Theory of Electric and Magnetic Susceptibilities, (Oxford University Press, 1932, New York) Chapter 9.

18. Mathematical and Physical Papers, Thompson (Kelvin) (Cambridge University Press, London, 1882) Vol. 1, p. 235 quoted in W. F. Giauque, Phys. Rev. 92, 1339 (1953).

19. T. L. Hill, Introduction to Statistical Thermodynamics (Addison-Wesley Publishing Co., Inc., Reading, Mass., 1960) Chap. 1.

20. N. Kurti and F. E. Simon, Phil. Mag. 26, 849 (1938).

21. J. H. Van Vleck, J. Chem. Phys. 5, 320 (1937).

22. M. H. Hebb and E. M. Purcell, J. Chem. Phys. 5, 338 (1937).

23. J. M. Daniels, Proc. Phys. Soc. London A66, 673 (1953).

24. R. J. Blin-Stoyle and M. A. Grace, Handbuch der Physik 42, 555 (Springer - Verlag, Berlin, 1957).

25. D. A. Shirley, Ann. Rev. Nucl. Sci. 16, 89 (1966).

26. J. M. Daniels, Oriented Nuclei: Polarized Targets and Beams (Academic Press, New York, 1965) Chap. II.

27. E. Ambler, Progress in Cryogenics (Heywood and Co., London, 1960) pp. 235-280.

28. W. J. Huiskamp and H. A. Tolhoek, Progress in Low Temperature Physics 3, ed. C. J. Gorter (North Holland Publishing Comp., Amsterdam, 1961) Chap. VIII.

29. M. J. Steenland and H. A. Tolhoek, Progress in Low Temperature Physics 2, ed. C. J. Gorter (North Holland Publishing Comp., Amsterdam, 1957) Chap. X.

30. S. R. de Groot, H. A. Tolhoek, and W. J. Huiskamp, Alpha-Beta-and-Gamma Ray Spectroscopy, ed. Kai Siegbahn (North Holland Publishing Comp., Amsterdam, 1965) Vol. 2, Chap. 19.

31. Nuclear Orientation, ed. M. E. Rose (Gordon and Breach, New York, 1963).

32. M. Ferentz and N. Rosenzweig, Table of F coefficients, Argonne National Laboratory Report ANL-5324, 1955.

33. A. Abragram and M. H. L. Pryce, Proc. Phys. Soc. London A 205, 135 (1951).

34. B. N. Samoilov, V. V. Sklyarevskii, and E. P. Stepanov, Zh. Eksperim. Teor. Fiz. 36, 644 (1959) (Soviet Phys. JETP 9, 448 (1959)).

35. E. Matthias and R. J. Holliday, Phys. Rev. Letters 17, 897 (1966).

36. J. E. Templeton and D. A. Shirley, Phys. Rev. Letters 18, 240 (1967).

37. R. V. Pound, Phys. Rev. 76, 1410 (1949).

38. R. M. Sternheimer, Phys. Rev. 80, 102 (1950).

39. J. Blok and D. A. Shirley, Phys. Rev. 143, 911 (1966).

40. J. Blok and D. A. Shirley, Phys. Rev. 143, 278 (1966).

41. B. Bleaney, Proc. Phys. Soc. London A64, 315 (1951) and Phil. Mag. 42, 441 (1951).

42. C. J. Gorter, Physica 14, 504 (1948).

43. M. E. Rose, Phys. Rev. 75, 213 (1949).

44. J. Blok, D. A. Shirley, and N. J. Stone, Phys. Rev. 143, 78 (1966).

45. Cryonetics Corporation, Burlington, Massachusetts (now defunct).

46. E. Ambler and R. B. Dove, Rev. Sci. Instr. 32, 737 (1961).

47. Mott Metallurgical Co., Hartford, Connecticut, drawing number A 3331-1.

48. Consolidated Vacuum Corporation, Rochester, New York.

49. W. M. Welch Manufacturing Co., Chicago, Illinois.

50. T. R. Roberts and S. G. Sydoriak, Phys. Rev. 102, 304 (1956).

51. R. A. Watkins, W. L. Taylor, and W. J. Haubach, J. Chem. Phys. 46, 1007 (1967).

52. A. Freddi and I. Modena, Cryogenics 8, 18 (1958).

53. R. H. Sherman, S. G. Sydoriak, and T. R. Roberts, J. Research NBS 68A (Phys. and Chem.), 579 (1964).

54. Spectromagnetic Industries, Hayward, California.

55. Rawson Electrical Instrument Co., Cambridge, Massachusetts.

56. George Associates, Berkeley, California.

57. Harshaw Chemical Corporation, Cleveland, Ohio.

58. Digital Equipment Corporation, Maynard, Massachusetts.

59. I am indebted to Miss Penny Collom for writing the program "TWIST" and several of the post-processing routines.

60. Hastings-Raydist, Inc., Hampton, Virginia.

61. A. Zalkin, J. D. Forrester, and D. H. Templeton, J. Chem. Phys. 39, 2881 (1963).

62. B. Bleaney, K. D. Bowers, and R. S. Trenam, Proc. Roy. Soc. London A228, 157 (1955).

63. T. L. Estle, H. R. Hart, and J. C. Wheatley, Phys. Rev. 112, 1576 (1958).

64. R. J. Lang, Can. J. Res. 14, 127 (1936).

65. M. J. M. Leask, R. Orbach, M. J. D. Powell, and W. P. Wolf, Proc. Roy. Soc. London A272, 371 (1963).

66. K. H. Hellwege, S. H. Kwan, W. Rummel, W. Schemps, and B. Schneider, Z. Phys. 167, 487 (1962).

67. R. P. Hudson and W. R. Hosler, Phys. Rev. 122, 1417 (1961).

68. J. H. M. Thornley, Phys. Rev. 132, 1492 (1963).

69. C. B. P. Finn, R. Orbach, and W. P. Wolf, Proc. Phys. Soc. London 77, 261 (1961).

70. J. A. Cowen and D. E. Kaplan, Phys. Rev. 124, 1098 (1961).

71. R. H. Ruby, H. Benoit, and C. D. Jeffries, Phys. Rev. 127, 51 (1962).

72. A. H. Cooke, H. J. Duffus, and W. P. Wolf, Phil. Mag. 44, 623 (1953).

73. O. S. Leifson and C. D. Jeffries, Phys. Rev. 122, 1781 (1961).

74. B. R. Judd, Proc. Roy. Soc. London A232, 458 (1955).

75. S. J. Williamson and J. A. Cape, Phys. Rev. Letters 21, 370 (1968).

76. C. A. Bailey, Phil. Mag. 4, 833 (1959).

77. J. R. Hull and R. A. Hull, J. Chem. Phys. 9, 465 (1941).

78. J. N. Haag, C. E. Johnson, D. A. Shirley, and D. H. Templeton, Phys. Rev. 121, 591 (1961).

79. J. N. Haag, D. A. Shirley, and D. H. Templeton, Phys. Rev. 129, 1601 (1963).

80. R. B. Frankel, Ph.D. Thesis, University of California, 1965 UCLRL 11871 (unpublished).

81. A. R. Brosi and B. H. Kettelle, Phys. Rev. 100, 169 (1955).

82. N. J. Stone, R. B. Frankel, and D. A. Shirley, Bull. Am. Phys. Soc. 9, 486 (1964).

83. R. B. Frankel, D. A. Shirley, and N. J. Stone, Phys. Rev. 136, B577 (1964).

84. L. E. Glendenin, K. F. Flynn, R. F. Buchanan, and E. P. Steinberg, Anal. Chem. 27, 59 (1955).

85. I am indebted to George Shalimoff for performing all the spectrochemical analyses.

86. DAP, Inc., Dayton, Ohio.

87. L. G. Parratt, Probability and Experimental Errors in Science (John Wiley and Sons, Inc., New York, 1961) Chapter 3.

88. M. J. L. Yates, Perturbed Angular Correlation, ed. E. Karlsson, E. Matthias, and K. Siegbahn (North Holland Publishing Comp., Amsterdam, 1963) Appendix 4.

89. J. W. Culvahouse (private communication).

90. M. E. Rose, Phys. Rev. 91, 610 (1953).

91. R. W. Kedzie, M. Abraham, and C. D. Jeffries, Phys. Rev. 108, 54 (1957).

92. Private communication from J. Felsteiner to R. C. Sapp. I am grateful to Professor Sapp for bringing this to my attention. See also reference 94.

93. J. W. Culvahouse, J. L. McNichols, and R. C. Sapp (private communication).

94. J. M. Daniels and J. Felsteiner, Can. J. Phys. 42, 1469 (1964).

95. M. W. Levi, R. C. Sapp, and J. W. Culvahouse, Phys. Rev. 121, 538 (1961).

96. J. W. Culvahouse, W. Unruh, and R. C. Sapp, Phys. Rev. 121, 1370 (1961).

97. E. Ambler, M. A. Grace, H. Halban, N. Kurti, H. Durand, C. E. Johnson, and H. R. Lemmer, Phil. Mag. 44, 216 (1953).

98. C. M. Schroeder, Ph.D. Thesis, Ohio State University, 1957 (unpublished).

99. F. Carboni and R. C. Sapp, Ann. Phys. (N.Y.) 1, 77 (1965).

100. J. L. Powell and B. Craseman, Quantum Mechanics (Addison-Wesley Publishing Company, Inc., Reading, Massachusetts, 1961).

101. A. Mookherji, Indian J. Phys. 23, 410 (1949).

LEGAL NOTICE

This report was prepared as an account of Government sponsored work. Neither the United States, nor the Commission, nor any person acting on behalf of the Commission:

A. Makes any warranty or representation, expressed or implied, with respect to the accuracy, completeness, or usefulness of the information contained in this report, or that the use of any information, apparatus, method, or process disclosed in this report may not infringe privately owned rights; or

B. Assumes any liabilities with respect to the use of, or for damages resulting from the use of any information, apparatus, method, or process disclosed in this report.

As used in the above, "person acting on behalf of the Commission" includes any employee or contractor of the Commission, or employee of such contractor, to the extent that such employee or contractor of the Commission, or employee of such contractor prepares, disseminates, or provides access to, any information pursuant to his employment or contract with the Commission, or his employment with such contractor.

TECHNICAL INFORMATION DIVISION
LAWRENCE RADIATION LABORATORY
UNIVERSITY OF CALIFORNIA
BERKELEY, CALIFORNIA 94720